Analysis of a Wedge Core Hypersonic Waverider for Use in Sub- Orbital Aerodynamic Re-Entry Experiment

A project present to
The Faculty of the Department of Aerospace Engineering
San Jose State University

in partial fulfillment of the requirements for the degree
Master of Science in Aerospace Engineering

By

Paul R. Linggi

December 2013

approved by

Dr. Periklis Papadopoulos
Faculty Advisor

San José State
UNIVERSITY

Approved by:

12/12/13

Periklis Papadopoulos Date
Committee Chair
Department of Aerospace Engineering, San José State University

Dec 12, 2013

Marcus Murbach Date
Committee Member
NASA Ames Research Center

Dec 13, 2013

Professor Nikola Djordjevic Date
Committee Member
Department of Aerospace Engineering, San José State University

Abstract

With the retirement of the Space Shuttle and the move to smaller capsules for transporting humans and scientific payloads, the ability to bring down scientific experiments and equipment is greatly hampered. In order to augment the capabilities, a hypersonic waverider can be used to bring materials down without the strong forces normally experienced during a capsule descent. In order to reduce costs and to make the vehicle practical in various situations, a proto-waverider is being developed at NASA Ames Research Center for use in Sub-Orbital Aerodynamic Re-Entry Experiments (SOAREX).

The proto-waverider is a lifting body without wings designed with the various high lift re-entry bodies of the past in mind. Using a variety of resources, the proto-waverider has been modeled and a computational fluid dynamic (CFD) analysis has been conducted on the body. This particular paper focuses on re-entry from the near International Space Station orbit from a sounding rocket where during re-entry the vehicle should undergo the highest heating conditions and the highest dynamic pressure conditions. For the highest heating condition the proto-waverider's nose will reach temperatures in excess of 1500 K while at the highest dynamic pressure the vehicle will experience pressures near 60 kPa. The data is also analyzed for various angles of attacks and two other conditions to further help design the proto-waverider so that it can one day be used in re-entry applications.

Acknowledgements

I would like to thank my parents first and foremost; they have supported me and encouraged me during this long, long, long process. Without them I doubt this would have ever been completed, and I thank them dearly for this. I would like to thank Dr. Periklis Papadopoulos, Marcus Murbach, and Nikola Djordjevic for their contributions to this report and for providing feedback throughout the years. I would particularly like to thank Marcus Murbach for the support and help obtaining the necessary resources for this project.

I would like to thank Kenny Boronowski, Joshua Benton, and especially Matthew Ringle for their help getting all the models and getting the programs to actually do what they are supposed to do. I would also like to thank my friends who have encouraged me (and distracted me) throughout this process. I would particularly like to thank Tommy Blackwell, Gabriel Alvarez, and particularly Andrew Muñoz for joining me for this descent into madness and providing support and encouragement to make it out the other side.

Table Of Contents

List of Nomenclature

Symbol	Description
C	Constant
C_D	Coefficient of Drag
C_f	Coefficient of Skin Friction
C_L	Coefficient of Lift
D	Drag
K	Temperature in Kelvin
kg	Kilogram
kPa	Kilopascal
L	Lift
m	Meter
M	Mach
$\dot{m}$	Mass flow
p	Pressure
r	Radial Direction
Re	Reynolds Number
T	Temperature
u	Horizontal Flow Speed Component
V	Velocity
V_r	Flow Velocity Along Conical Ray
z	Axial Direction
α	Second Angle of Correction; Angle of Attack

β	Shock Wave Angle
ε	Half Angle
ρ	Density
ω	Z-Component of Flow Velocity,
υ	Transverse Component of Flow Velocity; Vertical Flow Speed Component
μ	Viscosity
ϖ	Exponential Variation
ψ	Streamfunction Value
θ	Angle of a Ray; Incident Angle
γ	Specific Heat Ratio
ν	Prandtl-Meyer Function

Subscripts

e	Edge
j	Grid Point Location
w	Wall Location
x	Distance to Leading Edge
∞	Freestream
0	Total/Stagnation Condition
0, 1, … , 5	Locations

Superscripts

′ Reference

List of Figures

1. Introduction

The National Aeronautics and Space Administration (NASA) has recently ended the Space Transportation System (STS), more commonly known as the space shuttle, after thirty years of service. Since this transition, there have been no large crew missions to the International Space Station (ISS), as well as diminished payload returns due to the smaller size of the Soyuz capsules. Due to the size and shortage of orbiters, experiments will not be able to be returned from the ISS with regular frequency [1]. In order to increase the payload return capability, also known as “down-mass”, a simple wedge core hypersonic waverider will be analyzed for implementation within the Sub-Orbital Aerodynamic Re-Entry Experiments (SOAREX) program.

2. Hypersonic Waverider Overview

Hypersonic waveriders are aptly named, for they have the capability to ride a shock wave during high-speed maneuvers. When a hypersonic waverider is designed, the intention is for the shock wave generated at the front of the body to become attached along the wing’s leading edge. By having the shock wave attached to the leading edge, the high pressure cannot go around the edge to the low-pressure region and thus creates a “seal” so that the hypersonic waverider can hold (ride) the shock wave along its trajectory. Meanwhile, the top portion of the waverider is exposed to the hypersonic conditions and thus has a lower pressure due to the rapidly moving air over the surface. With this attached shock, the waverider does not need to be at an extreme angle of attack like other hypersonic vehicles since it prevents pressure from seeping out [2]. The hypersonic waverider will thus have a higher lift-to-drag ratio (L/D) than other lifting body designs that have been manufactured in the past (see Section 3). The design of the hypersonic waverider also has the advantage of allowing an engine to be mounted to the vehicle with known flow properties. As the conditions of the air flow around the waverider is known, an engine can be attached to the craft so that an inviscid flow with exact Mach design can be used to power the waverider for flights around the world [3]. For the purpose of using the wedge core hypersonic waverider ('proto-waverider') in SOAREX, there is no need to attach an engine, but it should be noted that many other designs include the addition of an engine.

2.1. Inviscid Flow Waveriders

Nonweiler designed the first hypersonic waveriders in 1959 under the assumption that the hypersonic flow was inviscid flow. He designed the first waverider after the known flow field of a planar oblique shock wedge. This shape, known as a caret wing waverider, allows the waverider to become a lifting surface and can be seen in Figure 1 [4].

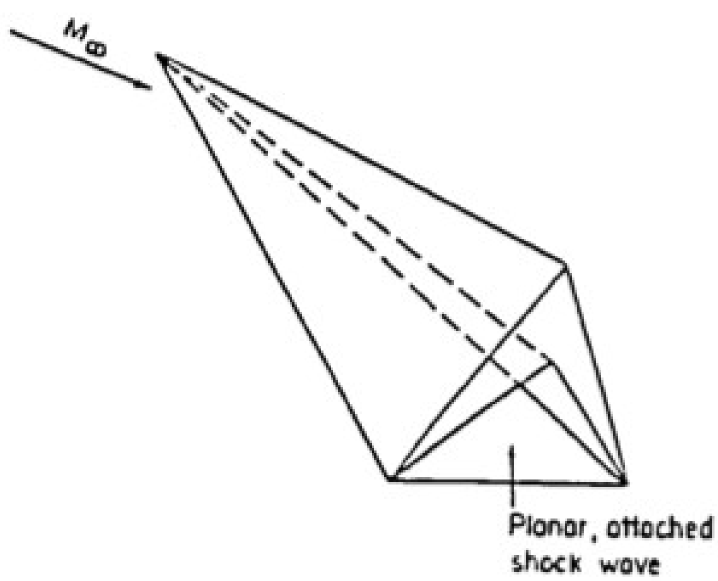

Figure 1. Simple caret wing waverider [4]

Initially when the inviscid flow waveriders were designed, the drag calculated was only wave drag and this led to large L/D values that seemed great on paper. However, since the calculations did not take into account the reality of skin drag, many in the field said that the waverider would have a much lower L/D value and thus was an unreasonable vehicle. This opinion lead to a halt in the development of waveriders until the computational power became available to model viscous waveriders, as discussed in the next section. The inviscid waveriders though are still important for in the initial planning of missions to other planets (non-terrestrial) where there is a high Mach number during entry. The boundary layers created during atmospheric entry will likely be laminar and therefore the viscous drag is less severe, making initial inviscid calculations significant in the mission design phase [2].

The inviscid hypersonic waverider seen in Figure 1 was initially calculated without the use of an optimizer as the base for inviscid optimized waveriders and was just to be the simplest form of a waverider. Bowcutt (et all) researched how to optimize an inviscid waverider by optimizing hypersonic waveriders without skin drag. By removing the skin drag and setting a Mach range from 6 to 25, they discovered that the optimized inviscid hypersonic waverider is actually the simple caret wing, as seen in Figure 2, proving Nonweiler's design [5].

Figure 2. Optimized inviscid waverider at Mach 10; a caret wing [5]

2.2. Viscous Flow Waveriders

As stated previously, hypersonic waveriders were initially dismissed given that the inviscid flow assumptions were unrealistic due to the drag associated with skin friction. Since the 1980's however, research has started up again into finding out about the viscous flow of hypersonic waveriders. In order to make the hypersonic waverider a possibility, the wetted surface area needs to be reduced so that the skin friction drag force can be reduced for a higher L/D ratio. When an optimizer program is used in conjunction with the skin friction (instead of initially assuming inviscid flow then taking into account the skin friction drag at the end), a capable high L/D waverider can be designed. Using this approach the designer initially designates a Mach speed and flow field by choosing a flow field; the flow field can be such shapes as a wedge, cone, or even a sweep angle. Once optimized for the chosen conditions, the waverider will no longer be the simple caret wing waverider and instead be something that works for the specified conditions [5]. An example of this can be seen with Figure 3 where the desired Mach number was six and the shock cone angle went from 11° to 14°.

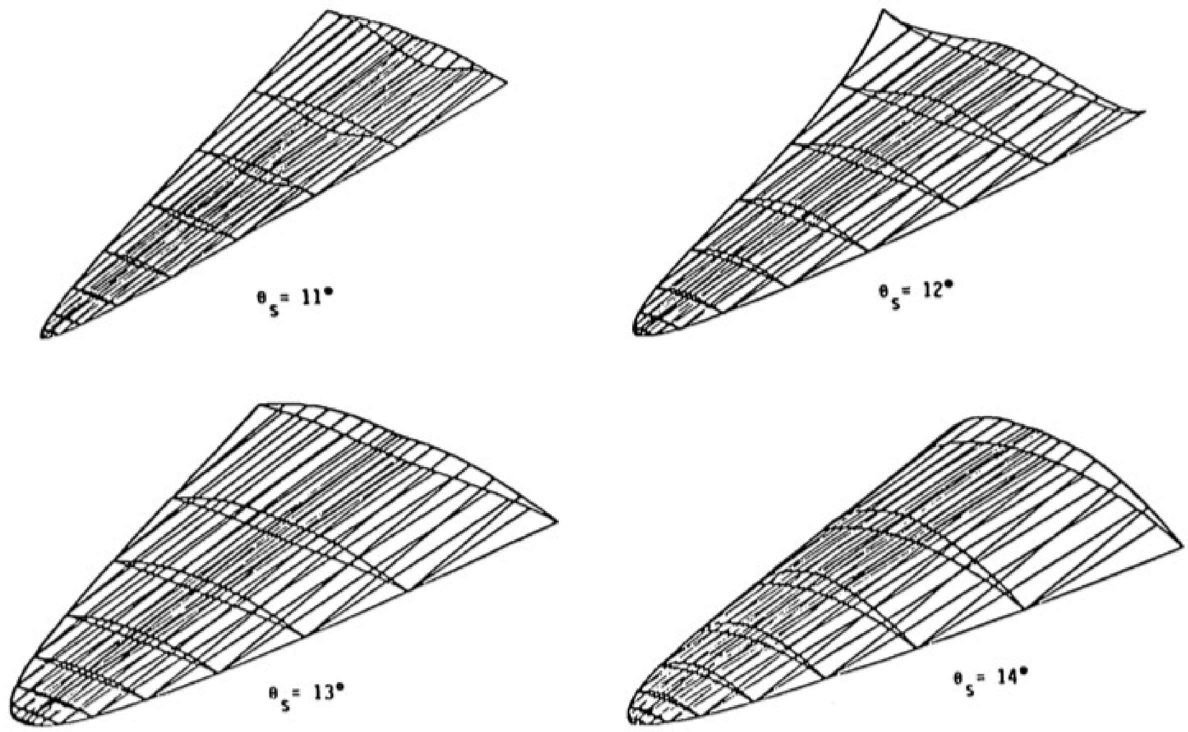

Figure 3. Hypersonic waveriders optimized for Mach 6 at varying shock cone angles [5]

2.3. Computational Fluid Dynamics (CFD)

Once the shape is defined (shock cone angle, wedge, etc) and Mach value chosen, the Taylor-Macoll equation can be used to model the flow field behind the shock. Once the shape has defined for the chosen conditions, multiple methods can be used to solve computationally the flow. Such methods such as the marching grid and Euler equations can be solved if you have the time or patience, while such programs as ESI, F3D, and Fluent can use their own methods to solve for the chosen conditions [6]. One example is a CFD solution of a wedge cone waverider conducted by Takashima and Lewis where they defined the flow field (a wedge cone), and the mach speed and before optimizing it, created a pressure contour to find the shock location so that the shock wave can be attached to the leading edge [7]. The wave-cone waverider can be seen in Figure 4 while the pressure contour can be seen in Figure 5.

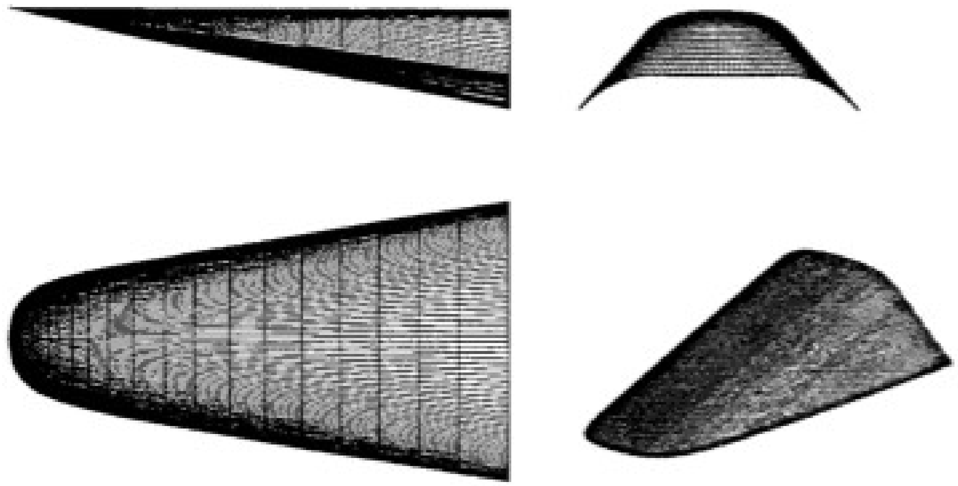

Figure 4. Wedge-cone hypersonic waverider [7]

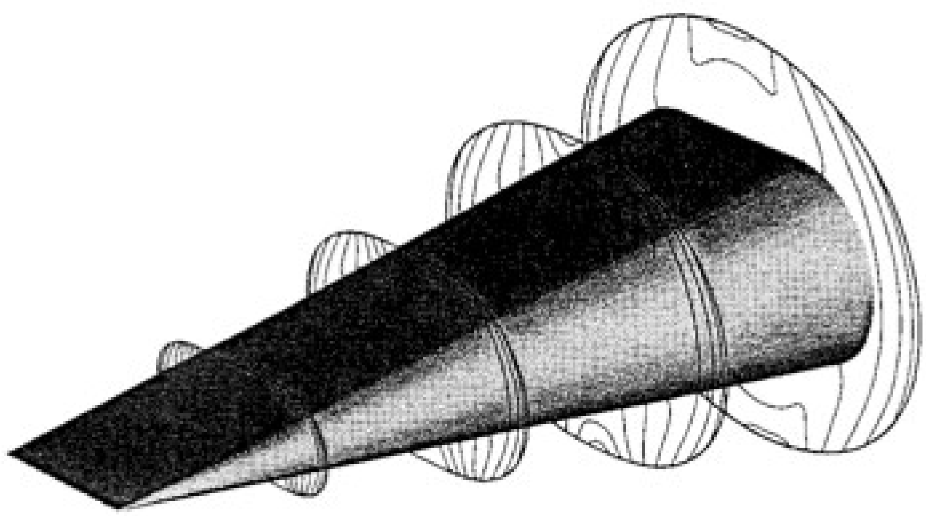

Figure 5. Wedge-cone pressure contours [7]

3. Hypersonic Vehicles

Though the hypersonic waverider was not initially used despite the concept in the late 1950's, other hypersonic re-entry vehicles have been theorized, developed, tested, and flown.

Though some do not have a high lift-to-drag ratio, it is important to study these vehicles. Using the information from these flights and tests, the hypersonic research has advanced information enough to bring the hypersonic waverider back into a reality.

3.1 Saenger Bomber/Glider

The Saenger bomber/glider (Figure 6) was developed in the 1940's by the Nazi's during World War II in order to reach the Glasgow shipyards or even the United States. The bombers and V-2 rockets of the time could not traverse the distance to Glasgow and thus the Allied Forces used the city to build ships, making Glasgow a prime target for this gliding rocket bomber. This vast distance would have been covered by skipping along the top of the atmosphere during re-entry and could then return after delivering the explosive payload.

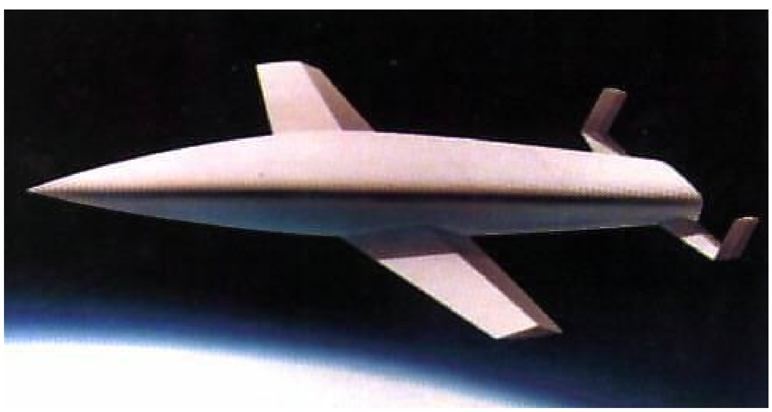

Figure 6. Saenger Bomber/Glider [8]

The Saenger Bomber/Glider was to be 28 m long, had a 15 m wingspan, and would have a gross mass of 133,773 kg. During the orbital boost and atmospheric travel phases when the Saenger would be traveling at hypersonic speeds, the Saenger design would have an impressive lift-to-drag ratio of 6.4 and during subsonic travel it would have an L/D of 7.5. This is an impressive feat for many hypersonic vehicles for many do not have such a high L/D value, as seen later with the X-20 Dyna-Soar and Langley HL20. While the Saenger Bomber/Glider design was never built and therefore cannot be authenticated, the proposal did help lead to the design of the Dyna-Soar Project for the United States [8].

3.2 X-20A Dyna-Soar

From the 1950's to the early 1960's the United States embarked on a project to build a manned spaceplane and the result was the X-20A Dyna-Soar (Dynamic Soarer) (Figure 7). The X-20A was originally designed to be an orbital bomber designed and built by Boeing. However, over the course of its lifespan the spaceplane's objective changed multiple times becoming a hypersonic test vehicle at one point and reconnaissance platform at another. In order to reach orbit, the X-20A would be launched on top of a rocket, replacing the rockets nose cone. The design-induced complications during ascent came from the natural lifting body of the X-20A, which would force the rocket off course unless large thrusters were installed on the rockets. One particular idea to solve this issue was to use large fins on the body of the boosting rocket. However the project was cancelled in 1963, so the X-20A Dyna-Soar would never be launched.

Figure 7. X-20A Dyna-Soar [9]

Based off the Saenger bomber/glider, the X-20A would also “skip” off the atmosphere and allow it to travel vast distances before landing. The X-20A Dyna-Soar would be 10.78 m long, have a 6.34 m wingspan where the delta wing was at 72.48°, and had an empty mass of 7,435 kg. At hypersonic speeds the X-20A would have a much smaller L/D ratio than the Saenger bomber/glider, only a value of 0.8 to 1.9. Though the X-20A Dyna-Soar was cancelled, the research into such a craft helped develop high temperature materials and even helped with the development of the Space Shuttle [9].

3.3 Langley HL-20

In 1986 the Space Shuttle experienced a setback with the destruction of the Challenger, and NASA started looking for new ways to replace the Space Shuttle in case the project was abandoned or permanently grounded. One such vehicle design that came to light was the Langley HL-20 (Figure 8) manned spaceplane. Based off of the Soviet BOR-4 design (the BOR-4 is discussed in section 3.7), the HL-20 would have the capability to land horizontally on a runway with a lower build and operational cost while maintaining a high flight safety rating.

Figure 8. Langley HL-20 [10]

The main intention of the HL-20 in particular was to be a Crew Emergency Rescue Vehicle (CERV) of the International Space Station (ISS). However, during the selection process for the ISS CERV, it was decided that the Soyuz Capsule would be used instead of developing the HL-20 and taking on the costs associated with development. The HL-20 was to be 8.84 m long, have a wingspan of 7.16 m, and a gross mass of 10,884 kg. During the hypersonic re-entry, the L/D of the HL-20 would be between 0.75 and 1.0, much less than both the Saenger bomber/glider and the X-20A Dyna-Soar (though the HL-20 would have only been used as a CERV and thus the L/D would not need to be high) [10].

3.4 X-38

As stated previously, when the ISS was built the Soyuz Capsule was chosen as the lifeboat over the HL-20. However, when the ISS crew size was to increase to 6 permanent members, a new lifeboat that could hold more people was needed and the suggestion was the X-38. The X-38 (Figure 9) was based off of the Spacewedge program and would use the landing technology already developed. Unlike other hypersonic vehicles, the X-38 was always intended for use as a Crew Return Vehicle (CRV). Though the X-38 was designed with Commercial Off-The-Shelf (COTS) parts and was fairly cheap in the grand scheme (a half million for the X-38 prototype and four vehicles), the project was still cancelled in 1999.

Figure 9. X-38 [11]

The X-38 did undergo drop tests from a B-52 approximately 15 km above the surface where the ram-air parafoil directed the unmanned test aircraft to a safe and accurate landing at NASA Dryden. There were three different drops from around the same altitude that were successful but before a higher drop test could be conducted the project was cancelled. The X-38 was 7.31 m long, had a 4.42 m wingspan, and a gross mass of 8,163 kg. While the X-38 was a lifting body, the L/D is not known [11].

3.5 X-37

The X-37 (Figure 10) is a joint project operated by NASA and the US Department of Defense in order to create a reusable maneuverable spaceplane. The X-37 is particularly designed to test the aerodynamic controls and the ability to fly at variable speeds. Like the X-38, the X-37 undertook five different drop tests from a B-52 at 12 km, which verified the autonomous landing as well as other X-37 specific tasks. The X-37 has launched multiple times and orbited the earth.

Figure 10. X-37 [12]

The X-37 has been shrouded in secrecy due to the Department of Defense, so the particular objectives of the flights are not currently known. The X-37 is 8.9 m long, has a 4.57 wingspan, and a gross mass of 3,200 kg. Like the Space Shuttle, the X-37 has a L/D of about 1 at hypersonic speeds during re-entry [12].

3.6 Hermes

Hermes (Figure 11) was developed to be a French manned spaceplane for independent European space access during the 1980's and early 1990's. At the time, Hermes would have pushed France/Europe into the record books as the third country to accomplish a manned spaceflight behind Russia and the United States. France initially funded the Hermes program, but Germany became a financial contributor once the large cost of the project was realized. For the Hermes to reach orbit, it was to sit atop an Ariane-5 rocket, which required heavy modification for such a spaceplane. This ran up the cost of the project even more, and with the design of the Hermes spaceplane being heavier than expected, the project was cancelled in 2002.

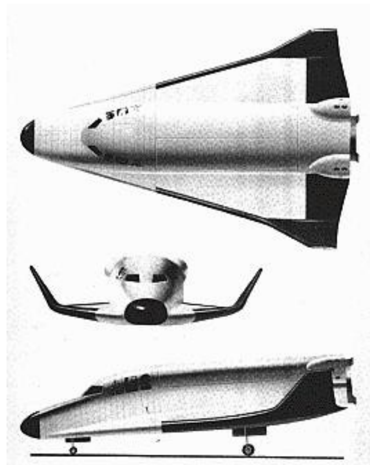

Figure 11. Hermes [13]

The Hermes was similar to the HL-20, and although they put a couple of years into this project, there are not many dimensions available. The gross mass of the Hermes was to be around 23,000 kg and could sit three astronauts. They concentrated heavily on a crew evacuation system (after the challenger accident), thus increased the vehicle weight and decreased the number of astronauts that it could transport. There is no listed L/D for this spaceplane [13].

3.7 Bor-4

The Bor-4 (Figure 12) was the successor to the Bor-1, -2, and -3. This particular model was an unmanned lifting body that deployed at high altitudes and reached Mach 25 during descent before crashing into a large body of water to be retrieved by the Soviet Space Program. The Bor-4 was a vital step in the design and development of a heat shield for the Buran [14]. The Bor-4 was launched four different times and it was from reconnaissance photos of an ocean recovery that the United States knew the approximate size and weight of the Bor-4 for the design of the Langley HL-20 [10].

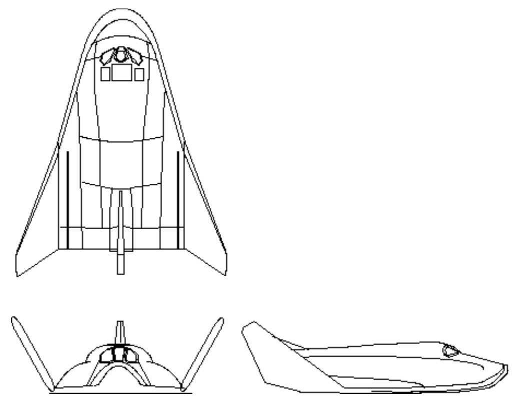

Figure 12. Bor-4 [14]

The Bor-4 was built at 3.859 m long and had a wingspan of 2.8 m. Before the spacecraft began the descent, it weighed 1,450 kg in orbit but would splashdown at 795 kg. The two outer wings are adjustable in order to maximize stability during re-entry. The L/D of the Bor-4 is unknown, but it should be similar to the HL-20 for they are both of similar design. The Bor-4 was a success and validated the new heat shields for the Buran, but a Bor-5 was created for a more accurate aerodynamic profile of the Buran [15].

3.8 ASSET

The Aerothermodynamic Elastic Structural Systems Environmental Test (ASSET) was originally part of the Dyna-Soar project (see Section 3.2). After the Dyna-Soar project was cancelled, the ASSET and the X-23 PRIME went to the United States Air Force under the START project. The ASSET, as seen in Figure 13, was originally designed to test the heat shield of the X-20 Dyna-Soar for it is the same shape as the nose cone section. The ASSET was launched atop of leftover Thor and Thor-Delta missiles and landed in the ocean. There was a total of six launches between 1963 and 1965. Only one ASSET test plane could be recovered, as the rest sank into the ocean.

Figure 13. ASSET [16]

During re-entry, ASSET reached speeds of Mach 25 and had a L/D of 1 at hypersonic speeds. The ASSET was only 1.75 m long, and had two small delta wings with a wingspan of 1.53 m. As such a small test vehicle, it only had a gross mass of 540 kg. Though under the Air Force, the ASSET was able to contribute re-entry data and heat shield experiments to the space shuttle program [16].

3.9 X-23 PRIME

The X-23 PRIME (Precision Recovery Including Maneuvering Entry) was part of the Dyna-Soar project in conjunction with the ASSET. The X-23 PRIME (Figure 14) focused on the maneuvering aspect of the Dyna-Soar project, where as the ASSET was focused on the structural aspect. The X-23 PRIME had spray on ablative heat shields and bears a close resemblance to the X-20 Dyna-Soar. Launched atop Atlas missiles for three different tests, only one X-23 PRIME was recoverable. The other two tests experienced parachute troubles and crashed into the ocean where they could not be recovered.

Figure 14. X-23 PRIME [17]

Like the ASSET, the X-23 PRIME had a lift to drag ratio of 1 at hypersonic speeds. The test vehicle was 2.07 m long, had a wingspan of 1.16 m, and had a gross mass of 405 kg. Though the X-23 PRIME and ASSET were part of a cancelled project, they both made great strides towards hypersonic re-entry vehicles and the development of spaceplanes [17].

3.10 M2-F1

The M2-F1 was a NASA project for a manned lifting body aircraft. The subsonic craft was towed behind a 1963 Pontiac Convertible initially until they could manage sustained flight, and later behind a C-47 airplane. The M2-F1 (Figure 15) had a maximum speed of 150 mph and fell at 4,000 feet per minute during testing from the C-47 [18]. The M2-F1 was 6.1 m long, had a 4.32 m wingspan, and had an empty mass of 454 kg. The M2-F1 retired in 1966 with 77 air-towed flights and in the vicinity of 400 car-towed flights [19].

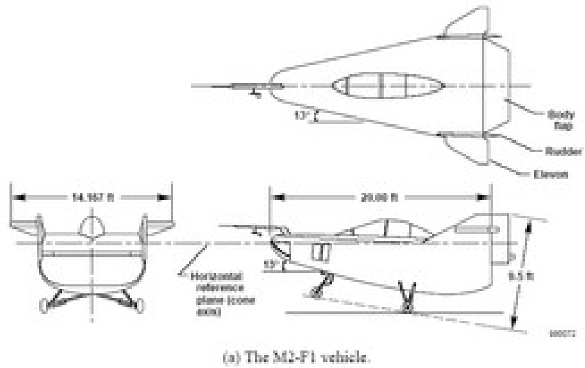

Figure 15. M2-F1 [18]

3.11 M1-L Half Cone

The M1-L Half Cone was proposed in 1962 with the M2-F1 and the Langley Lenticular. The M1-L Half Cone had a 40° half cone (much wider than the 13° M2-F1) and an inflatable rubber tail that would boost the L/D value during landing. The M1-L Half Cone is the center craft in Figure 16 [19]. The size and characteristics of the M1-L Half Cone are not known for it was never fully developed.

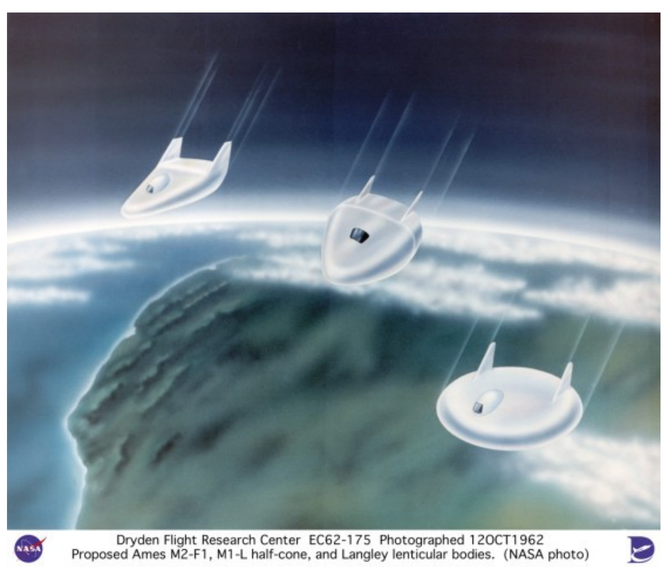

Figure 16. M1-L Half Cone (Middle) [19]

3.12 Langley Lenticular

The Langley Lenticular (Figure 17), known also as the Kehlet Lenticular, was proposed and studied in the early 1960's with nothing much coming out of the project. It was shaped like a saucer but with fixed wings for atmospheric maneuverability. The thick underbelly and shape gave the Langley Lenticular the ability to reduce the structural mass required for heat shields and landing gear, for the large belly would be able to skid across rough terrain during landing without severely damaging the spacecraft. The wings would be able to contract during re-entry and would expand for the landing [20]. The size and characteristics of the Langley Lenticular are not known for the spacecraft was never fully developed for it was cancelled within a year of the study.

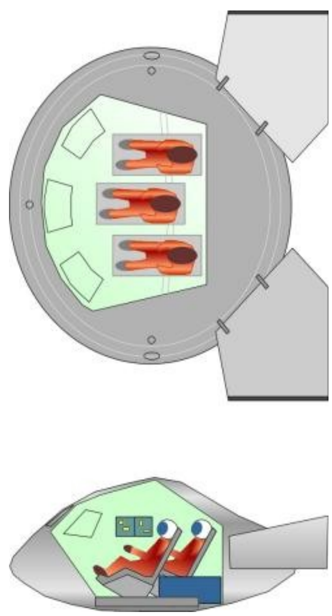

Figure 17. Langley Lenticular [20]

3.13 SHARP

The Slender Hypervelocity Aerothermodynamic Research Probe (SHARP) is designed to test materials in true conditions owing to a sharp leading edge. The project was started by NASA

Ames Research Center and had contributions from Santa Clara University and Montana State University [21]. The SHARP (Figure 18) has not been launched, and there is no data available.

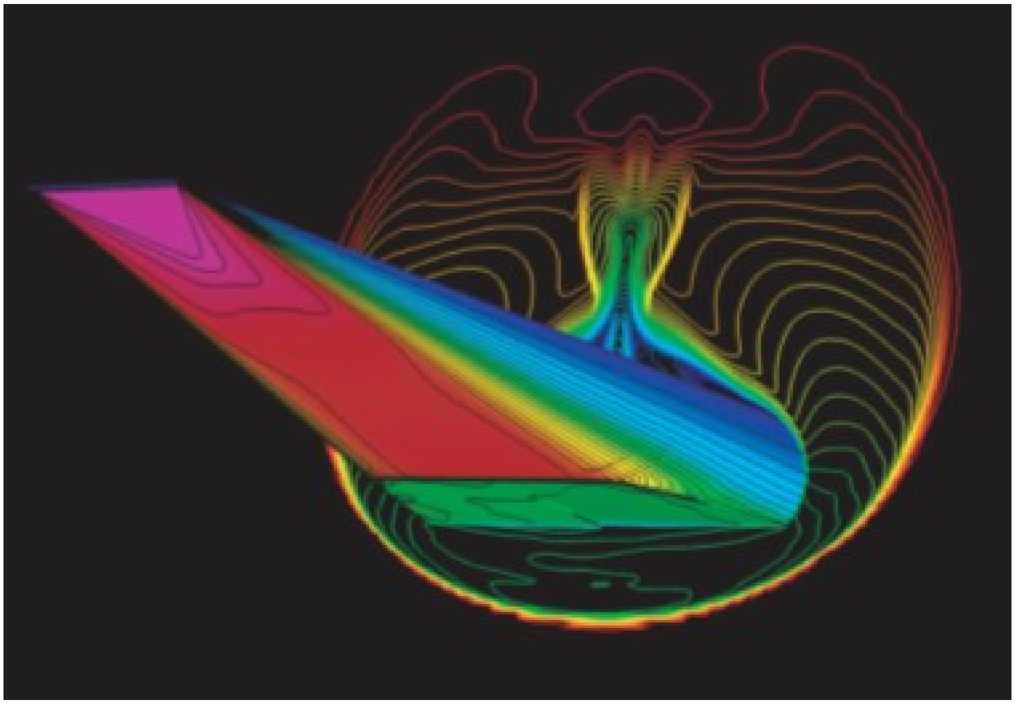

Figure 18. SHARP [21]

4. Design Process of a Hypersonic Waverider

In the technical paper by John D. Anderson [22], a step-by-step approach to creating and designing a hypersonic waverider is given. The following sections are the summery of that process.

4.1 Generate Inviscid Flowfield

The first step in creating a hypersonic waverider is to define the flowfield for which the waverider is based off of. The inviscid flowfield is created using simple shapes such as the wedge or cone as a base and then modifying them to fit the flight conditions and desired performance capabilities. Within this paper by Anderson there are two different approaches, one that uses a conical flowfield and the other that uses a general axisymmetric flowfield.

4.1.1 Conical Flow

When generating a flowfield for conical bodies, as most hypersonic waveriders are conical, the Taylor-Maccoll equation is used. This is an ordinary differential equation that is solved with the fourth-order Runge-Kutta Method and is shown in Eqn. 1 where V_r is the flow velocity along the conical body ray, θ is the angle of the ray (in reference to the cone's axis), and γ is the ratio of specific heat.

$$\frac{\gamma-1}{2}\left[1-V_r^2-\left(\frac{dV_r}{d\theta}\right)^2\right]\left[2V_r+\frac{dV_r}{d\theta}\cot\theta+\frac{d^2V_r}{d\theta^2}\right]-\frac{dV_r}{d\theta}\left[V_r\frac{dV_r}{d\theta}+\frac{dV_r}{d\theta}+\frac{dV_r}{d\theta}\frac{d^2V_r}{d\theta^2}\right]=0 \qquad \text{Eqn 1.}$$

4.1.2 General Axisymmetric Flowfield

In generating a flowfield for axisymmetric bodies such as a wedge, the Euler equations are used as seen in Eqn. 2 where Eqn. 3, Eqn. 4, and Eqn. 5 define G, E, and H respectively. In Eqn. 3 through Eqn. 5 ρ is the density, ω is the z-component of the flow velocity, υ is the transverse component of the flow velocity and p is the pressure.

$$\frac{\partial G}{\partial z}=-\frac{\partial E}{\partial r}-H \qquad \text{Eqn. 2}$$

$$G=\begin{bmatrix}\rho\omega \\ p+\rho\omega^2 \\ \rho\upsilon\omega\end{bmatrix} \qquad \text{Eqn. 3}$$

$$E=\begin{bmatrix}\rho\upsilon \\ \rho\upsilon\omega \\ p+\rho\upsilon^2\end{bmatrix} \qquad \text{Eqn. 4}$$

$$H = \begin{bmatrix} \rho\upsilon \\ \rho\upsilon\omega \\ \rho\upsilon^2 \end{bmatrix} \qquad \text{Eqn. 5}$$

In order to solve Eqn. 2 through Eqn. 5, a MacCormack scheme is used. This scheme is used in both the z (axial) and r (radial) directions with a step approach denoted by Δz. Δz is shown in Eqn. 6 where Δz is the increment in the z-direction, Δr is the distance in the r-direction, n is the grid point location in the z-direction whereas j is the grid point location for the radial direction, and C is a constant between 0 and 1. The nose tip, though part of an axisymmetric body, is still assumed to be conical and thus the θ is the angle of the ray in reference to the cone's axis still and α is the second angle of correction to resume the general axisymmetric flowfield.

$$\Delta z = C\frac{\Delta r}{\tan(\theta+\alpha)} \qquad \text{Eqn. 6}$$

Now that the incremental march defined, the Euler Equations (Eqn. 2 through Eqn. 5) can be applied where the solution of the flow is bounded by both the physical body and the shock wave produced. This produces the scheme that is shown in Eqn. 7 and Eqn. 8. Note that these equations use all the terms defined above.

$$G_j^{\overline{n+1}} = G_j^n - \frac{\Delta z}{\Delta r}\left(E_{j+1}^n - E_j^n\right) - \Delta z H_j^n \qquad \text{Eqn. 7}$$

$$G_j^{n+1} = \frac{1}{2}G_j^n + G_j^{\overline{n+1}} - \frac{\Delta z}{\Delta r}\left(E_j^{\overline{n+1}} - E_{j-1}^{\overline{n+1}}\right) - \Delta z H_j^{\overline{n+1}} \qquad \text{Eqn. 8}$$

4.2 Generate Leading Edge Shapes

Now that the flow field has been established for both the conical body and axisymmetric body, a waverider shape can be extrapolated from the flow. To illustrate this extrapolation,

Figure 19 shows the streamlines and how the leading edge follows the streamline and defines the lower surface of this particular waverider. The shape defining streamline goes from the leading edge of the shock wave off the flow generating body to the traveling edge of that same shockwave. Optimization of the leading edge takes place later in the process, but it is important to note that it is the flow conditions that you are designing this waverider for, not for an all-purpose body.

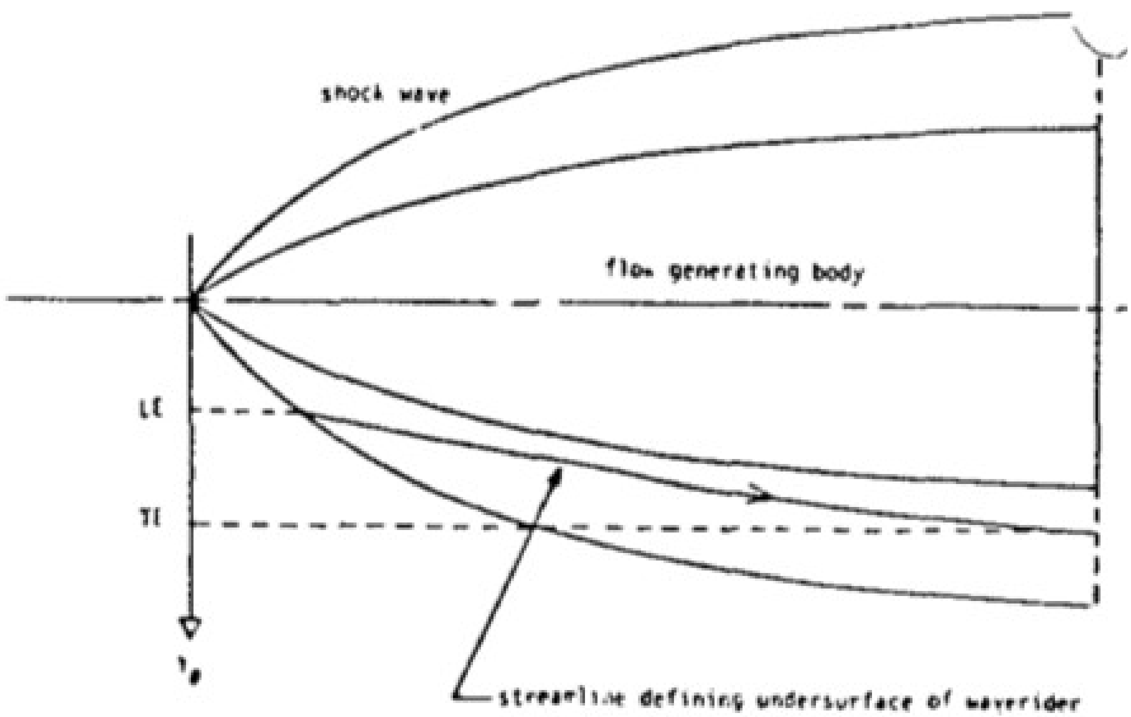

Figure 19. Leading Edge Cutting Streamline for Waverider Body [15]

4.3 Streamline Tracing

As seen from Figure 19, the streamline starts at the leading edge and pass through the known flowfield of the generated shockwave. In order to trace the streamline to define the lower and upper surface of the waverider, Eqn. 9 is used where ψ is the value of the streamfunction, j is still the grid point index in the radial direction, and $\dot{m}$ is the mass flow between j and j+1. This is done for both the lower and upper surface, but the upper surface has the freestream pressure (p_∞).

$$\psi_{j+1} = \psi_j + \dot{m} \qquad \text{Eqn. 9}$$

4.4 Skin Friction Calculation

When shaping a hypersonic waverider, it is important to take into account the skin friction. Some waveriders could be designed for maximum lift to drag with inviscid flow, but if they do not incorporate skin friction then they are worthless. In order to find the skin friction the Reynolds number needs to be calculated for the laminar and turbulent flow, as well as the reference temperature and the exponent of variation.

The Reynolds number of a flat plate for laminar flow can be seen in Eqn. 10 and for turbulent flow in Eqn. 11. In these two equations ρ_∞ is the freestream density, V_∞ is the freestream velocity, x is the distance from the leading edge of the plate, and μ_∞ is the freestream viscosity. For turbulent flow it is important to note that ρ' is the reference density for reference temperature T', as well as μ' is the reference viscosity.

$$\mathrm{Re}_x = \frac{\rho_\infty V_\infty x}{\mu_\infty} \qquad \text{Eqn. 10}$$

$$\mathrm{Re}'_x = \frac{\rho' V_\infty x}{\mu'} \qquad \text{Eqn. 11}$$

Now that the Reynolds numbers have been calculated, the reference temperature T' can be calculated with Eqn. 12. With the results of Eqn. 12, we can now calculate the exponential variation ϖ. For both equations, T_∞ is the freestream temperature, M_∞ is the freestream Mach number, and T_w is the wall temperature.

$$\left(\frac{T'}{T_\infty}\right) = 1 + 0.032 M_\infty^2 + 0.58\left(\frac{T_w}{T_\infty} - 1\right) \quad \text{Eqn. 12}$$

$$\left(\frac{\mu'}{\mu_\infty}\right) = \left(\frac{T'}{T_\infty}\right)^{\varpi} \quad \text{Eqn. 13}$$

From the results of Eqn. 10 through Eqn. 13, the skin friction for a flat plate can now be calculated. The skin friction (C_f) for a flat plate in laminar flow can be seen with Eqn. 14 where as the skin friction for a flat plate in turbulent flow can be seen with Eqn. 15.

$$C_f = 0.664 \frac{1}{\sqrt{\mathrm{Re}_x}} \left(\frac{T'}{T_\infty}\right)^{\frac{\varpi - 1}{2}} \quad \text{Eqn. 14}$$

$$C_f = \frac{0.0592}{\left(\mathrm{Re}_x'\right)^{0.2}} \quad \text{Eqn. 15}$$

Though this measurement form is simple in nature, the results obtained are typically within 10% of results from the complex integral boundary layer method.

4.5 Boundary Layer Transition

In order to find the boundary layer transition Reynolds number, you need to know the edge Mach number (M_e) and apply it to Eqn. 16. While finding the boundary layer transition point is not vital to the skin friction calculation, it is important to note for the overall design of the hypersonic waverider.

$$\log_{10} \mathrm{Re}_{x_t} = 6.421 e^{1.209 \times 10^{-4} M_e^{2.641}} \quad \text{Eqn. 16}$$

4.6. Aerodynamic Forces and Moments

In order to calculate the aerodynamic forces and moments for the hypersonic waverider, the shear stress and pressure need to be integrated over the entire surface of the waverider. This step is used to determine if the conditions are met for a set lift to drag value.

5. Proto-Waverider

5.1 Proto-Waverider Model

In order to study hypersonic waveriders, Marcus Murbach from NASA Ames Research Center lent an already built proto-waverider shape modeled after the SHARP in order to make a Computer Aided Design (CAD) model. The proto-waverider has a length of nearly three and a half feet, and at the widest point is just over 15.25 inches. This proto-waverider is made of metal that is two millimeters thick, and has an open component bay on top for instrumentation. Figures 20-24 are pictures of the proto-waverider that has been supplied and used for CAD modeling.

Figure 20. Isometric View of Proto-Waverider

Figure 21. Side View of Proto-Waverider

Figure 22. Front View of Proto-Waverider

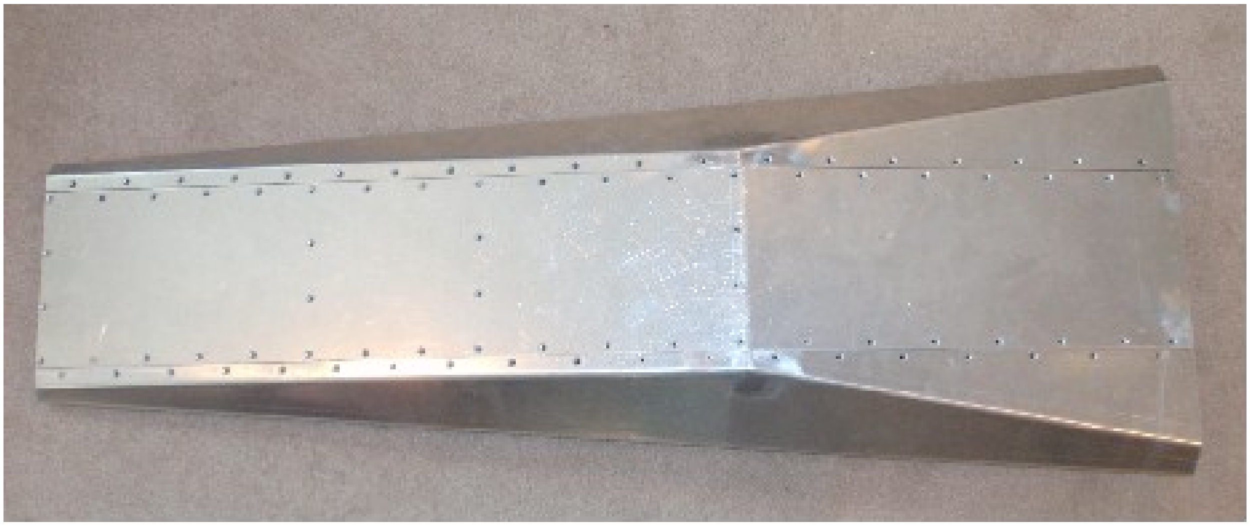

Figure 23. Bottom View of Proto-Waverider

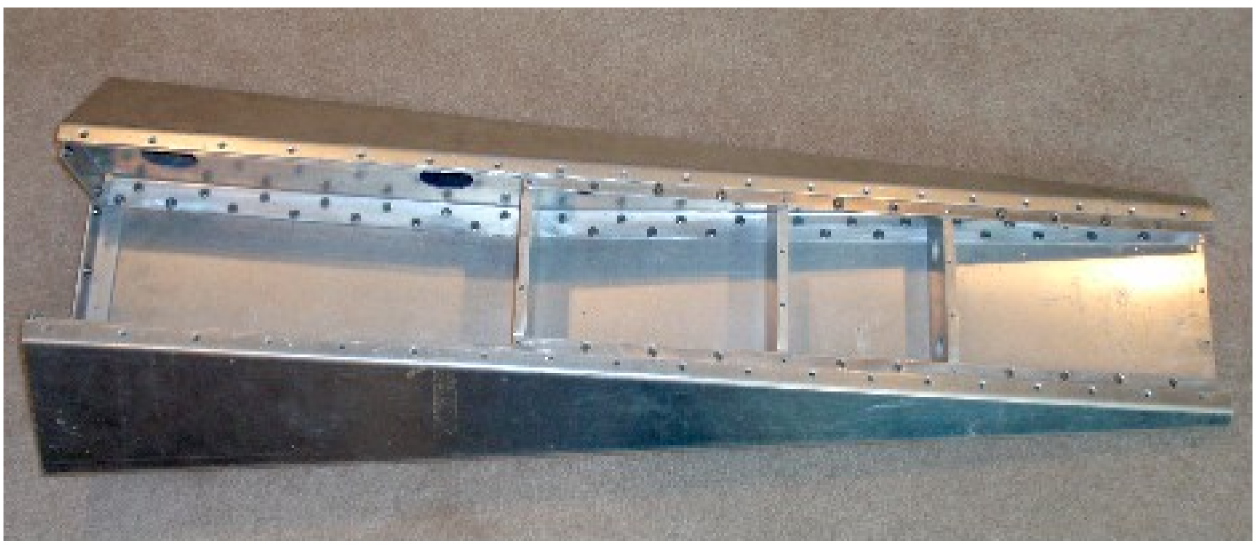

Figure 24. Top View of Proto-Waverider

5.2 CAD Model

Using the supplied proto-waverider model, dimensions were taken of each part of the waverider and inputted into SolidWorks (a CAD program). Some of the problems encountered with measuring the proto-waverider were with the sides of the waverider, for they were at angles and it affected the measurement process. Though multiple methods where used, the angles did contribute to errors within the CAD model. The proto-waverider also has rounded edges (as seen in Figure 23), and thus when measuring they made it difficult to find the true end of one part of the waverider and the beginning of the next part. The different sides were constructed with the measured dimensions, and the CAD assembly process was started.

5.2.1 Assembly Method

The CAD model original attempt was to be placed together via “mate” function. This method is illustrated in this section, as well as how the attempt turned out. Figure 25 illustrates that the sides and bottom flare piece of the proto-waverider were not measured correctly, for they pieces did not properly interact. Measurements were taken again but came up with the same results. Figure 26 shows that the stern of the proto-waverider is misshapen, or that the sides may be at an improper length. Figures 27, 28, and 29 show three views of the waverider; Figure 28 is missing part of the top as mating issues prevented the piece from joining the edges, as clearly seen in Figure 27. Figure 29 exemplifies that while the stern of the proto-waverider might be properly sized and assembled, the back is clearly not.

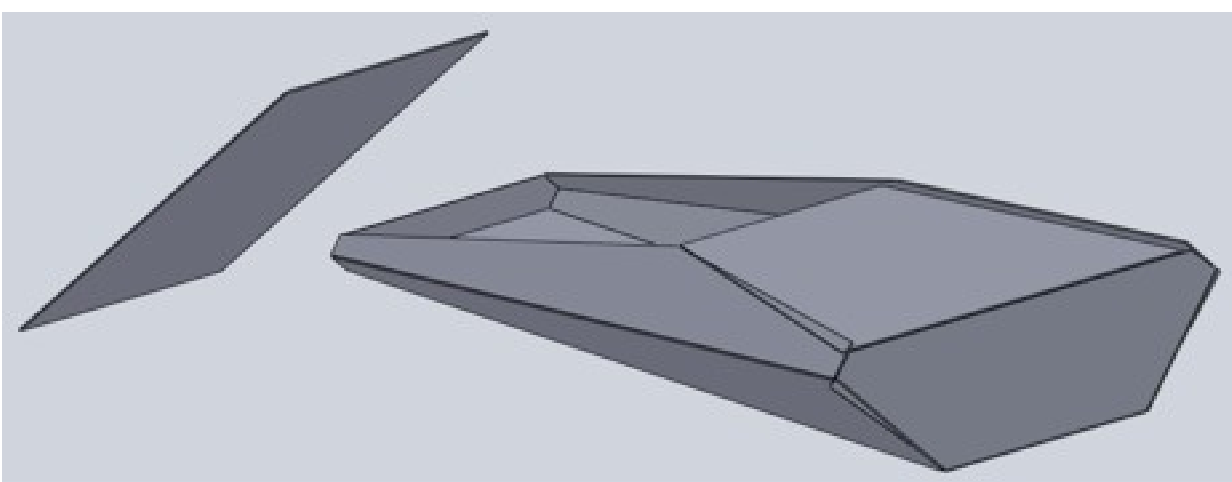

Figure 25. Proto-Waverider Model Assembly Attempt

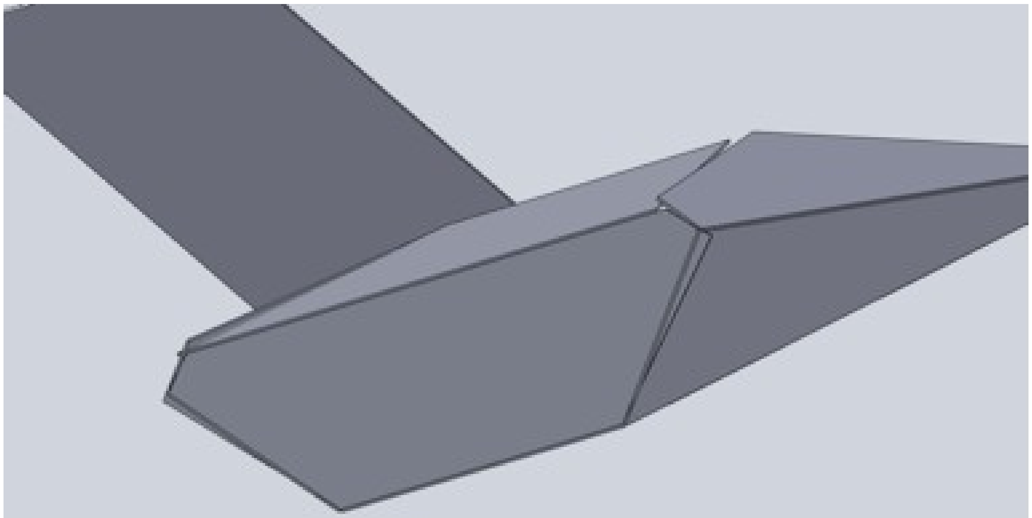

Figure 26. Proto-Waverider Stern Assembly Issue

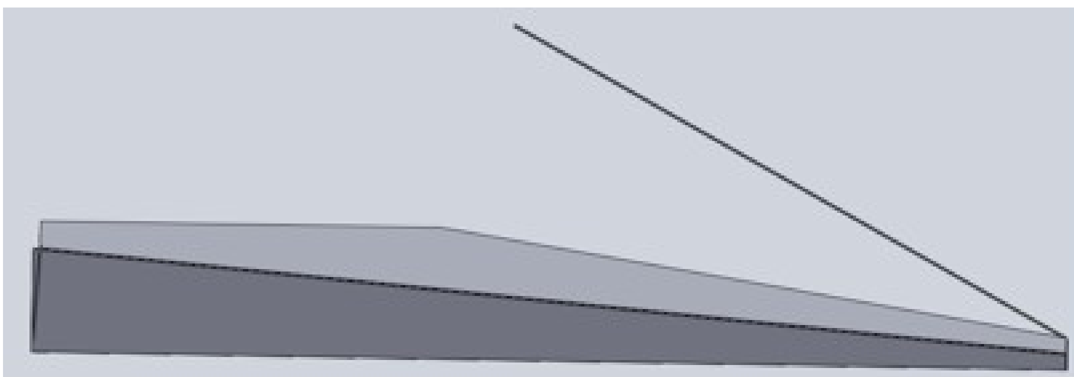

Figure 27. Side View of Proto-Waverider by Assembly Method

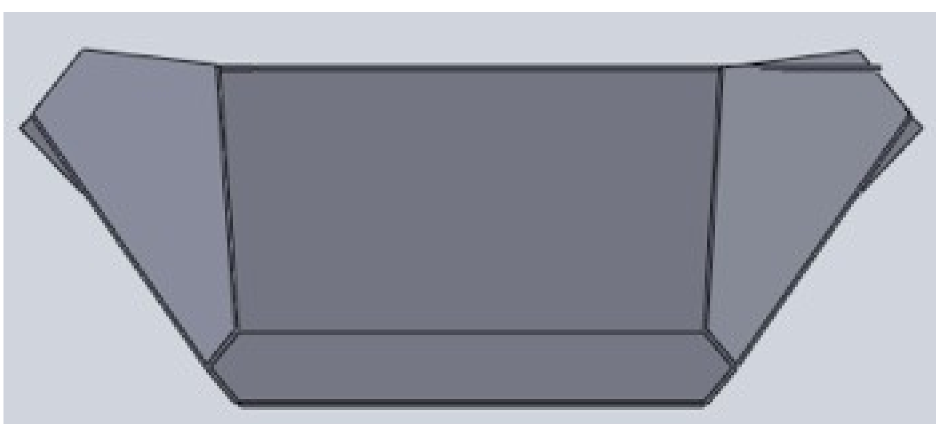

Figure 28. Front View of Proto-Waverider by Assembly Method

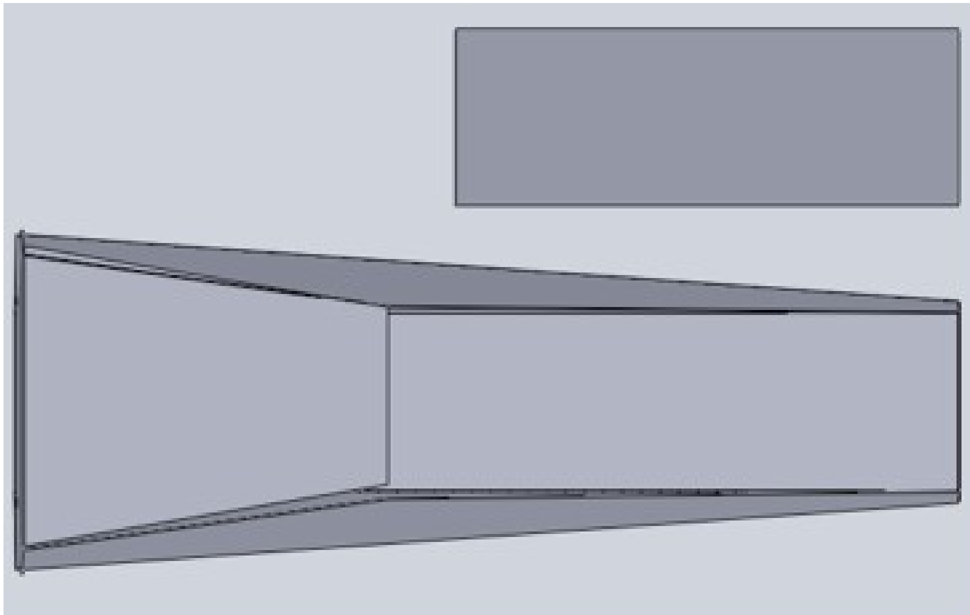

Figure 29. Bottom View of Proto-Waverider by Assembly Method

5.2.2 Loft Method

Confronted with the issues of a proto-waverider that could not seem to be assembled, a local skilled SolidWorks classmate, Andrew Muñoz, was able to help out and create a more accurate model. He utilized a “loft” method where the bow profile is first created then expanded out to the next profile face. This first loft took place from the bow to the point where the bottom of the proto-waverider flares outward, the second profile in this particular model. The second loft was from the initial point of the flare to the stern of the proto-waverider, the third profile. The results of the loft method can be seen in Figure 30 through Figure 35. The results clearly show that this is the proper method of assembly, and the waverider was re-measured with profiles in mind so that the loft method can be used.

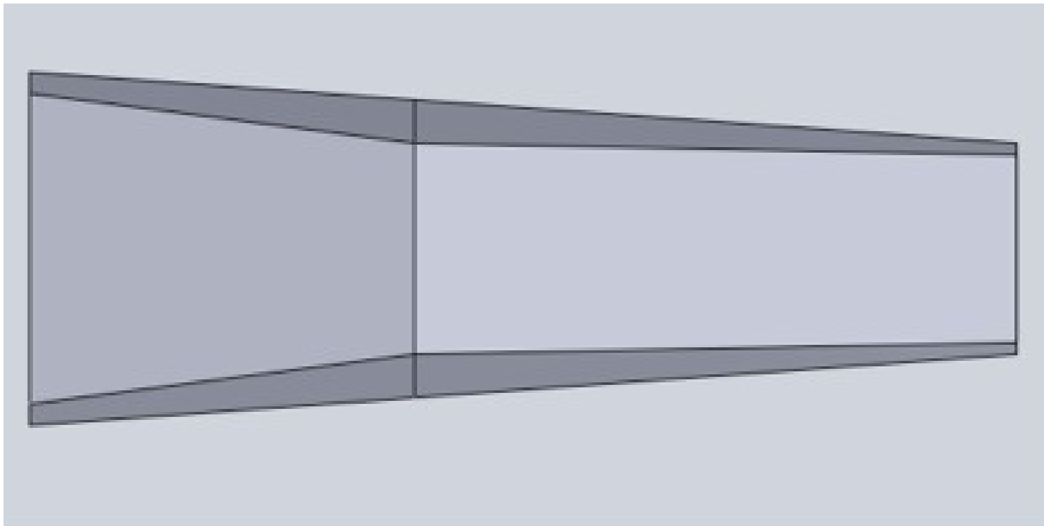

Figure 30. Bottom View of Proto-Waverider by Loft Method

Figure 31. Side View of Proto-Waverider by Loft Method

Figure 32. Bow View of Proto-Waverider by Loft Method

Figure 33. Stern View of Proto-Waverider by Loft Method

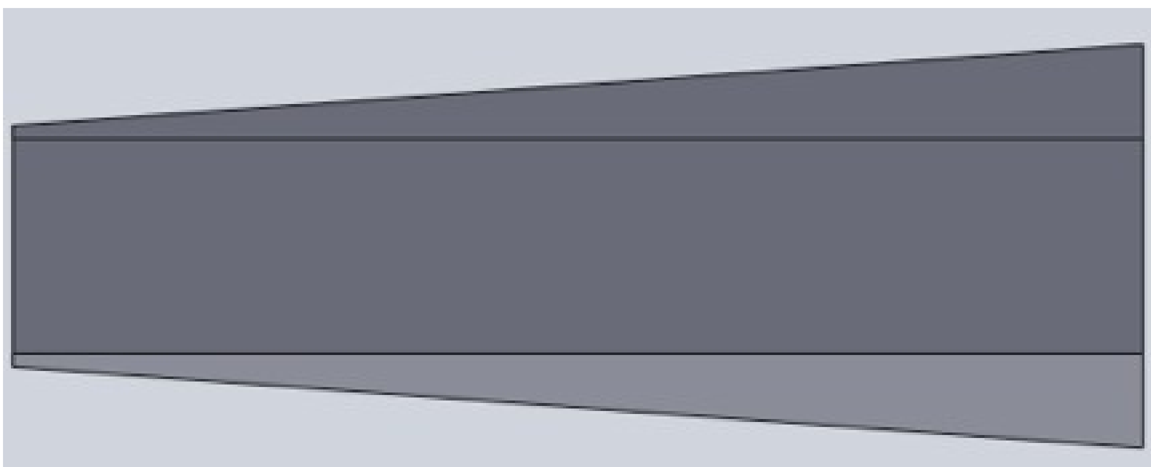

Figure 34. Top View of Proto-Waverider by Loft Method

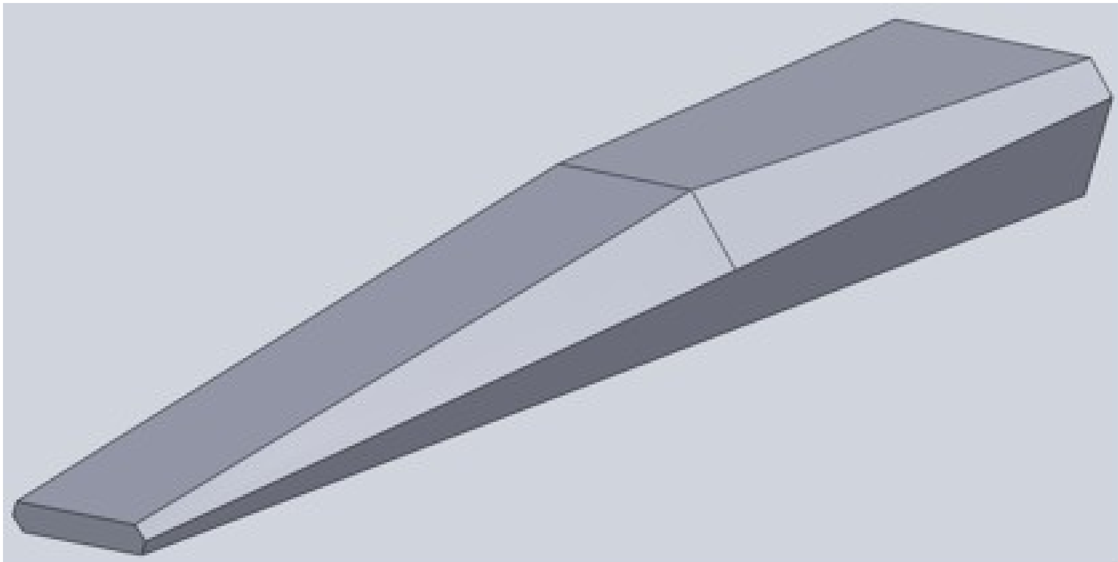

Figure 35. Isometric View of Proto-Waverider by Loft Method

It is important to note that the loft method profiles were not as exact, since this was secondhand information. It should also be observed that in Figure 33 the proto-waverider bottom body is above the stern, showing that the profile used was not exact for they should be flush.

5.2.2 Actual Waverider Model

After working with the above models, the proper CAD files were discovered in a misplaced external hard drive. It is important to note that the files showed the proper sizing for a nose cone that was not included in the other two versions. For use in Computational Fluid Dynamics, the nose was cut to a diameter of 0.271 inches then fillet was applied with a 0.100 inch radius leaving a 0.072 inch wide flat at the tip, large enough to properly mesh while small enough to keep a sharp enough edge during re-entry. The side edges have a fillet in order to reduce sharp edges that would have made computational modeling nearly impossible as well as closer representation to the physical proto-waverider. The isometric view of the proto-waverider can be seen in Figure 36, and the winged version can be seen in Figure 37. While no computational analysis will be conducted on the winged version, it is important to note what the future design will be once a proper modeling of the proto-waverider is completed.

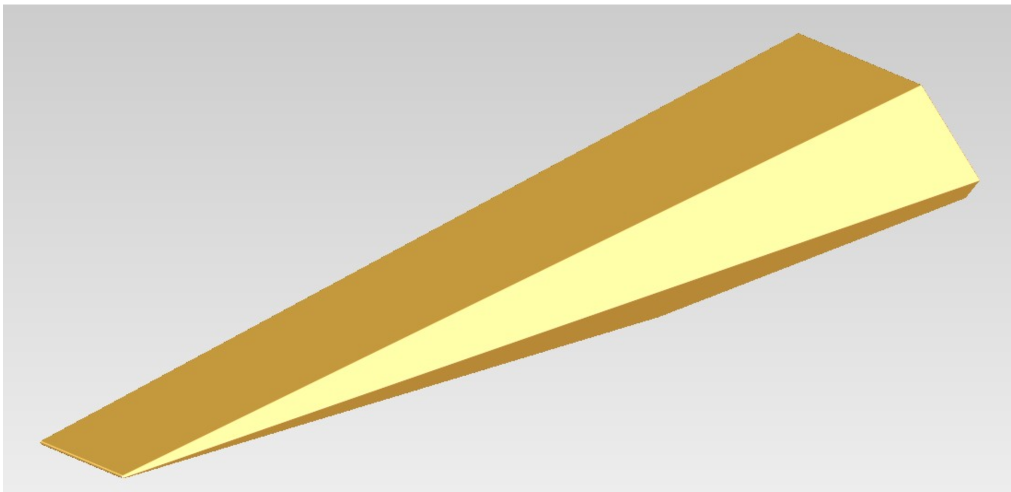

Figure 36. Isometric View of Proto-Waverider

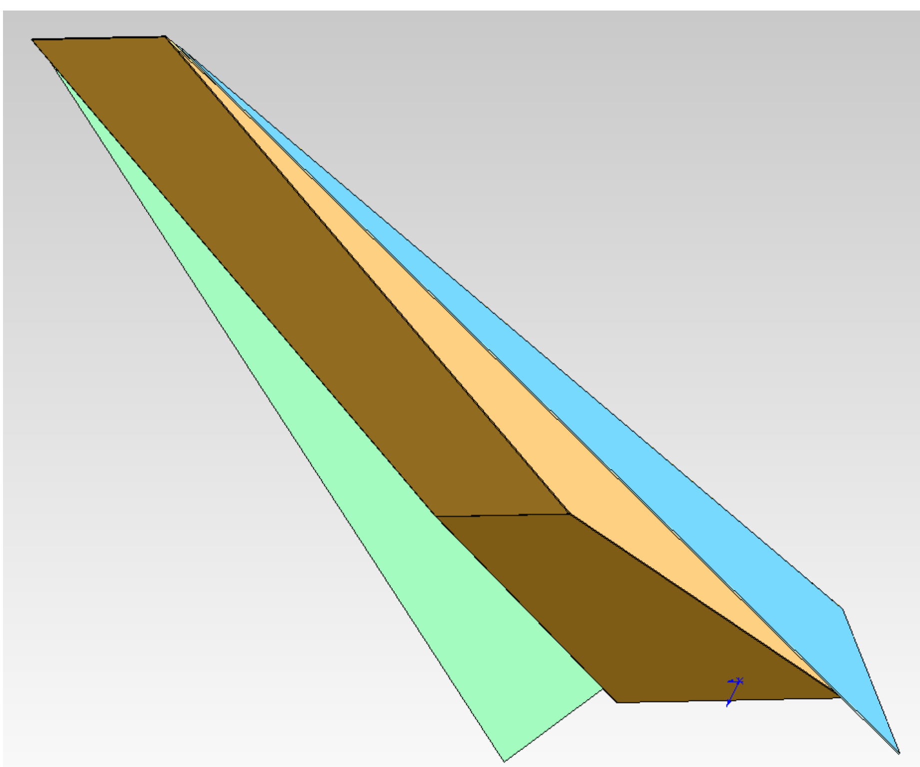

Figure 37. View of Winged Waverider

6. Hypersonic

While the hypersonic waverider utilizes an attached leading edge to catch and seal shock waves, calculation of such an interaction normally requires the use of Computational Fluid Dynamics (CFD) or a computer with plenty of time. The basic hypersonic conditions should not be ignored though. Shock waves, expansion fans, and theoretical calculations (such as Newtonian flow) are still vital for the development of hypersonic waveriders even though they cannot give the same degree of accuracy as CFD.

6.1 Hypersonic Shock Waves

A hypersonic shock wave is created when the flow has been re-directed back upon itself in any manner, whether by 0.1° or a full 90° wall as seen in Figure 38. When the flow has turned into itself, it creates a backpressure and the static shock wave forms where the flow undergoes changes in pressure, density, temperature, and speed. The shock wave is only about 10^{-5} cm thick, and although the shock technically is continuous, most calculations assume that they are discontinuous [23].

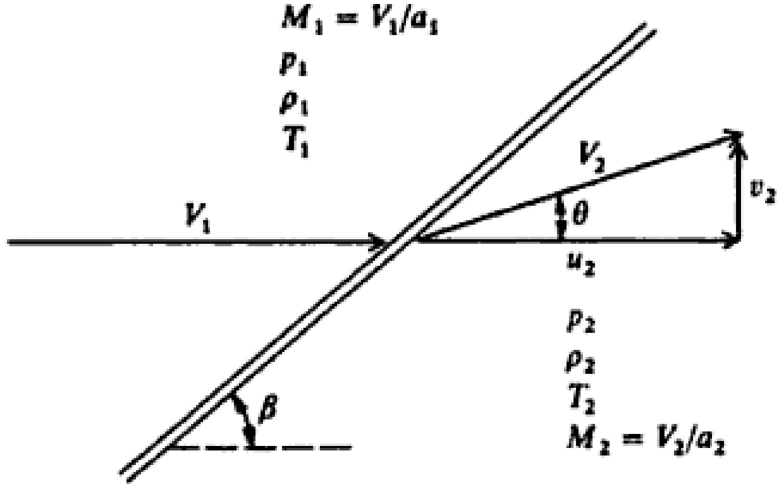

Figure 38. Oblique Shock Wave [23]

In order to calculate the conditions behind the shock wave, the following equations are used. Eqn. 17 defines the pressure ratio of the shock wave, while Eqn. 18 defines the density ratio. Eqn. 19 defines the temperature ratio across the shock, while Eqn. 20 defines the coefficient of pressure. Eqn. 21 and Eqn. 22 define the ratio in horizontal speed changes and the ratio of the vertical to horizontal speed respectively [23].

$$\frac{p_2}{p_1} = \frac{2\gamma}{\gamma+1} M_1^2 \sin^2 \beta \qquad \text{Eqn. 17}$$

$$\frac{\rho_2}{\rho_1} = \frac{\gamma+1}{\gamma-1} \qquad \text{Eqn. 18}$$

$$\frac{T_2}{T_1} = \frac{2\gamma(\gamma-1)}{(\gamma+1)^2} M_1^2 \sin^2 \beta \qquad \text{Eqn. 19}$$

$$C_p = \left(\frac{4}{\gamma+1}\right) \sin^2 \beta \qquad \text{Eqn. 20}$$

$$\frac{u_2}{V_1} = 1 - \frac{2\sin^2 \beta}{\gamma+1} \qquad \text{Eqn. 21}$$

$$\frac{\upsilon_2}{V_1} = \frac{\sin(2\beta)}{\gamma+1} \qquad \text{Eqn. 22}$$

In these equations, p is pressure, T is temperature, M is the mach number, β is the shock wave angle, θ is the incident angle of the impending body, ρ is the density, V is the velocity of the flow, u is the horizontal flow speed component, υ is the vertical flow speed component, and γ is the heat capacity ratio (1.4 for normal air) [23].

6.2 Hypersonic Expansion-Waves

Unlike shock waves, expansion waves occur when the flow has a chance to expand in a new direction and thus create an infinite number of Mach waves. The hypersonic expansion can be seen in Figure 39. It is possible to calculate the speed, incident angle, and pressure ratio by using the following equations in this section. Expansion will be prevalent in the hypersonic waverider [23].

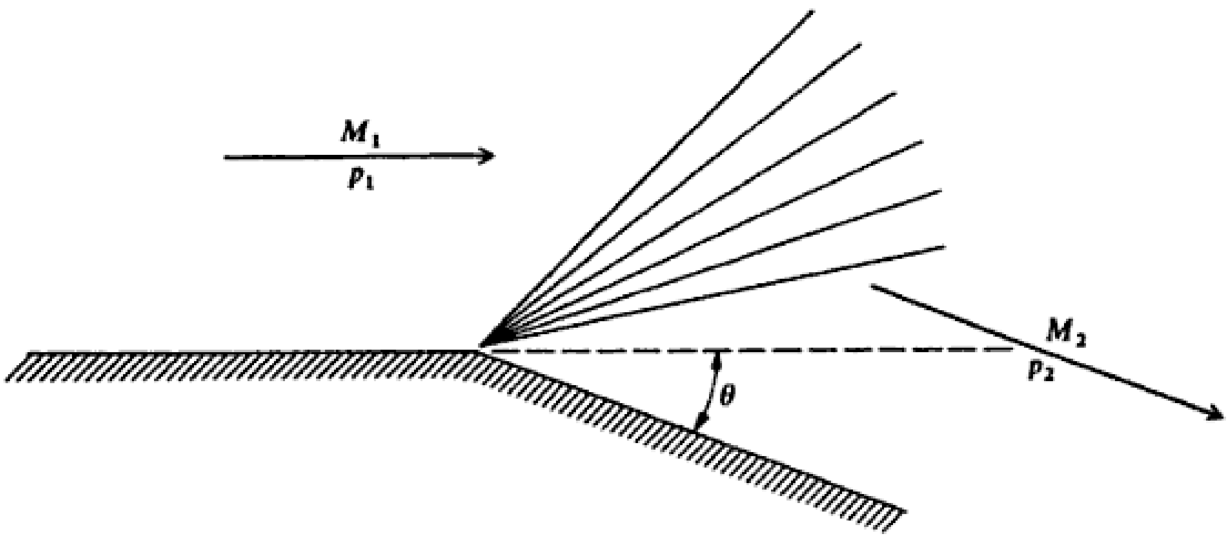

Figure 39. Centered Expansion Wave [23]

Eqn. 23 and Eqn. 24 can be used to find the incident angle of the expansion wave, while Eqn. 25 is the pressure differential. Eqn. 26 is the Prandtl-Meyer function. For the equations M is the mach number, p is the pressure, θ is the incident angle, ν is the Prandtl-Meyer function (based off Mach number), and γ is the heat capacity ratio [23].

$$\theta = \nu(M_2) - \nu(M_1) \qquad \text{Eqn. 23}$$

$$\theta = \frac{2}{\gamma - 1}\left(\frac{1}{M_1} - \frac{1}{M_2}\right) \qquad \text{Eqn. 24}$$

$$\frac{p_2}{p_1} = \left(1 - \frac{\gamma - 1}{2} M_1 \theta \right)^{\frac{2\gamma}{\gamma - 1}} \qquad \text{Eqn. 25}$$

$$\nu(M) = \sqrt{\frac{\gamma+1}{\gamma-1}} \left[\tan^{-1} \sqrt{\frac{\gamma-1}{\gamma+1}\left(M^2 - 1\right)} \right] - \tan^{-1} \sqrt{M^2 - 1} \qquad \text{Eqn. 26}$$

6.3 Proto-Waverider Calculations

In order to show the effect of the proto-waverider design, calculations were performed to the conditions set for in SOAREX IV- First Full Waverider Test by Marcus Murbach. Here the angle of attack α is listed at 10° while traveling at Mach 10. In Figure 40, the proto-waverider is set at a 10° angle of attack at Mach 10.

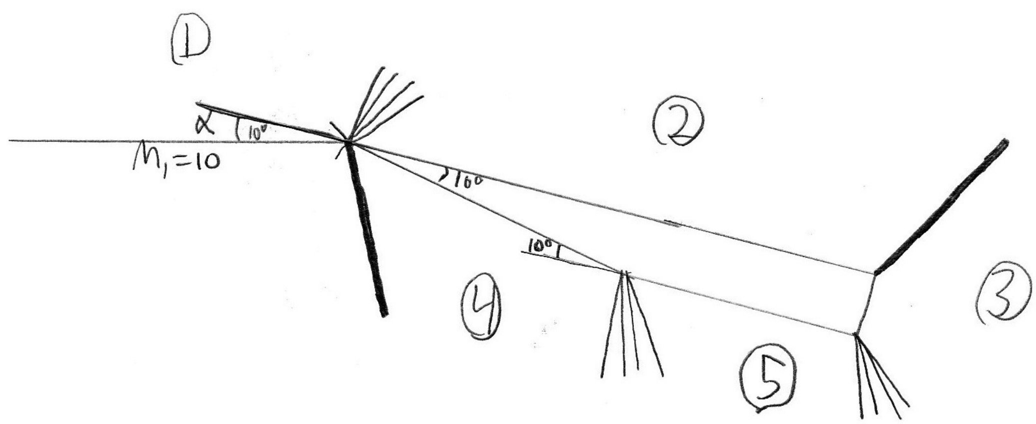

Figure 40. Proto-Waverider Diagram

From the CAD model, the half angle is 10° for the first angle near the bow, and 10° for the second angle where the proto-waverider flares. From Appendix A calculations, we find that the L/D for the proto-waverider is 2.88. From the SOAREX literature, the L/D value for the proto-waverider traveling at this speed should be 3.5, a difference of 17.8%. It is important to note that at this time, region 3 of Figure 40 could not be calculated for the flow coming off the top of the airfoil passes through a shock wave and interacts with the flow coming off an expansion wave from the bottom of the proto-waverider.

7. Proto-Waverider CFD Setup

As previously established in Section 5, a proto-waverider CAD model was eventually found. In order to reduce the fruitless and unnecessary information in this paper, the following sections will all use the supplied CAD model despite the amount of work that went into using the loft-model. Using this model, a CFD study can be performed on the attributes and the flow characteristics of the proto-waverider in its current form. In order to do this, the model needs to be imported from the CAD software to grid generating software, and then exported for use in a CFD solver. The first step is to set up the CAD for use in the grid generator. It should be noted that while the following approach is described, there are multitude of other methods, models, programs, and approaches that were used to try to analyze the proto-waverider. Those techniques attempted spanned two years and did not yield practical results, and thus will be left out of this paper.

7.1 Computer Aided Design Setup

In order to utilize a CFD solver, a grid must be created. Due to the complexity of the proto-waverider design, a grid generation program will be used. For this project, the grid generator will be Pointwise. Since the CFD solver chosen is a body mesh only, the proto-waverider does not have to be placed inside a box or have a domain created around it. A mesh of the body with clustering around key areas is all that is required.

7.2 Grid Generation

In order to create a grid, the file must be uploaded and domains set. The file originally starts off as seen in Figure 41. For the proto-waverider surface, an unstructured mesh of varying grid point dimensions needs to be created. The grid points along all edges of the proto-waverider are grid independent (multiples of eight), and the result can be seen in Figures 42, 43, 44, 45, and 46. Figure 47 is an enhanced view of the nose, where you can see the increased cell count for this important section of the proto-waverider.

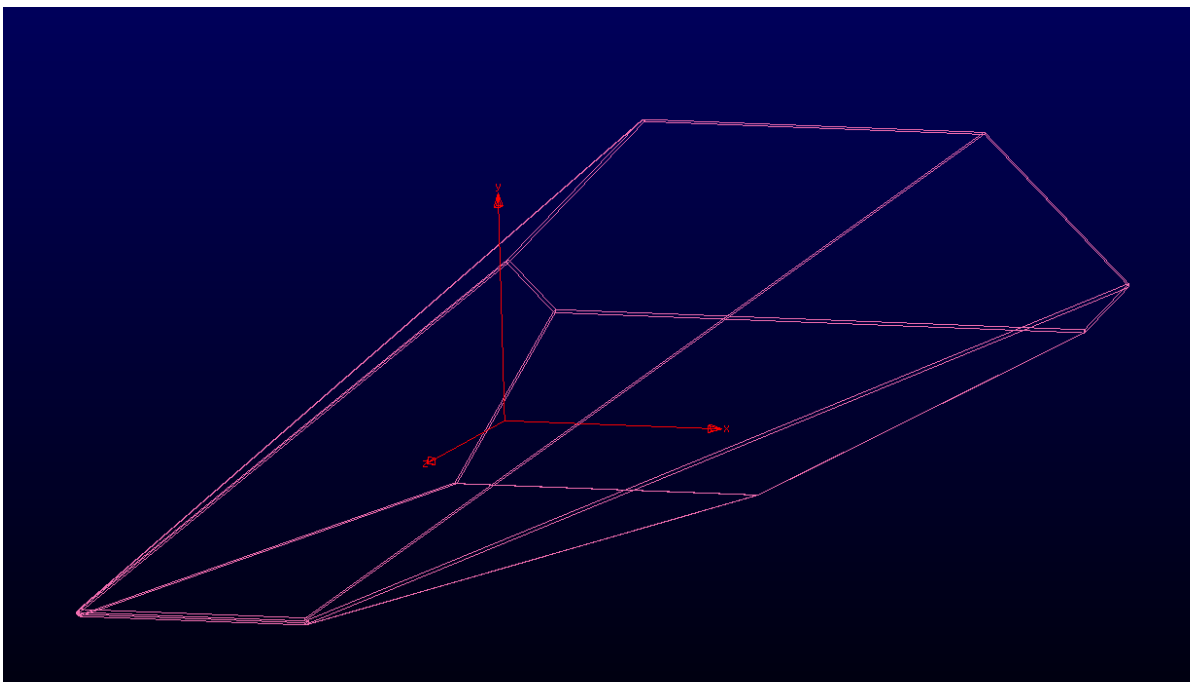

Figure 41. Proto-Waverider Before Mesh

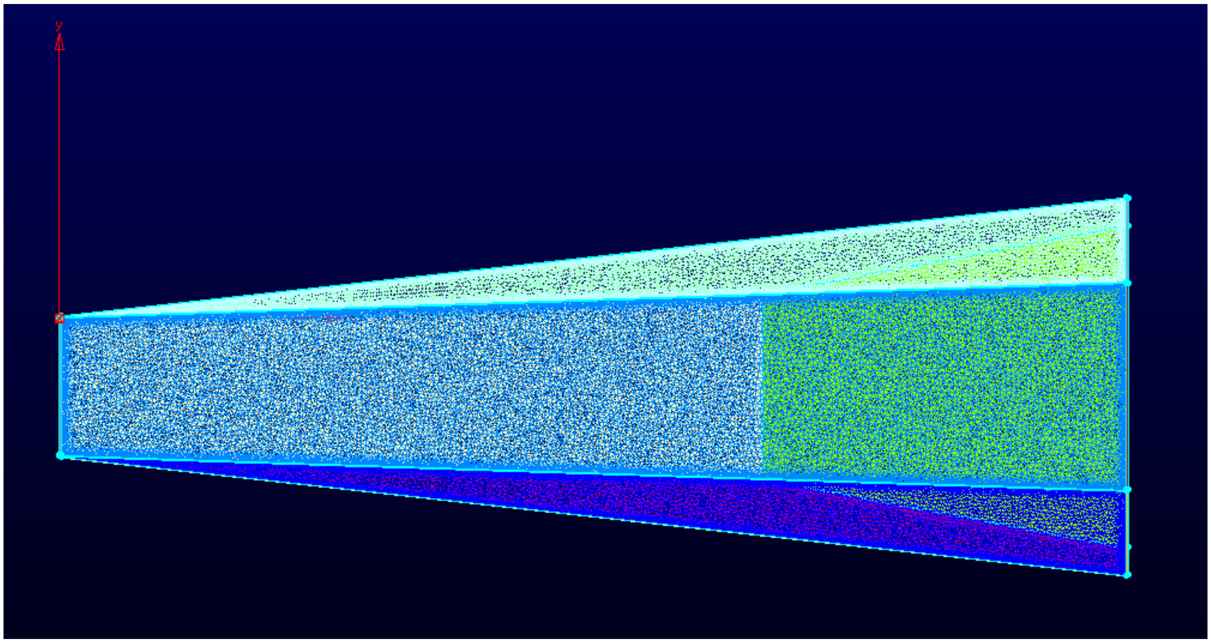

Figure 42. Top View of Waverider Mesh

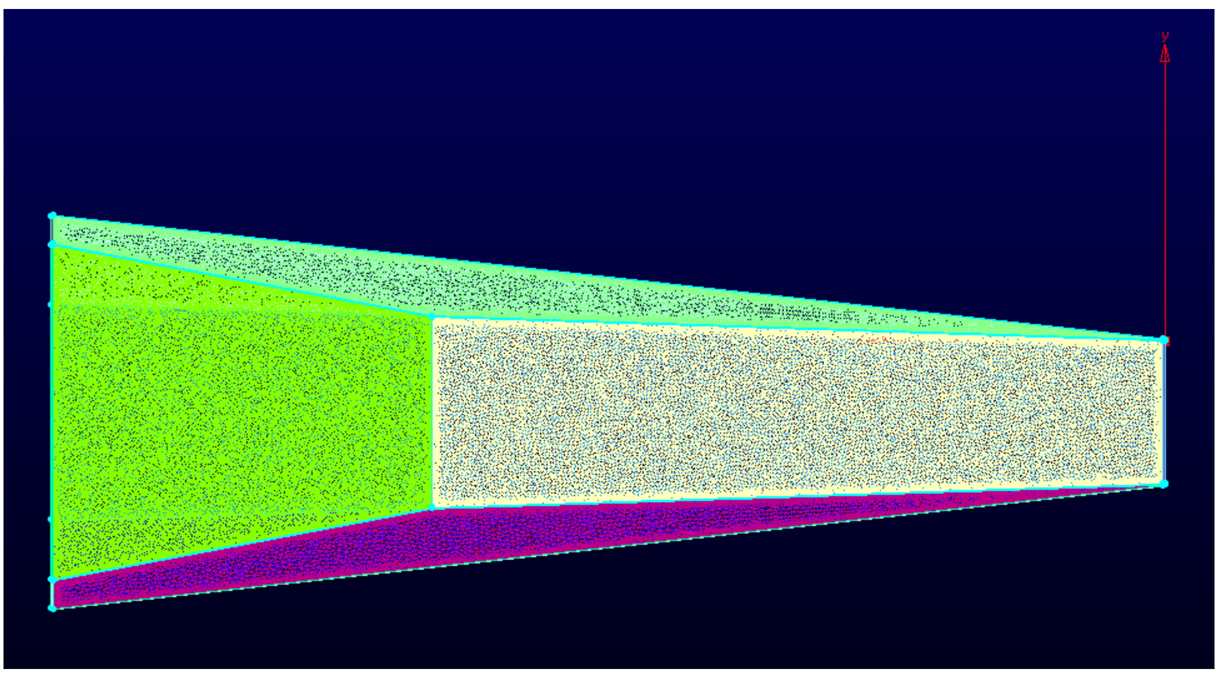

Figure 43. Bottom View of Waverider Mesh

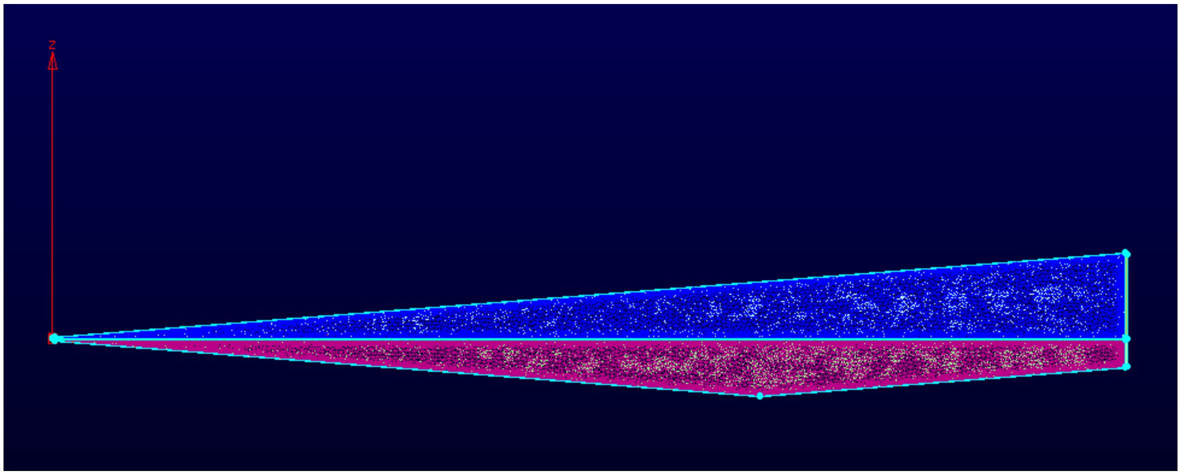

Figure 44. Side View of Waverider Mesh

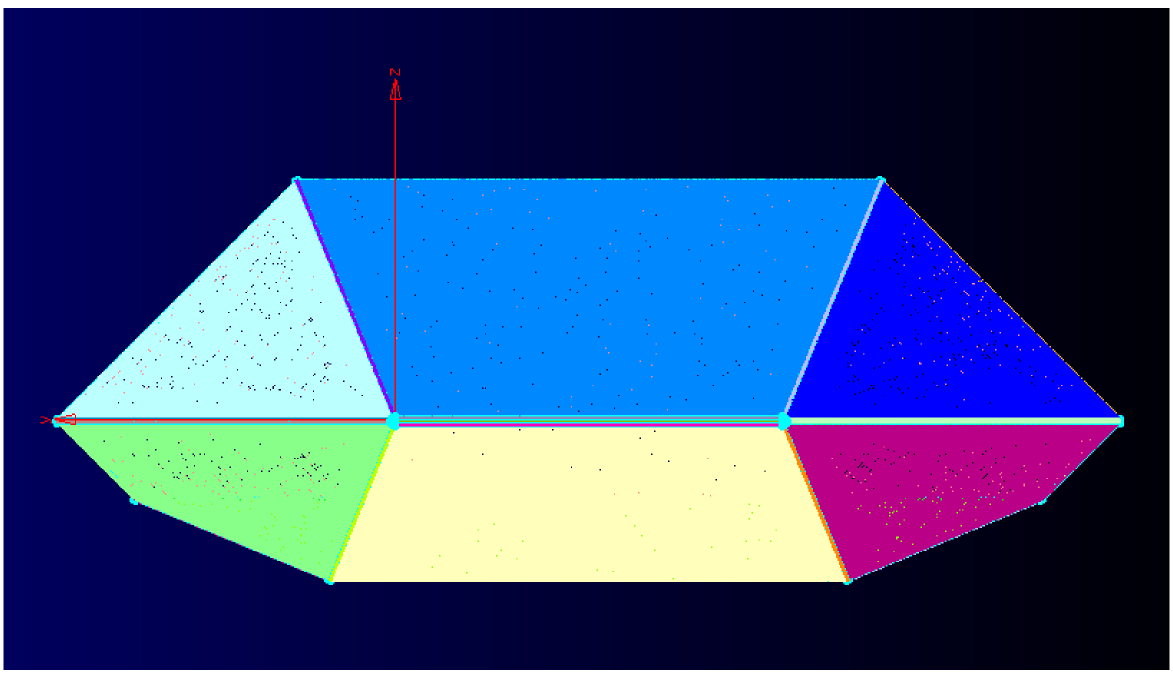

Figure 45. Front View of Waverider Mesh

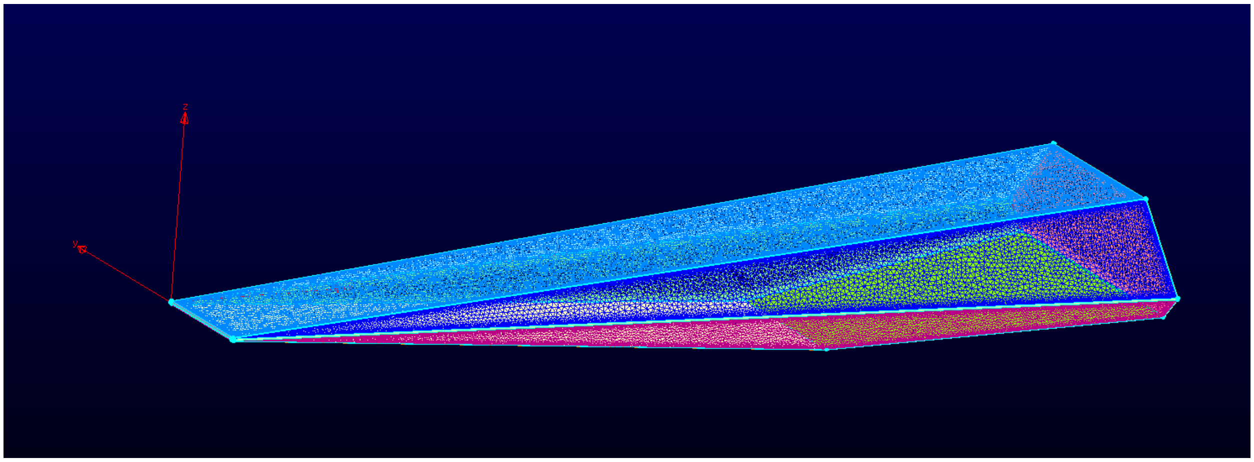

Figure 46. Diametric View of Waverider Mesh

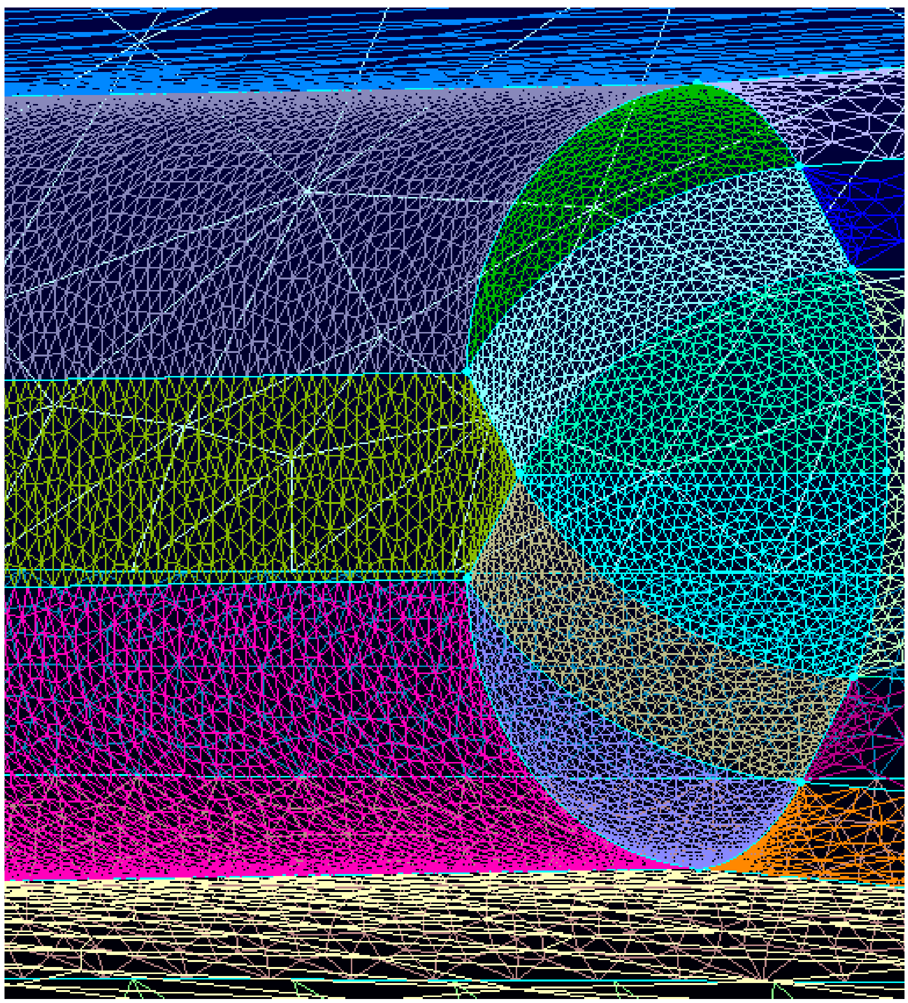

Figure 47. Proto-Waverider Enhanced View of Nose Tip

The cell count for this particular mesh is 889,155 cells with 472,405 points and is nearly ready to be imported into the CFD solver.

7.3 Pre-CFD Solver Setup

In order to import the designed mesh into the CFD solver CBAERO, the mesh must be altered into a specific format. This is operation is performed using a specific software supplied by Dr. Periklis Papadopoulos. The new file is then imported into CBAERO.

8. Proto-Waverider CFD

8.1 Conditions

Using proprietary NASA software, a trajectory from the SHARP (the most similar body) was used to determine initial conditions for the proto-waverider to be tested at and selective data is supplied in Appendix B. The trajectory is from 300 km (near space station orbit), simulates the launch out of a sounding rocket, and reaches a top speed of Mach 6.85 at 39.25 km above the surface of earth. At this point of the trajectory, the waverider will experience its max heating. The max dynamic pressure will be experienced at 28.77 km when the proto-waverider is moving at Mach 5.73. Further along the descent, there is a miniature maximum heating spike at 30.27 km while at Mach 2.59 and a miniature spike in the dynamic pressure at 28.24 km while at Mach 2.39. With the secondary spike in heating and dynamic pressure, it should be noted that the waverider actually skips across the atmosphere and increases in altitude before coming back down to the present conditions. This flight path can be seen in Figure 48 and some of the trajectory numbers can be found Appendix B. These four Mach numbers and dynamic pressures will be used for eleven different angles of attack to gain as much information as possible for future testing and designs. Only four of the angles of attack will be discussed here.

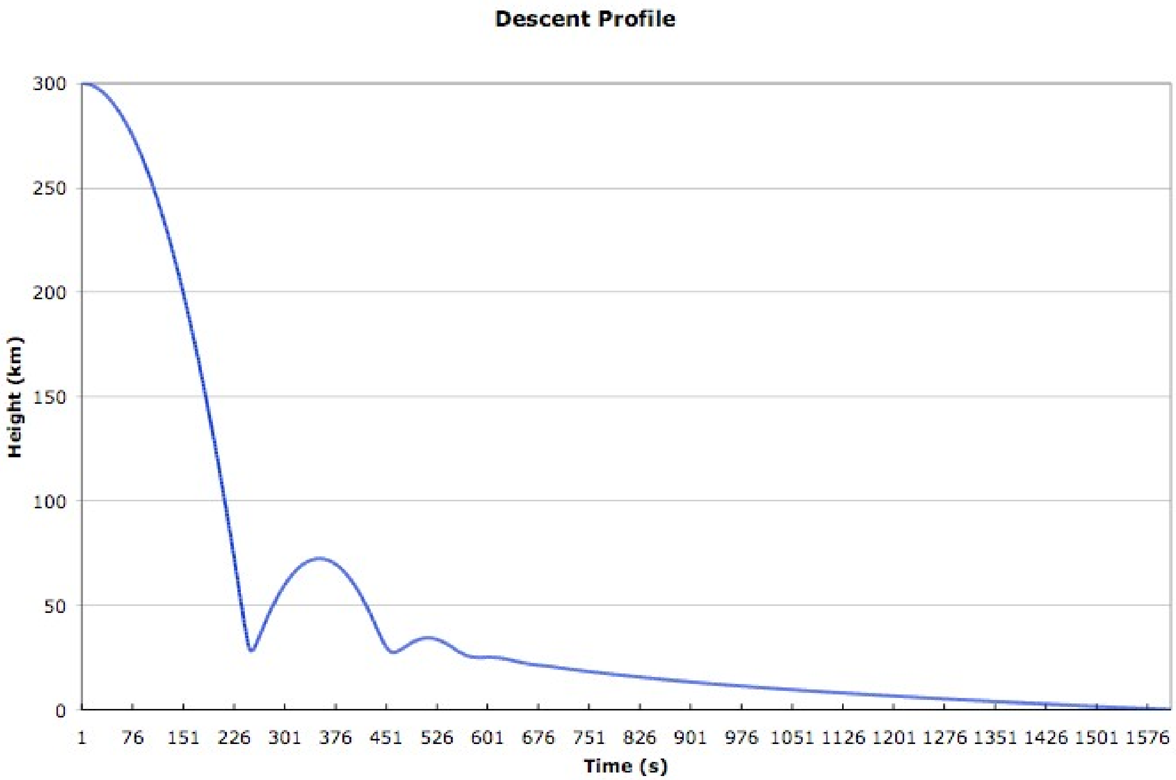

Figure 48. Trajectory Height by Time

8.2 Results

Using CBAERO, the proto-waverider was simulated at the conditions listed above with a catalytic flow. Since the vehicle is still undergoing design specifications, the emissivity was set to the default of 0.8 and no center of gravity was specified. It should be noted that some meshing changes were made to the proto-waverider in CBAERO in order to run the program, but the clustering and refinement on key areas are still in place. While eleven different angles of attack were calculations, the four that will be looked at are 0°, 4°, 8°, and 12°. The 0° angle of attack (AOA) is the most important one for that is the base for much of the design, and thus the results will have more information for this state. The maximum temperatures and pressures for the runs can be seen in Appendix C and Appendix D respectively. The coefficient of lift (C_L) values for the runs can be seen in Appendix E while the coefficient of drag (C_D) results can be seen in Appendix F.

8.2.1 Results from Max Heating Simulations (Mach 6.85, 39.25 km)

In Figures 49 and 50 the wall temperature and pressure for 0° angle of attack at Mach 6.85 can be seen.

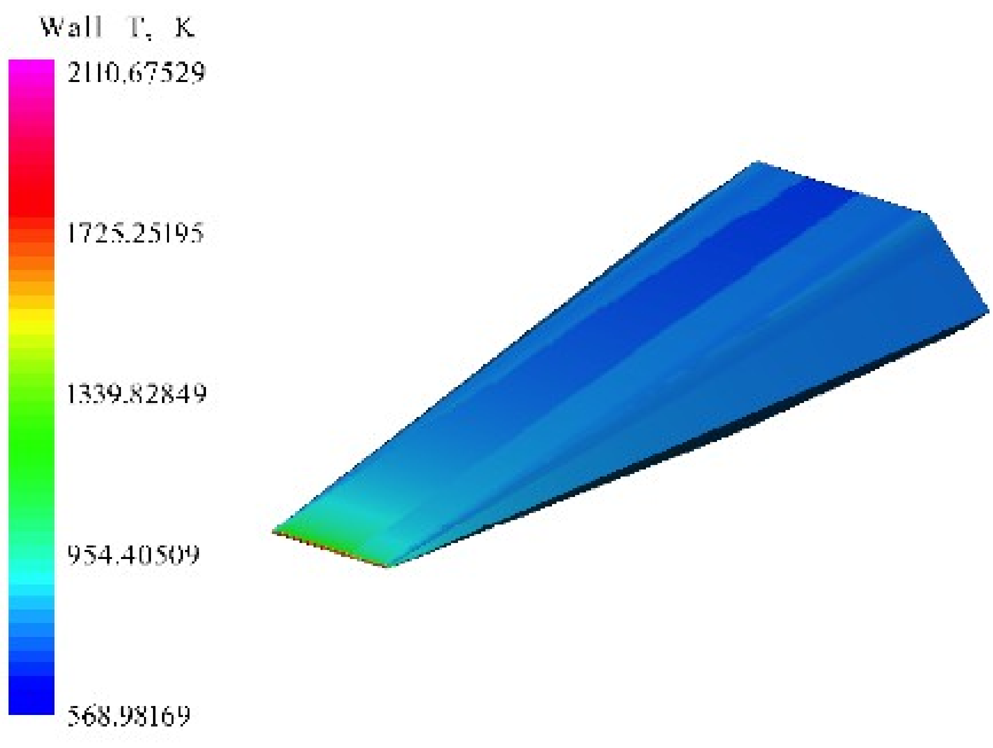

Figure 49. Proto-Waverider Temperature at Mach 6.85, 39.25 km Altitude, and 0° AOA

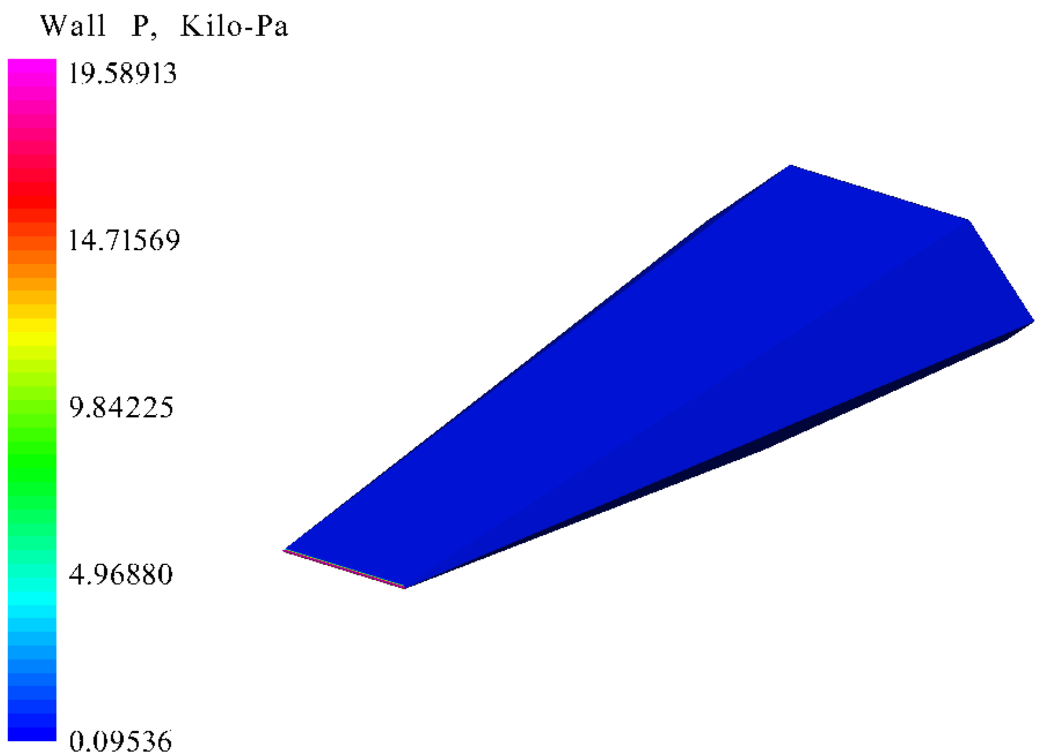

Figure 50. Proto-Waverider Pressure at Mach 6.85, 39.25 km Altitude, and 0° AOA

At these conditions we can see that most of the heating is at the nose of the proto-waverider with a temperature high of around 2111 K. It should be noticed that the temperature along the top and sides of the vehicle is also fairly high, around 900 K. For Figure 50 we can see that the pressure at the tip is the highest pressure at 19.6 kPa. We can see in the close up of the nose in Figure 51 that the nose cone for the proto-waverider will experience the highest temperatures. The slightly blunt nature of the nose, though small, illustrates how the lower and upper portions of the nose will experience the high temperatures, not the very flat tip of the proto-waverider where it is a stagnation point. Figure 52 shows the temperature profile for the underside of the proto-waverider and just like the topside, the highest temperatures are at the nose tip while the back flare has no significant temperature increase.

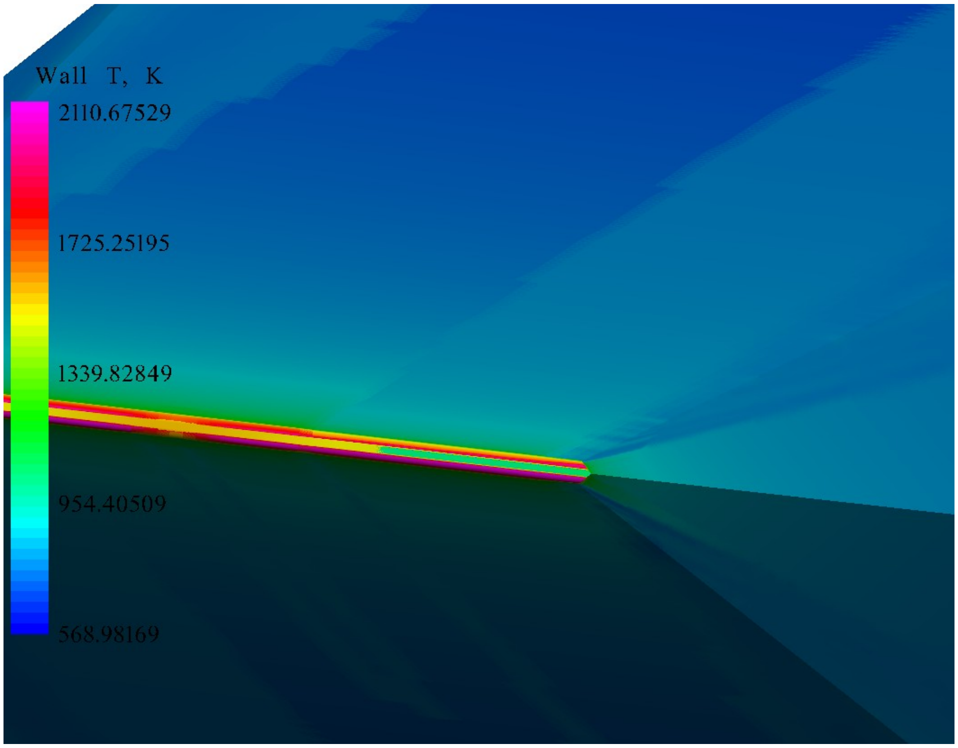

Figure 51. Proto-Waverider Nose Temp. at Mach 6.85, 39.25 km Altitude, and 0° AOA

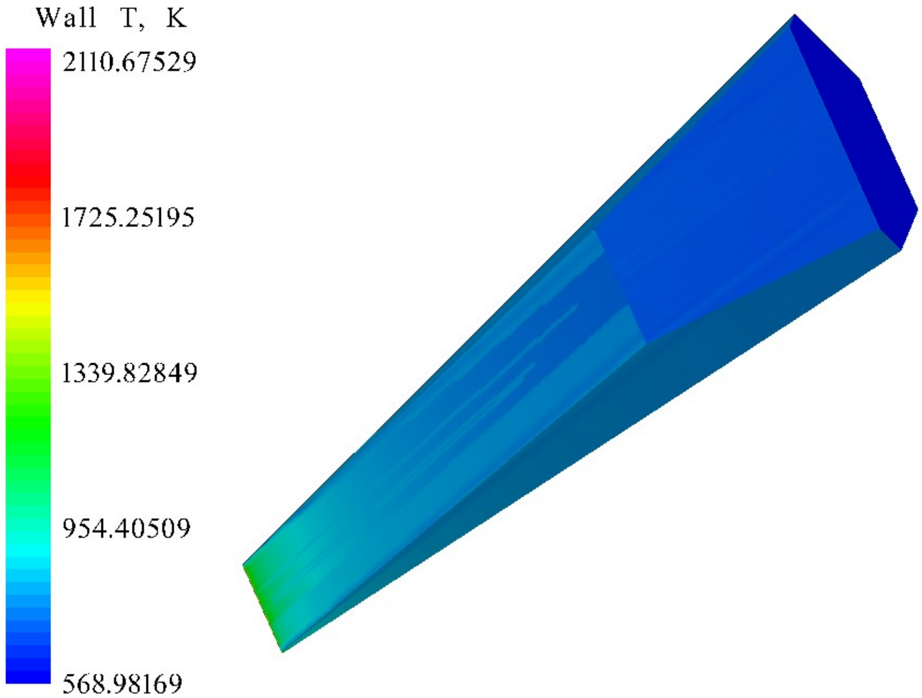

Figure 52. Proto-Waverider Bottom Temp. at Mach 6.85, 39.25 km Altitude, and 0° AOA

The C_L in this run is -0.0069 while the C_D is 0.0110, a L/D of 0.63 in the downward direction. In Figures 53 and 54 the temperature and pressure values for a 4° angle of attack are shown.

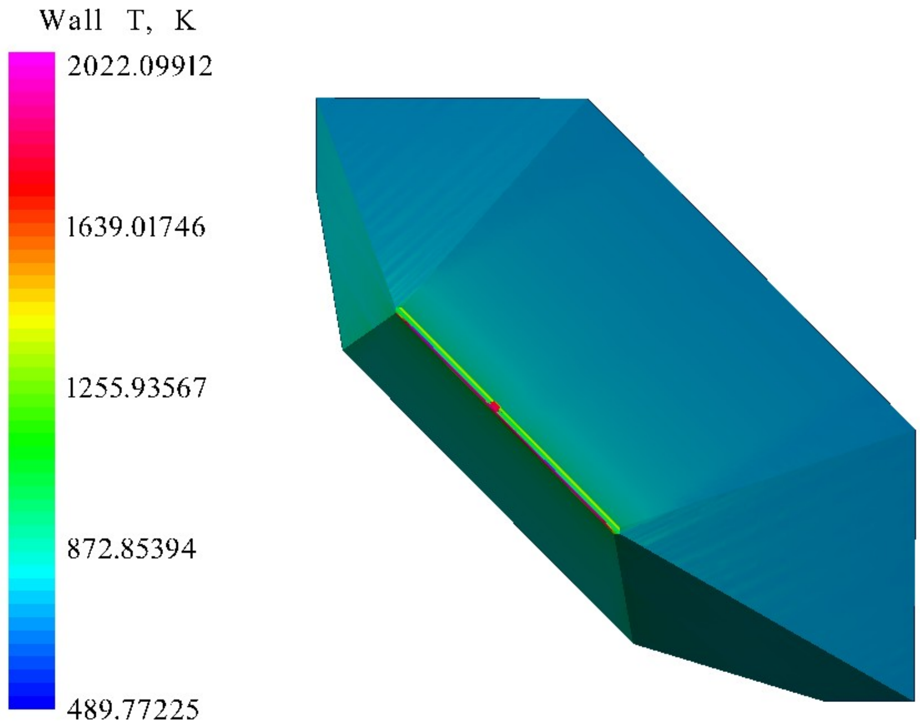

Figure 53. Proto-Waverider Temperature at Mach 6.85, 39.25 km Altitude, and 4° AOA

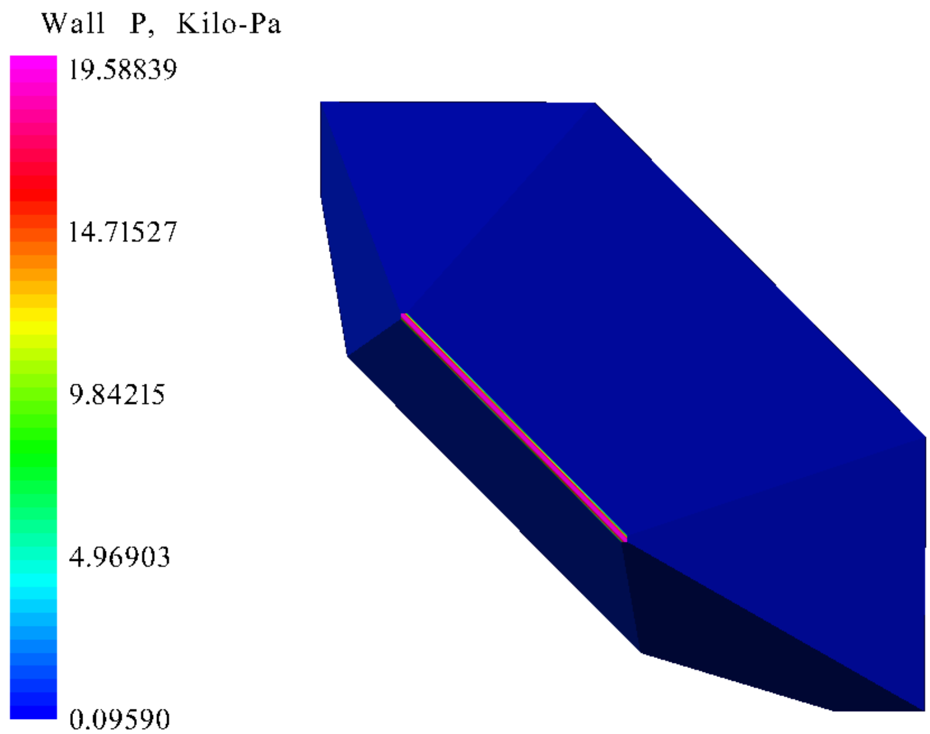

Figure 54. Proto-Waverider Pressure at Mach 6.85, 39.25 km Altitude, and 4° AOA

For this run there is a maximum temperature around 2022 K, with a maximum pressure of 13.40 kPa. In Figure 53, we can see in the CFD simulation there was a high temperature point near the middle of the nose but this is must likely an anomaly. In earlier runs, it would sometimes be noted that the middle of the nose might not resolve correctly, and while steps were taken so that the majority of the results would be accurate, it did not always turn out so. For these conditions the C_L is 0.0228 and the C_D is 0.0130 with a L/D of 1.75. The Figures 55 and 56 show the temperature and pressure values at 8° angle of attack.

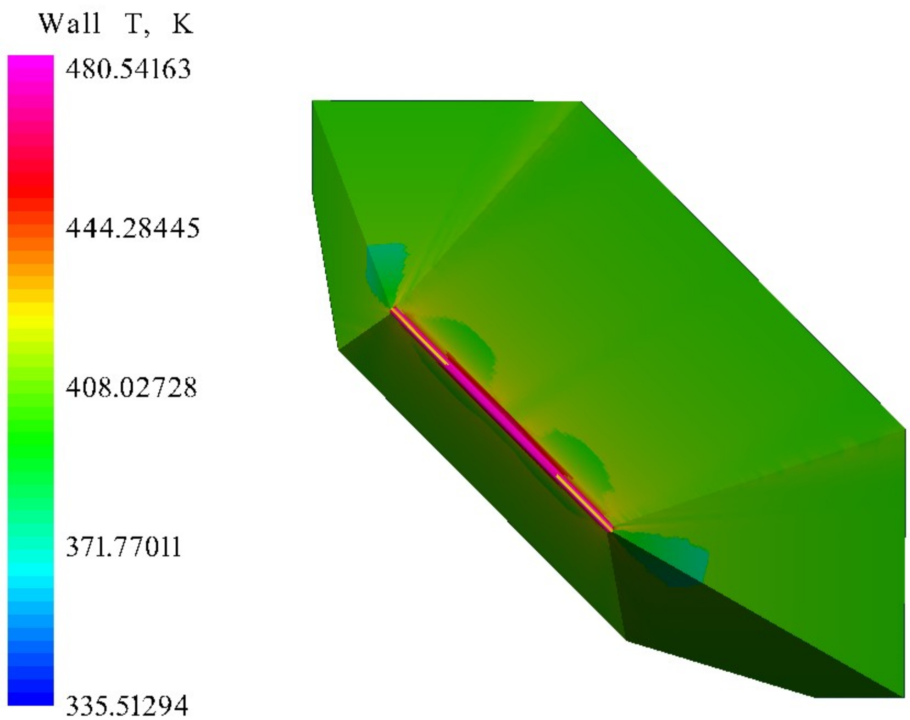

Figure 55. Proto-Waverider Temperature at Mach 6.85, 39.25 km Altitude, and 8° AOA

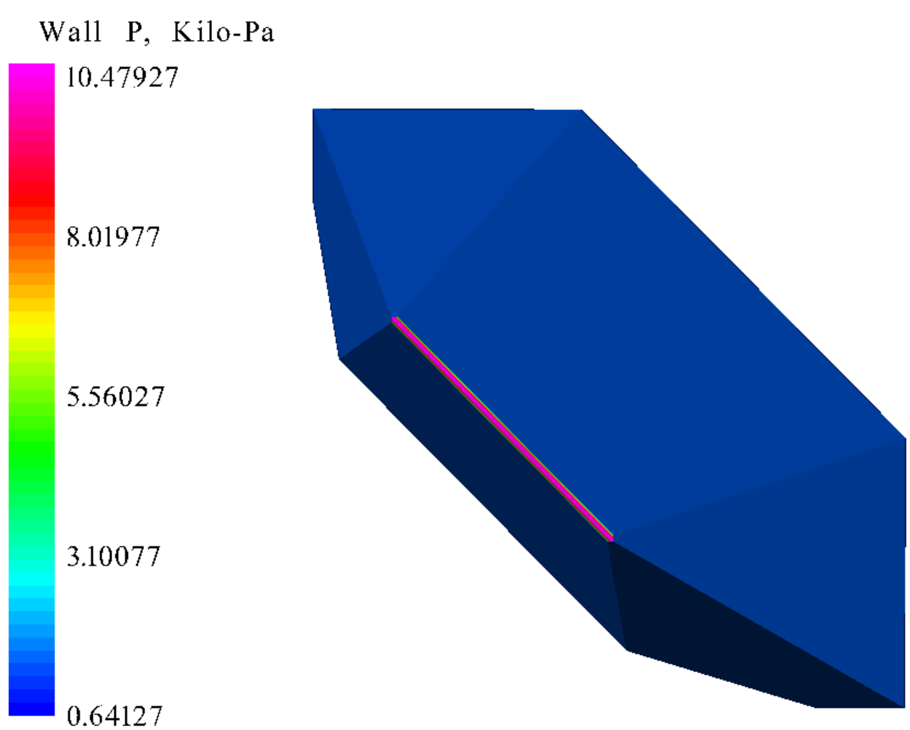

Figure 56. Proto-Waverider Pressure at Mach 6.85, 39.25 km Altitude, and 8° AOA

These results show that at the larger angles of attack, the vehicle is not subject to extreme conditions as the lower angles of attack, for the wall temperatures only reach around 480 K while the maximum temperature is 2070 K. It is important to remember that this is run in a catalytic flow thus the maximum temperature will be higher than the wall temperature. The maximum pressure is 12.85 kPa and in this run the C_L is 0.0568 while the C_D is 0.0214. The L/D for this case is therefore 2.65 for the proto-waverider body at 8° AOA. The temperature and pressure values for a 12° angle of attack can be seen in Figures 57 and 58 respectively.

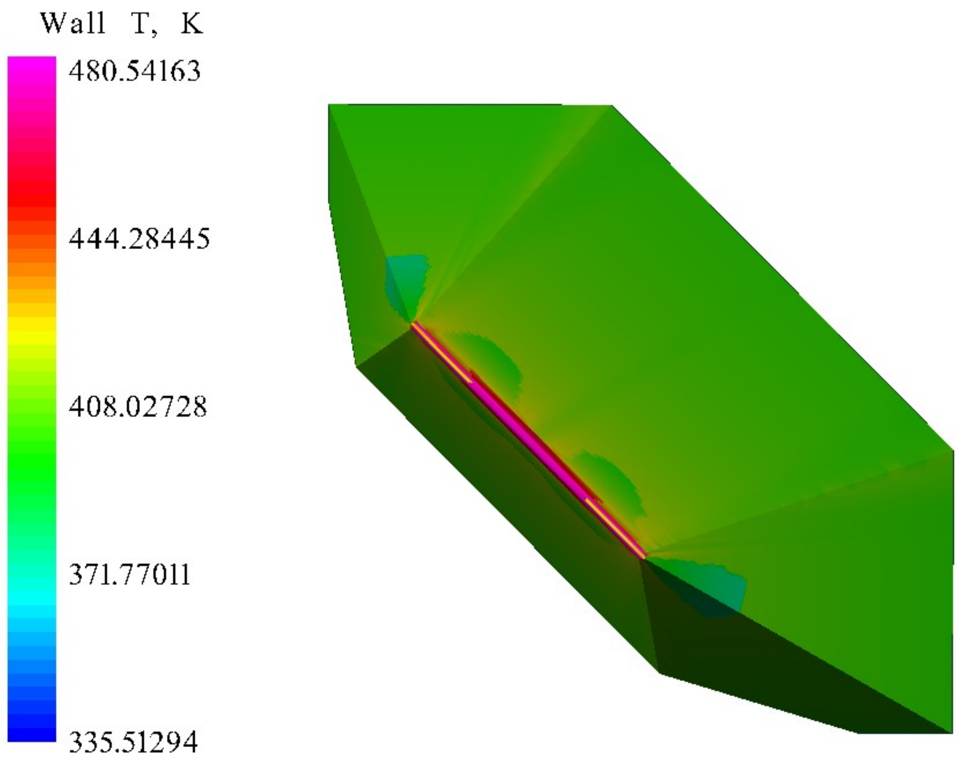

Figure 57. Proto-Waverider Temperature at Mach 6.85, 39.25 km Altitude, and 12° AOA

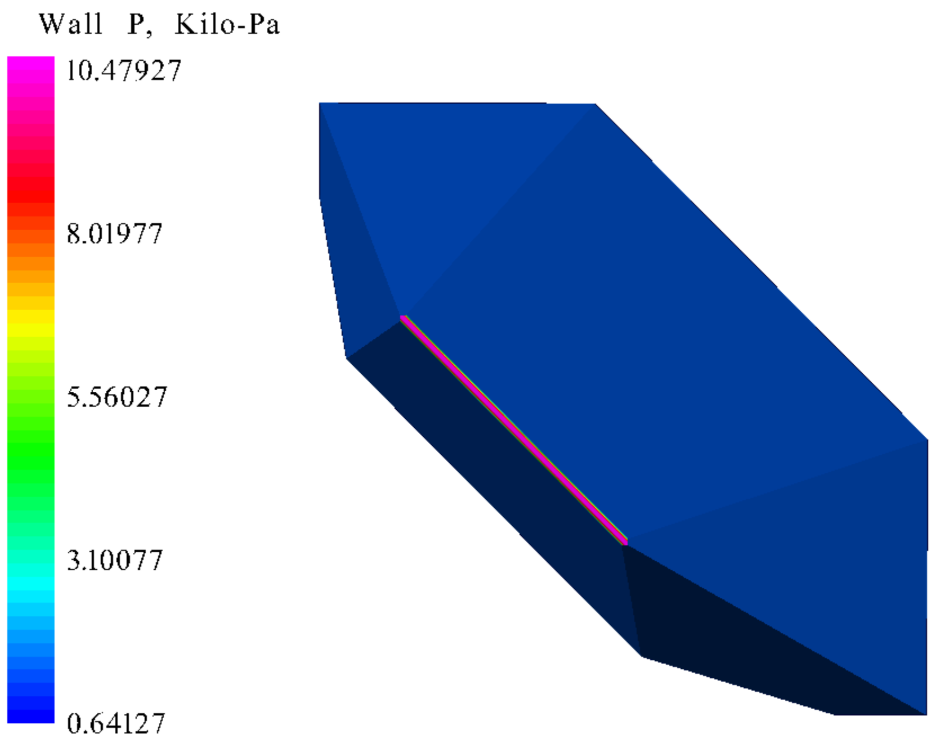

Figure 58. Proto-Waverider Pressure at Mach 6.85, 39.25 km Altitude, and 12° AOA

At an AOA of 12°, the vehicle is not subject to extreme conditions, for the wall temperatures only reach around 480 K while the maximum temperature is around 2022 K. The maximum pressure is 13.35 kPa and in this run the C_L is 0.1033 while the C_D is 0.0378. The L/D for this case is therefore 2.73 for the proto-waverider body at 12° AOA. As a reminder, this case was for the maximum heating found during the trajectory analysis of a similar re-entry vehicle.

8.2.2 Results from Max Dynamic Pressure Simulations (Mach 5.73, 28.77 km)

In Figures 59 and 60 the wall temperature and pressure for 0° angle of attack at Mach 5.73 can be seen where the proto-waverider is traveling at 28.77 km.

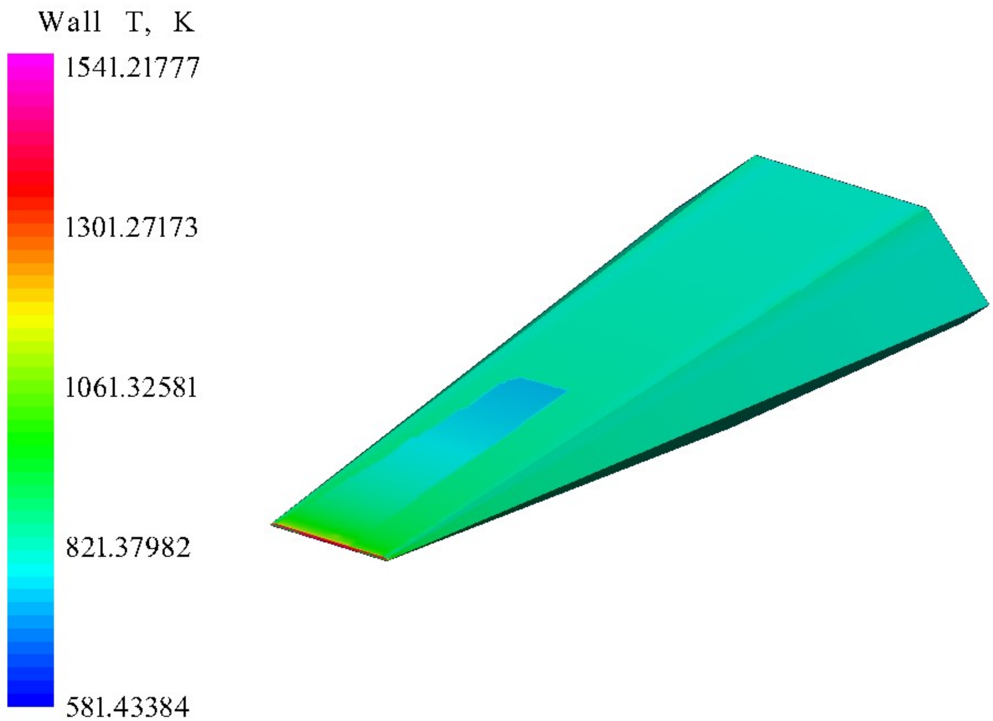

Figure 59. Proto-Waverider Temperature at Mach 5.73, 28.77 km Altitude, and 0° AOA

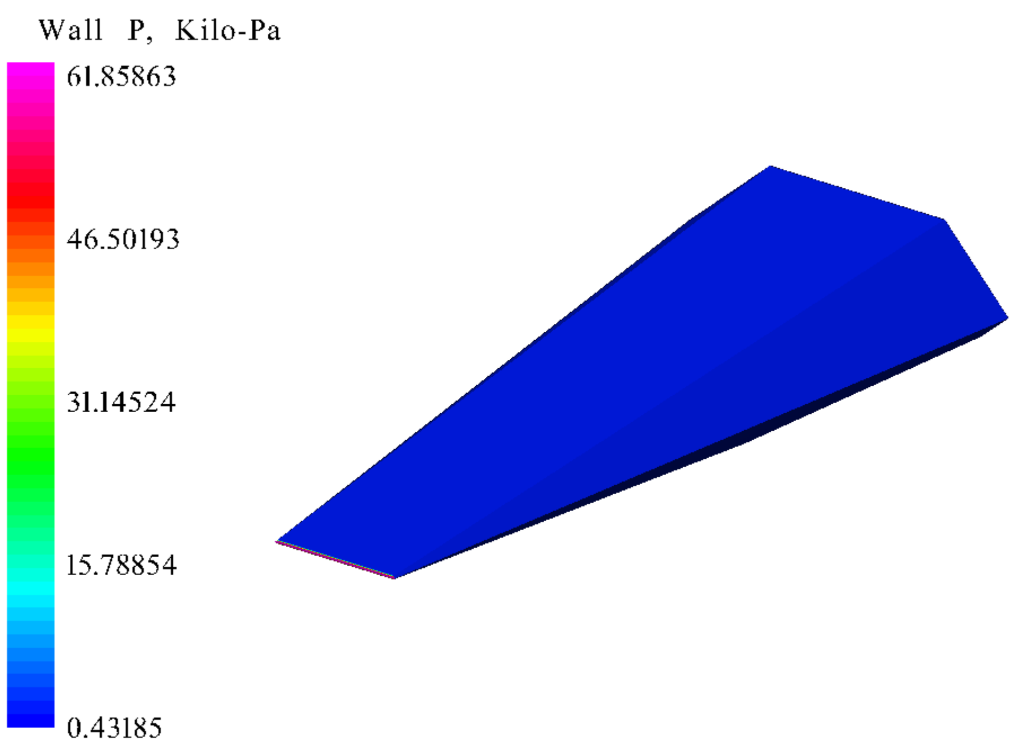

Figure 60. Proto-Waverider Pressure at Mach 5.73, 28.77 km Altitude, and 0° AOA

Like the earlier trajectory case, the highest temperature on the body take place on the nose of the proto-waverider and reach a high of around 1541 K but is over 500 K cooler than the first case. It should be noticed that the temperature along the top and sides of the vehicle is also fairly high, around 900 K just like the Mach 6.85 case. For Figure 60 we can see that the pressure at the tip is the highest pressure at 57.01 kPa, which is nearly 40 kPa higher than the Mach 6.85 case. We can see in the close up of the nose in Figure 61 that the nose cone for the proto-waverider will experience the highest temperatures, but the temperature profile is fairly even. Figure 62 shows the temperature profile for the underside of the proto-waverider and just like the topside, the highest temperatures are at the nose tip while the back flare has a noticeably decreased temperature than the rest of the body (except for the back of the vehicle).

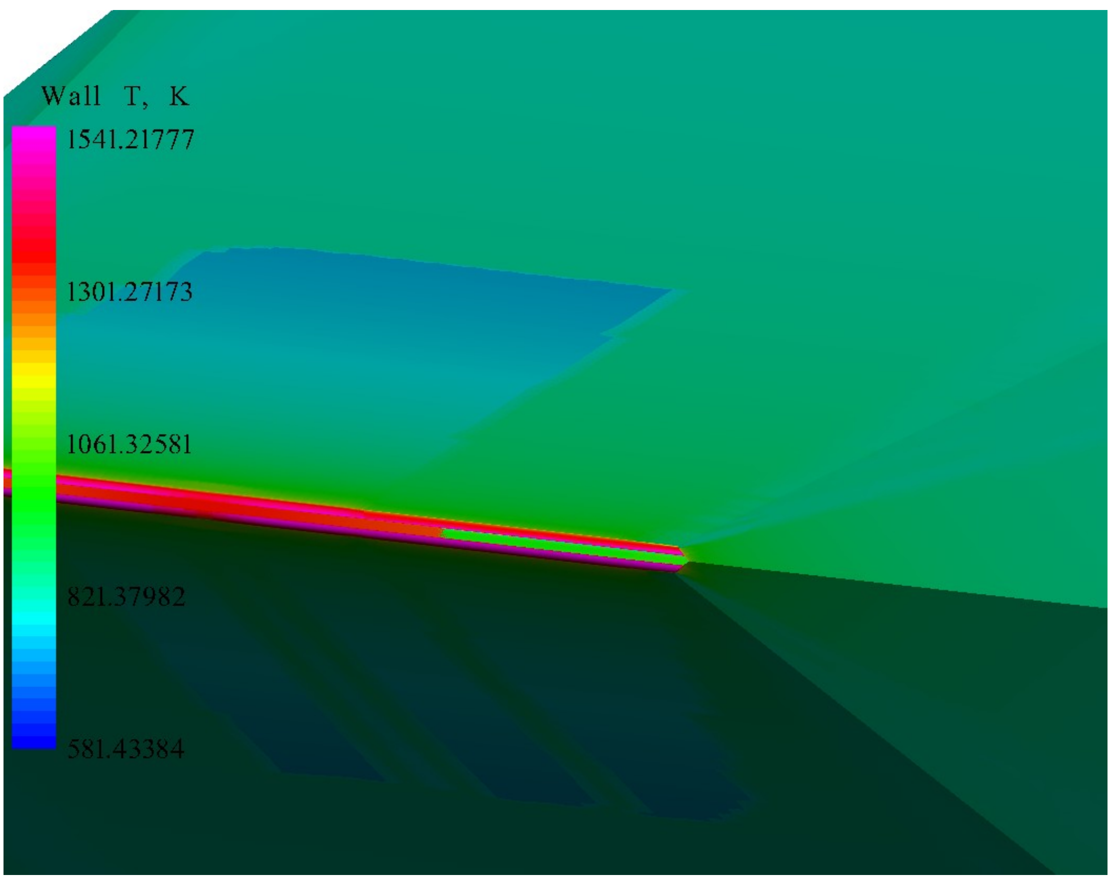

Figure 61. Proto-Waverider Nose Temp. at Mach 5.73, 28.77 km Altitude, and 0° AOA

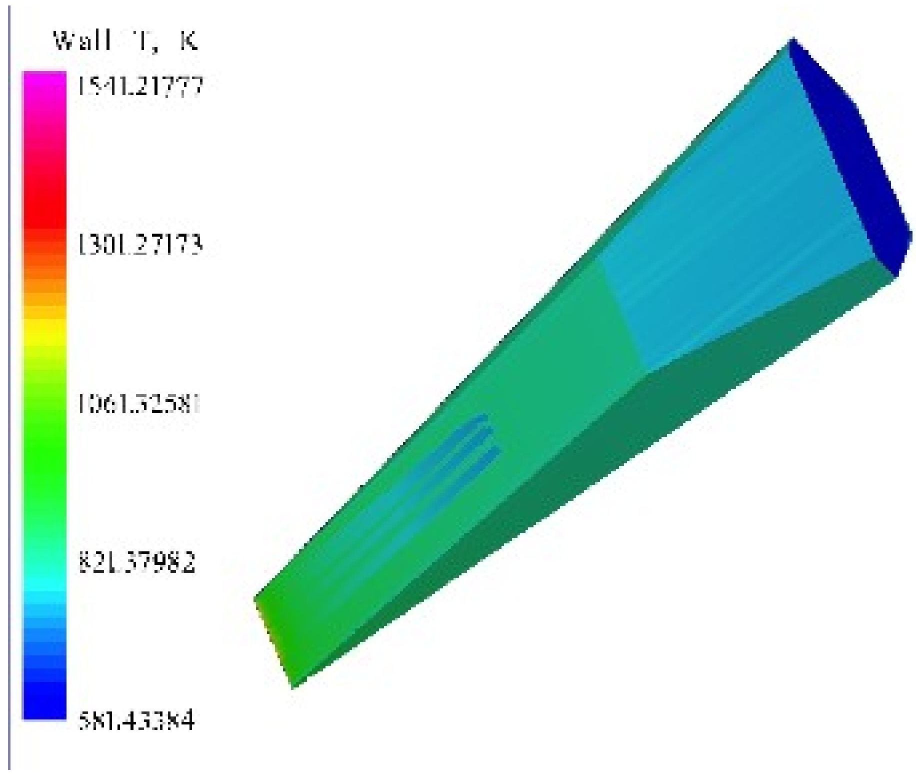

Figure 62. Proto-Waverider Bottom Temp. at Mach 5.73, 28.77 km Altitude, and 0° AOA

The C_L in this run is -0.0080 while the C_D is 0.0111, a L/D of 0.72 in the downward direction. In Figures 63 and 64 the temperature and pressure values for a 4° angle of attack at the maximum dynamic pressure is shown.

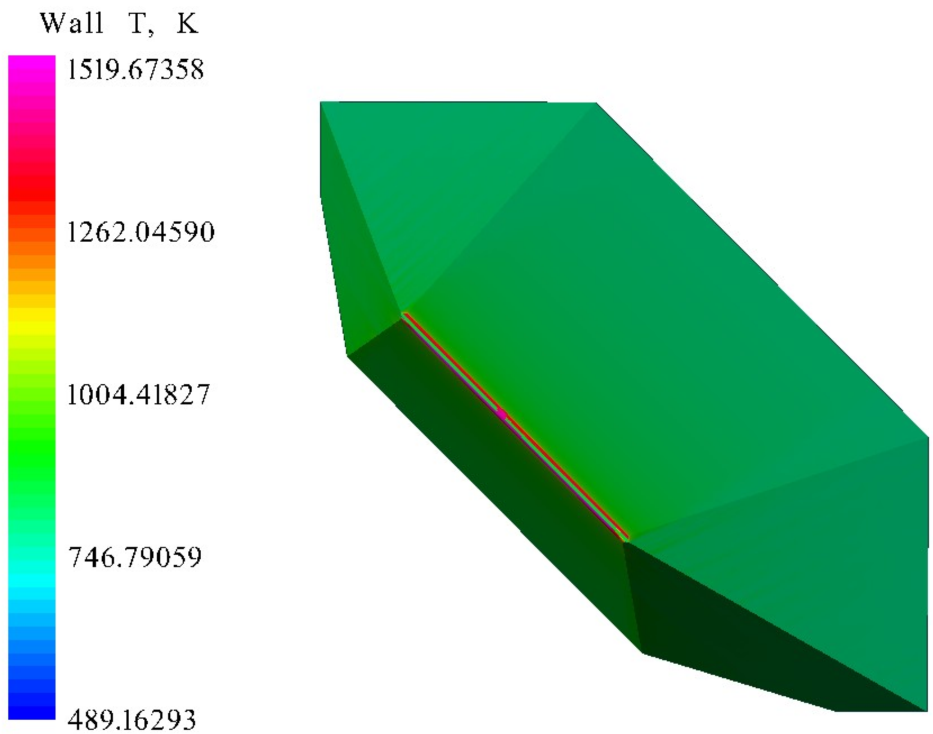

Figure 63. Proto-Waverider Temperature at Mach 5.73, 28.77 km Altitude, and 4° AOA

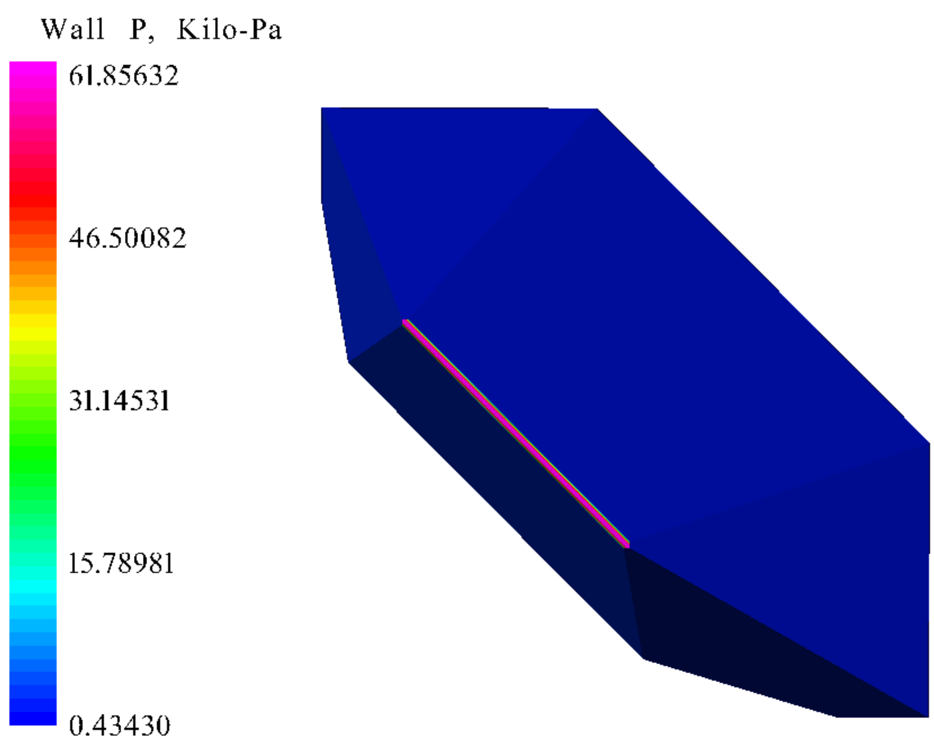

Figure 64. Proto-Waverider Pressure at Mach 5.73, 28.77 km Altitude, and 4° AOA

For this run there is a maximum temperature around 1520 K, with a maximum pressure of 52.41 kPa. In Figure 63, like in Figure 53, the temperature point along the nose returns. However, looking at the nose once more reveals that the nearby area are both at this high temperature so there is no need for further concern. For the Mach 5.73 and 4° AOA condition the C_L is 0.0225 and the C_D is 0.0131 with a L/D of 1.75 (practically the same as the 4° AOA for the maximum heating case earlier). In Figures 65 and 66 the temperature and pressure values at 8° angle of attack are illustrated.

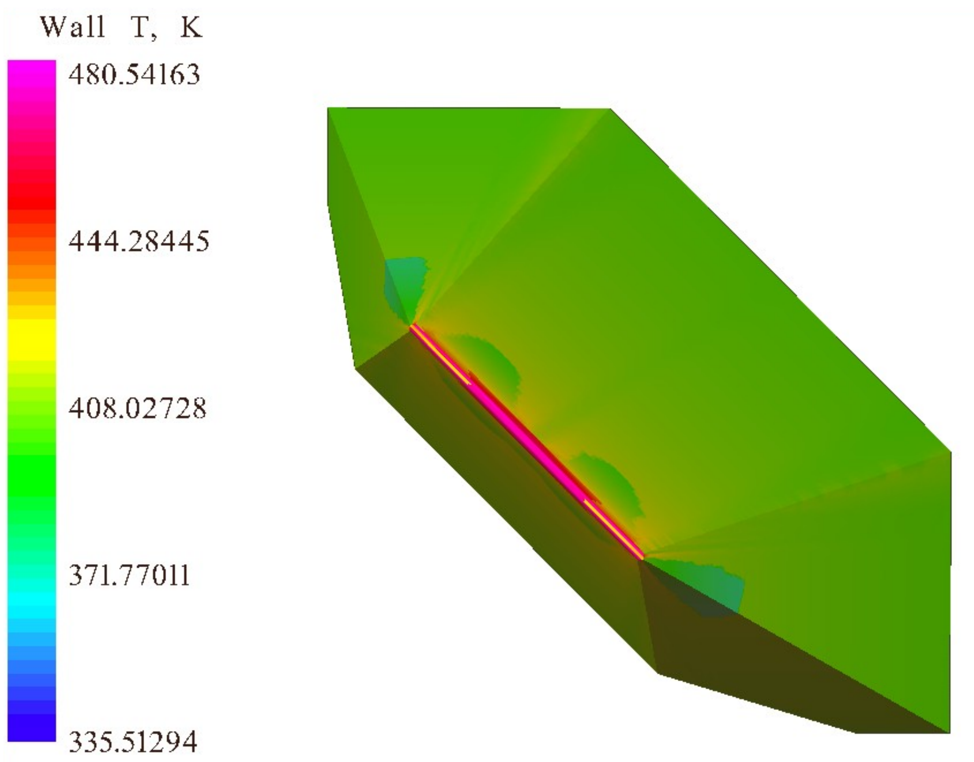

Figure 65. Proto-Waverider Temperature at Mach 5.73, 28.77 km Altitude, and 8° AOA

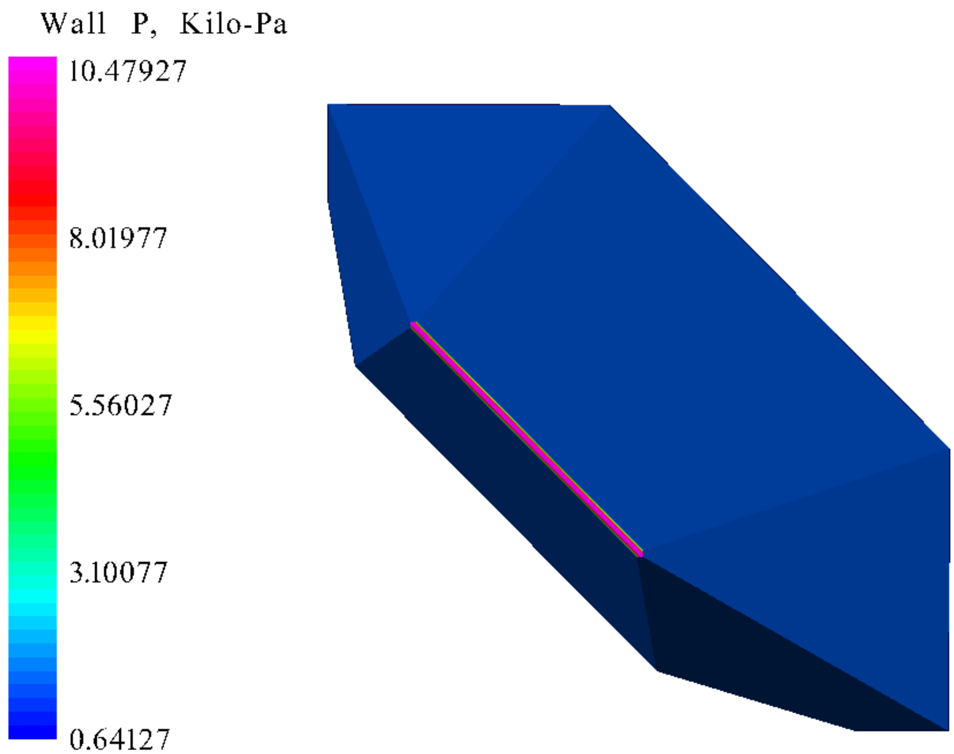

Figure 66. Proto-Waverider Pressure at Mach 5.73, 28.77 km Altitude, and 8° AOA

These results show that at the larger angles of attack, the vehicle is not subject to extreme conditions, for the wall temperatures only reach around 480 K while the maximum temperature is 1540 K. The maximum pressure is 56.40 kPa (as seen in Appendix D) while the maximum wall pressure is only 10.48 kPa as seen in Figure 66. The C_L at 8° AOA is 0.0584 while the C_D is 0.0212 resulting in a L/D of 2.75. The temperature and pressure values for a 12° angle of attack can be seen in Figures 67 and 68 respectively.

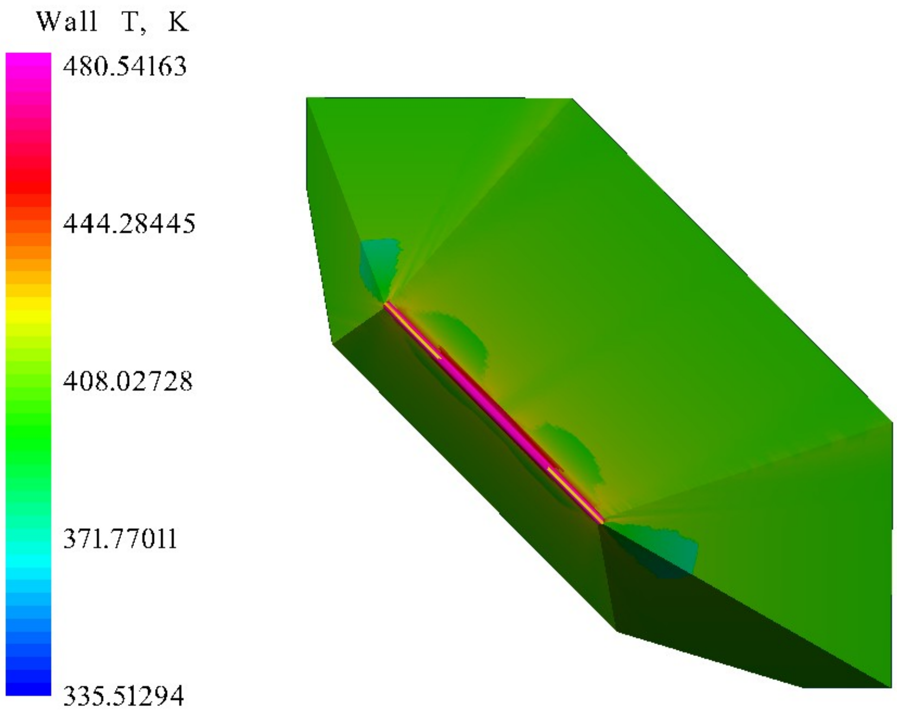

Figure 67. Proto-Waverider Temperature at Mach 5.73, 28.77 km Altitude, and 12° AOA

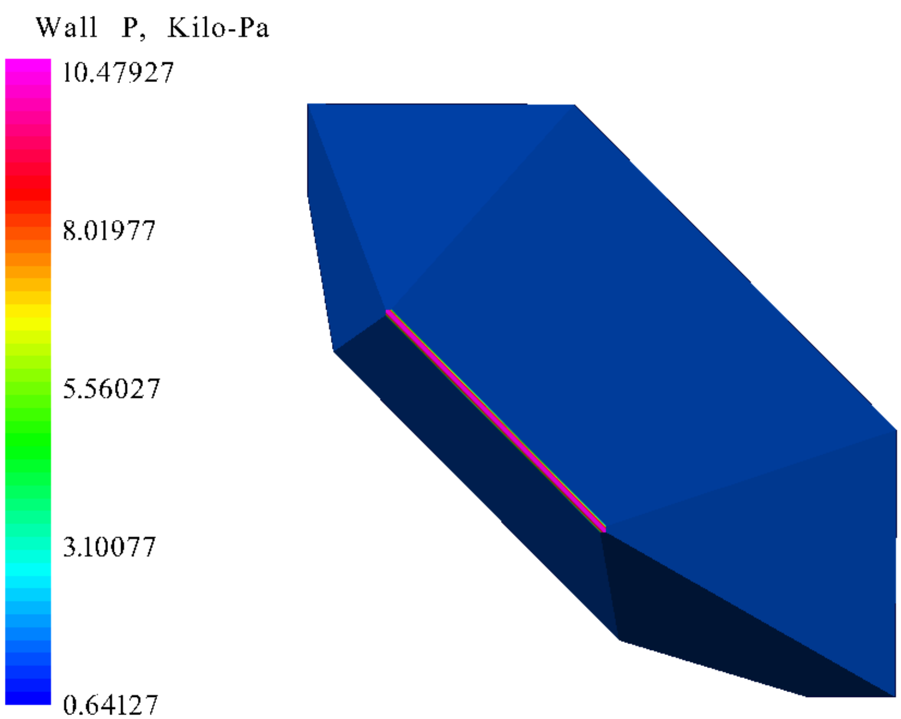

Figure 68. Proto-Waverider Pressure at Mach 5.73, 28.77 km Altitude, and 12° AOA

At an AOA of 12°, the vehicle is not subject to extreme conditions, for the wall temperatures only reach around 480 K while the maximum temperature is around 1535 K. The maximum pressure is 51.74 kPa with a maximum wall pressure of around 10.5 kPa at the nose. In this run the C_L is 0.1071 while the C_D is 0.0378. The L/D for this case is therefore 2.83 for the proto-waverider body at 12° AOA.

8.2.3 Results from Secondary Heating Spike Simulations (Mach 2.59, 30.27 km)

In Figures 69 and 70 the wall temperature and pressure for 0° angle of attack at Mach 2.59 can be seen where the proto-waverider is traveling at 30.27 km having skipped along the atmosphere and began its descent again.

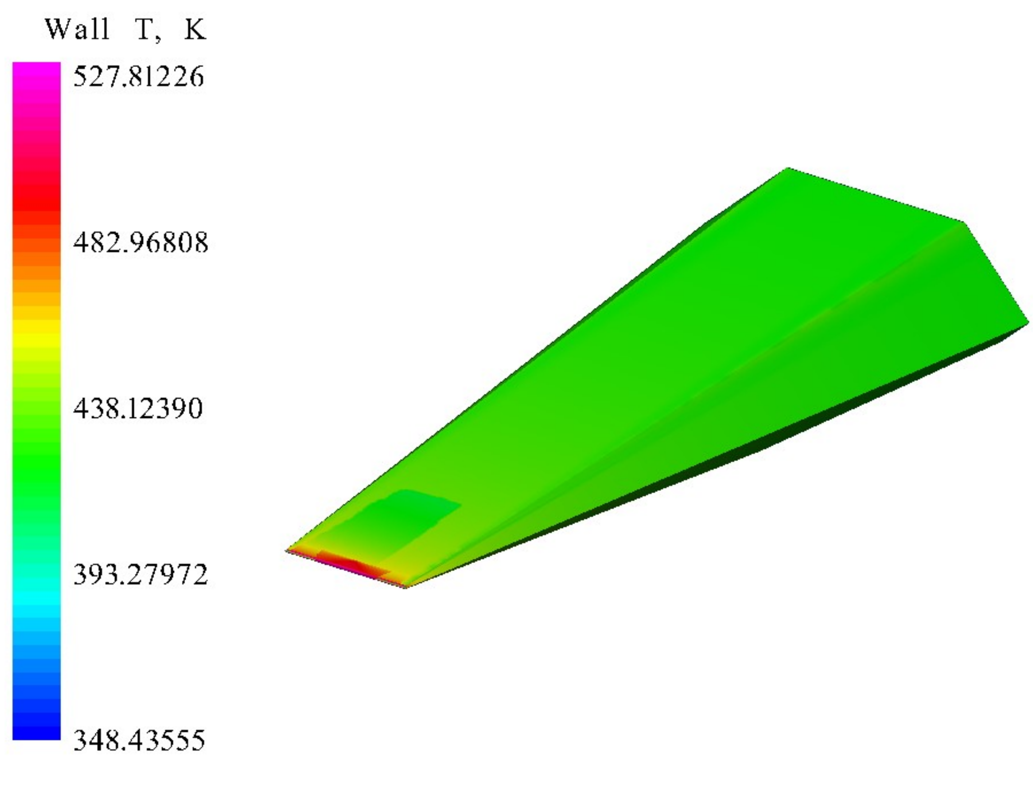

Figure 69. Proto-Waverider Temperature at Mach 2.59, 30.27 km Altitude, and 0° AOA

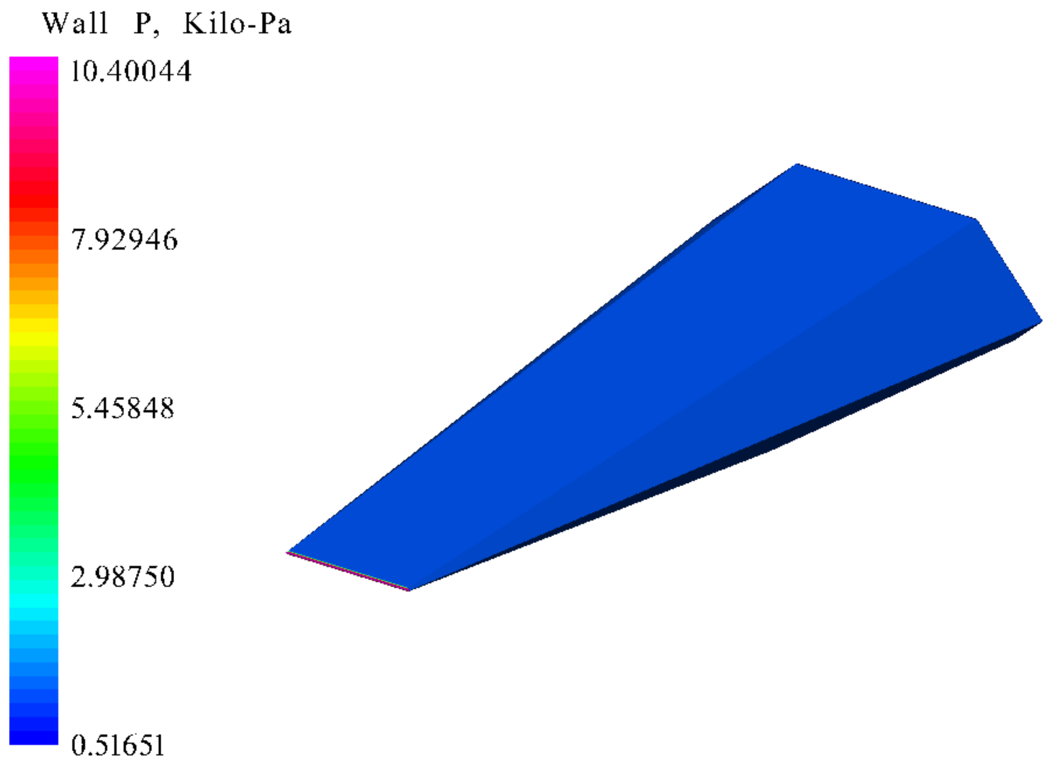

Figure 70. Proto-Waverider Pressure at Mach 2.59, 30.27 km Altitude, and 0° AOA

As the vehicle is coming back in, the temperature and pressure conditions that the proto-waverider will experience will not be as extreme as the first two cases. In this condition, secondary maximum heating spike has a high temperature of only 528 K with the temperature along the top and sides of the vehicle only slightly over 400 K. For Figure 70 we can see that the pressure at the tip is only around 10 kPa. In Figure 71 that the nose cone for the proto-waverider will experience the highest temperatures but the outer edges will significantly decrease in temperature. Figure 72 shows the temperature profile for the underside of the proto-waverider and most of the proto-waverider experiences temperatures around 400 K as noted earlier.

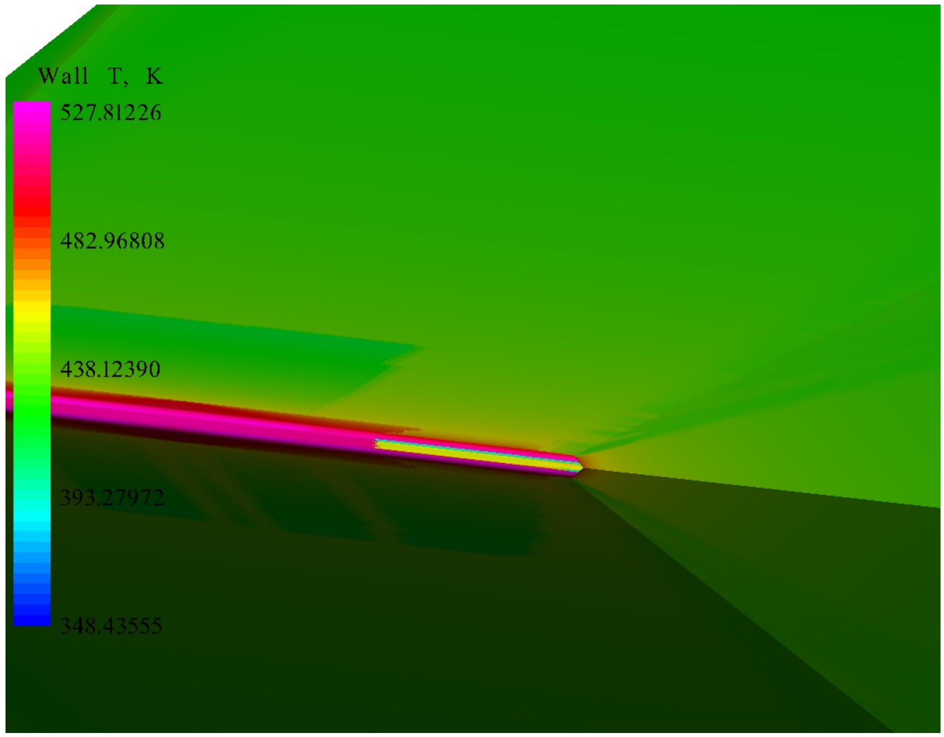

Figure 71. Proto-Waverider Nose Temp. at Mach 2.59, 30.27 km Altitude, and 0° AOA

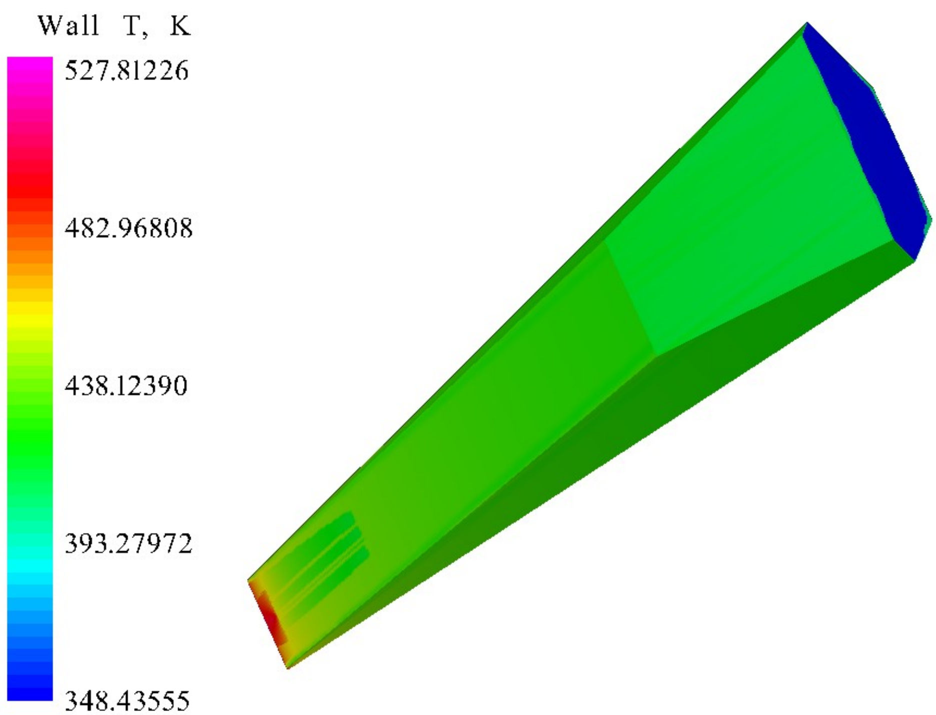

Figure 72. Proto-Waverider Bottom Temp. at Mach 2.59, 30.27 km Altitude, and 0° AOA

The C_L for this secondary maximum heating condition is -0.0200 while the C_D is 0.0255, a L/D of 0.78 in the downward direction. The angle of attack is increased to 4° in Figures 73 and 74 where the temperature and pressure values are shown correspondingly.

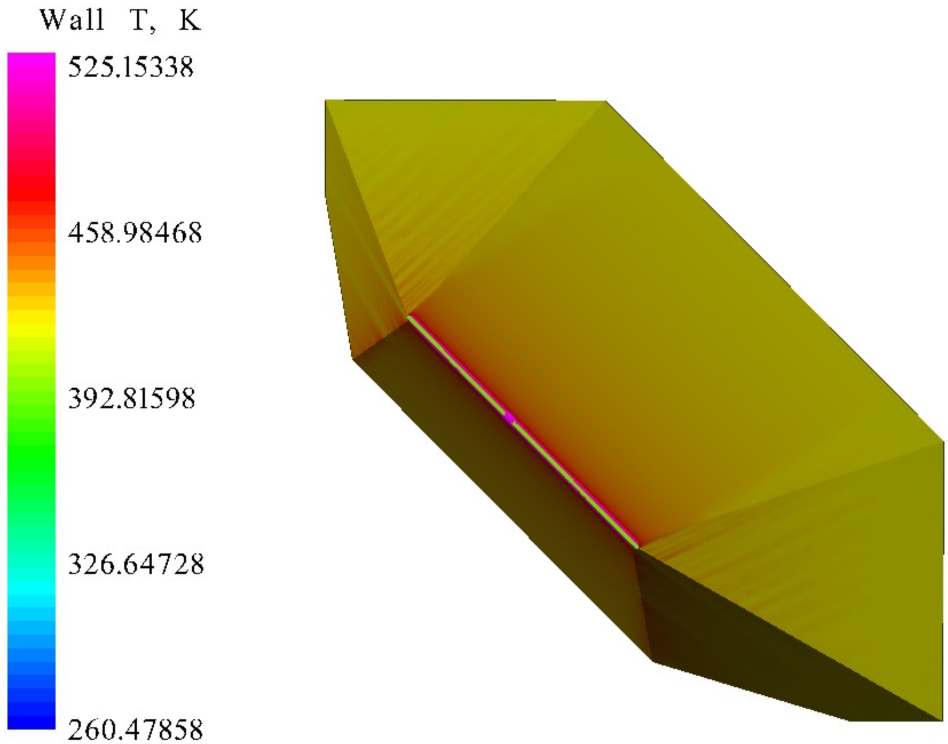

Figure 73. Proto-Waverider Temperature at Mach 2.59, 30.27 km Altitude, and 4° AOA

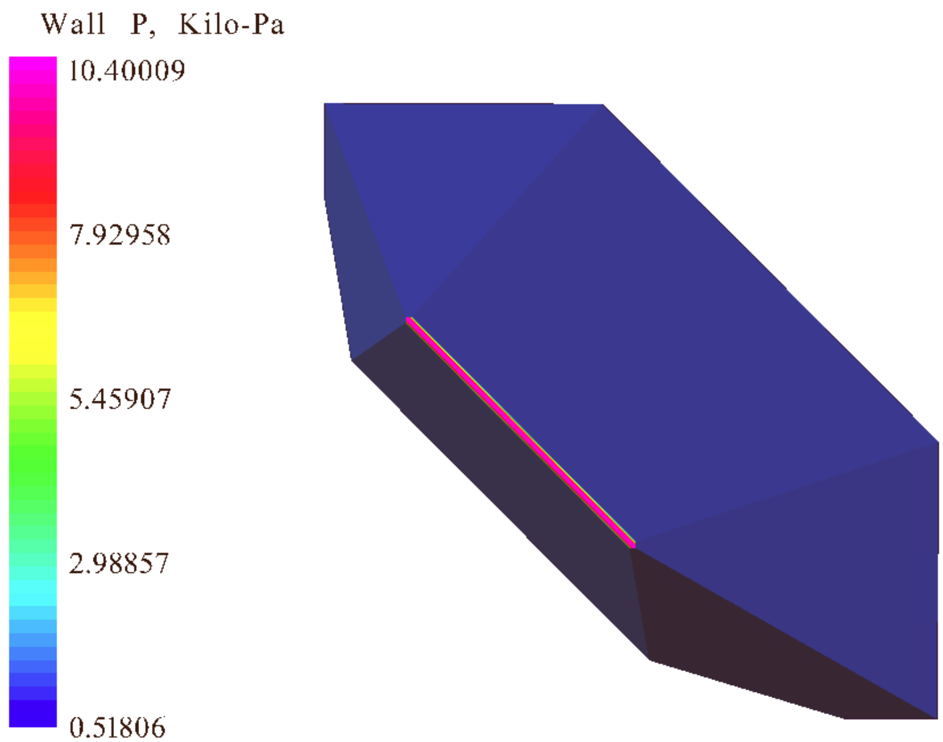

Figure 74. Proto-Waverider Pressure at Mach 2.59, 30.27 km Altitude, and 4° AOA

The vehicle reaches a maximum temperature around 525 K, with a maximum pressure of 10 kPa for Mach 2.59 at 30.27 km. Once more, in Figure 73, like in the other two cases, the temperature point along the nose returns. For this 4° AOA condition the C_L is 0.0190 and the C_D is 0.0263 with a L/D of 0.72, which is greatly reduced from the 4° AOA L/D values in the previous cases. In Figures 75 and 76 the temperature and pressure values at 8° angle of attack are displayed.

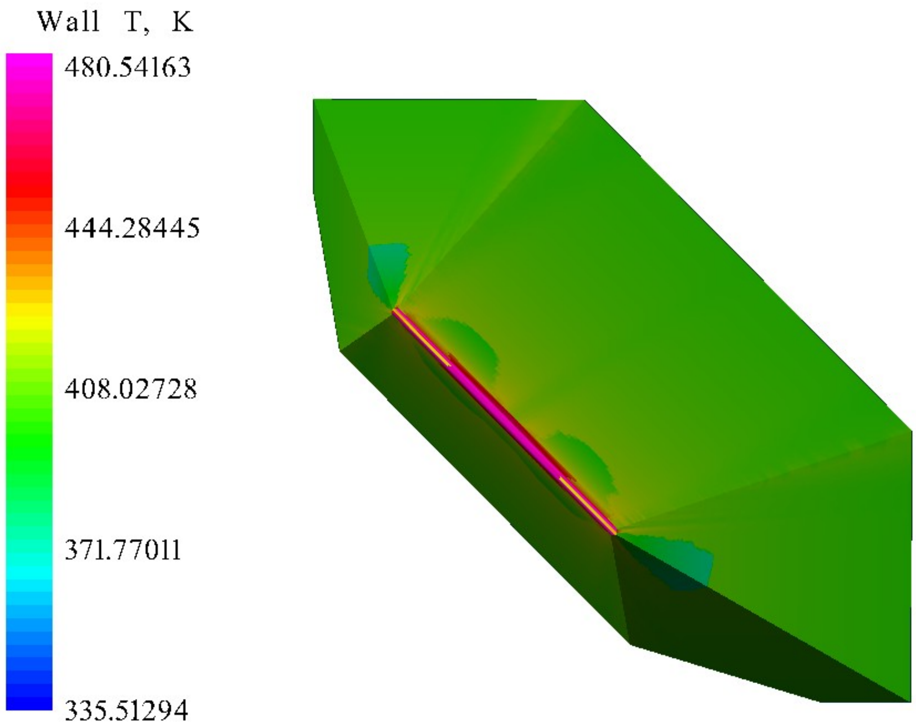

Figure 75. Proto-Waverider Temperature at Mach 2.59, 30.27 km Altitude, and 8° AOA

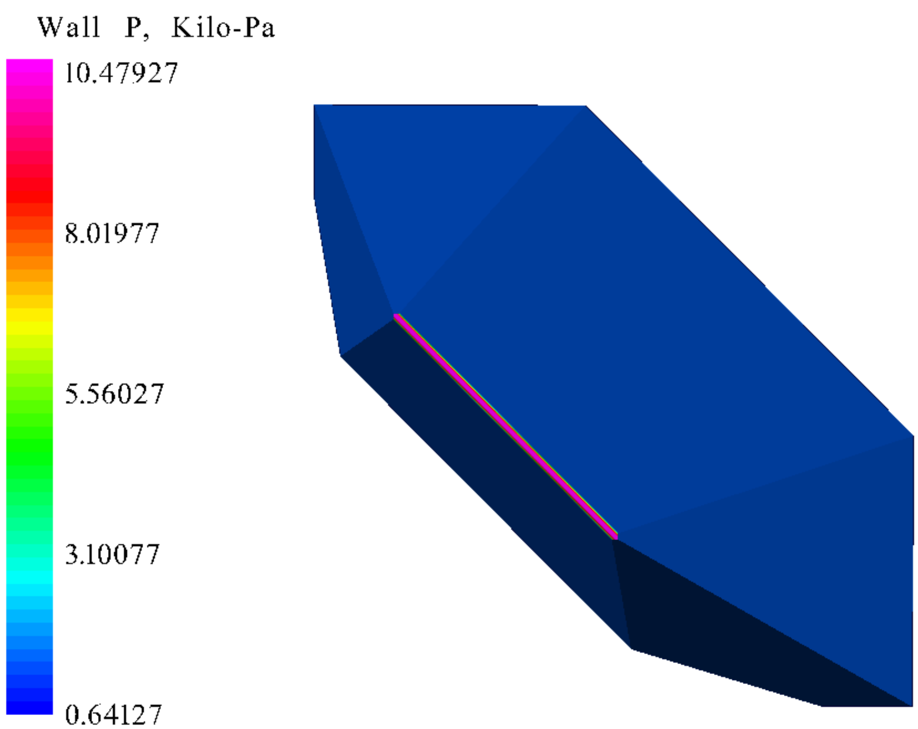

Figure 76. Proto-Waverider Pressure at Mach 2.59, 30.27 km Altitude, and 8° AOA

The wall temperatures only reach around 480 K while the maximum temperature is 527 K. The maximum wall pressure is only around 10 kPa as seen in Figure 76. The C_L at 8° AOA is 0.0764 while the C_D is 0.0350 resulting in a L/D of 2.18. The temperature and pressure values for a 12° angle of attack at 30.27 km altitude traveling at Mach 2.59 can be seen in Figures 77 and 78 respectively.

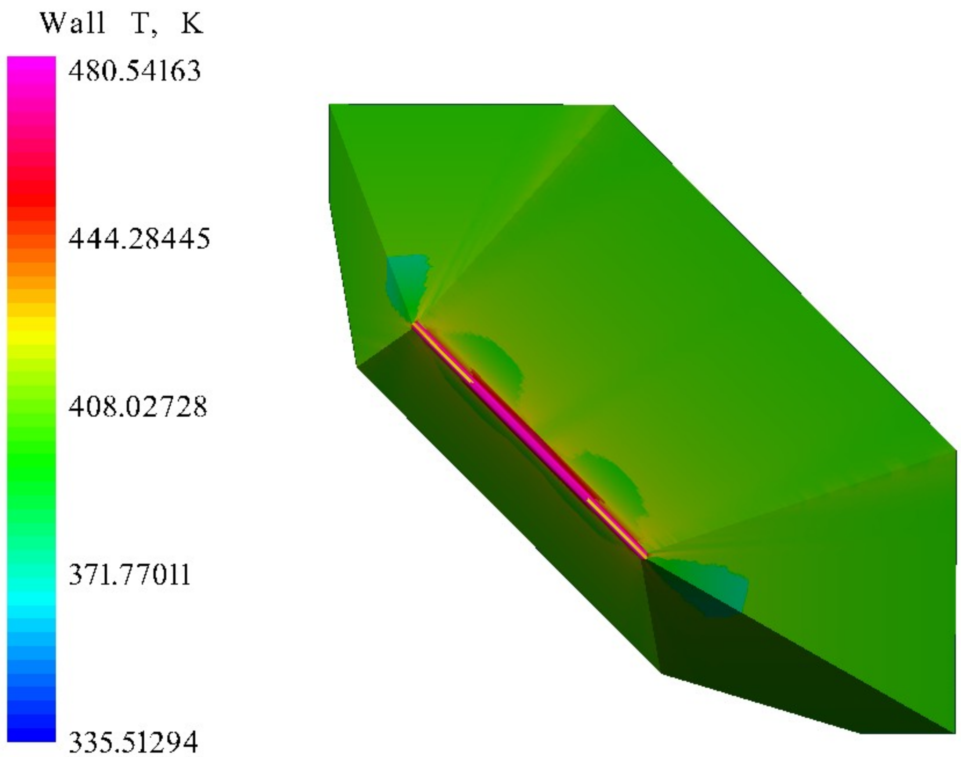

Figure 77. Proto-Waverider Temperature at Mach 2.59, 30.27 km Altitude, and 12° AOA

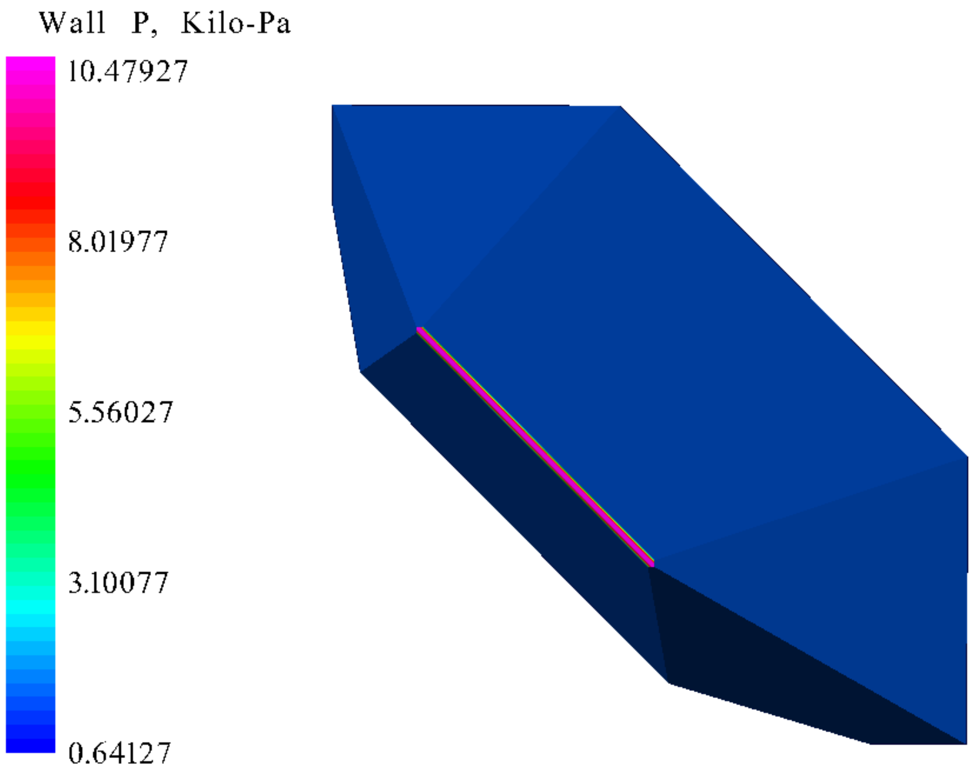

Figure 78. Proto-Waverider Pressure at Mach 2.59, 30.27 km Altitude, and 12° AOA

At an AOA of 12°, the nose of the proto-waverider reaches approximately 480 K while the maximum temperature is around 527 K. Like the 8° AOA, the maximum pressure is only around 10 kPa. In this run the C_L is 0.1484 while the C_D is 0.0550. The L/D for this case is 2.70, which is to be expected as the vehicle is descending at a slower rate.

8.2.4 Results from Secondary Dynamic Pressure Spike Simulations (Mach 2.39, 28.24 km)

The wall temperature and pressure for 0° angle of attack at Mach 2.39 can be seen in Figures 79 and 80. The proto-waverider is traveling at 28.24 km having skipped along the atmosphere and began its descent again. This particular case was identified in the trajectory data as being another high dynamic pressure condition.

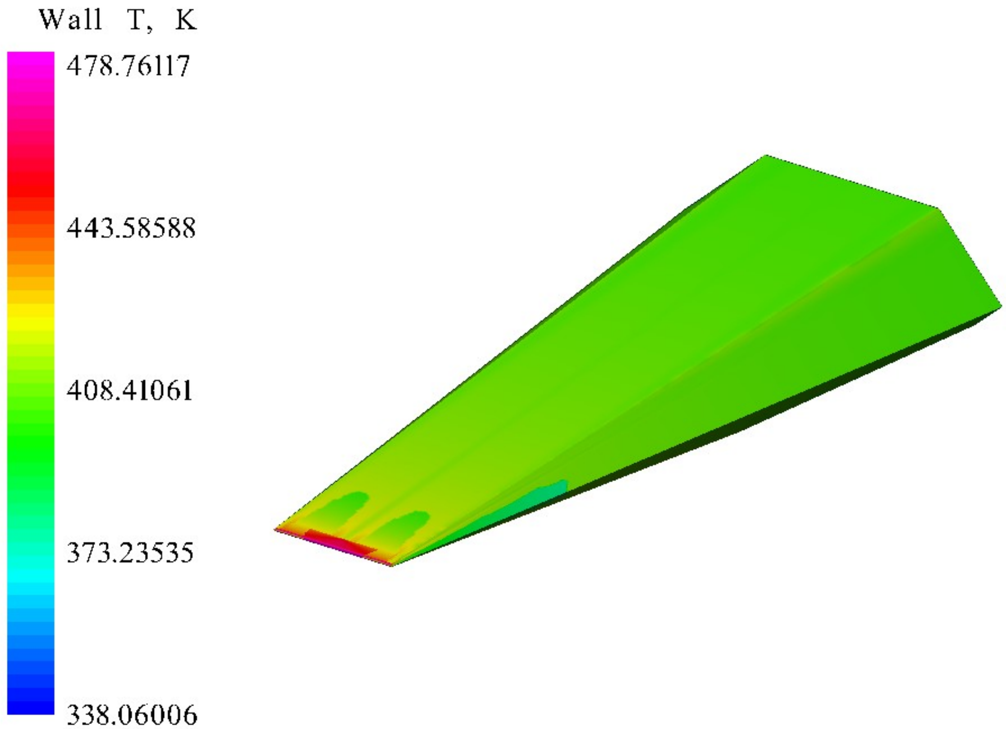

Figure 79. Proto-Waverider Temperature at Mach 2.39, 28.24 km Altitude, and 0° AOA

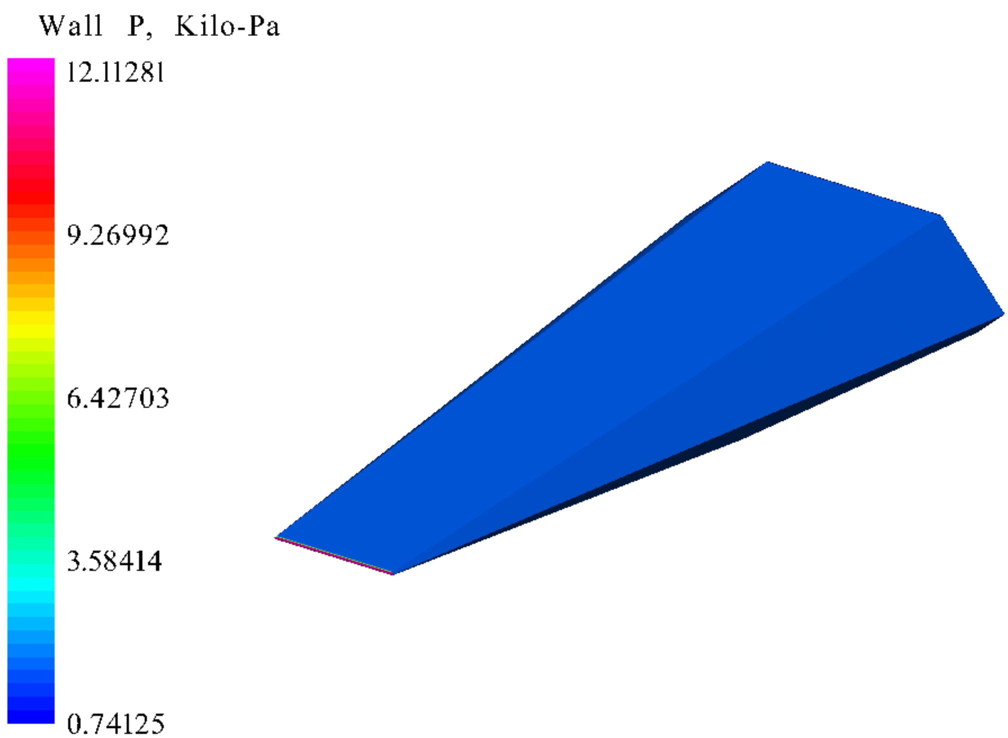

Figure 80. Proto-Waverider Pressure at Mach 2.39, 28.24 km Altitude, and 0° AOA

In this condition, secondary maximum dynamic pressure spike has a high temperature of only 479 K with the temperature along the top and sides of the vehicle around 400 K. For Figure 80 we can see that the wall pressure at the tip is only around 12 kPa while Appendix D gives a maximum pressure of 11.57 kPa. Figure 81 shows a very similar profile to Figure 71, though the high temperature section in the exact middle of the nose on the upper portion is not as large. Figure 82 shows the temperature profile for the underside of the proto-waverider and most of the proto-waverider experiences temperatures around 400 K as noted.

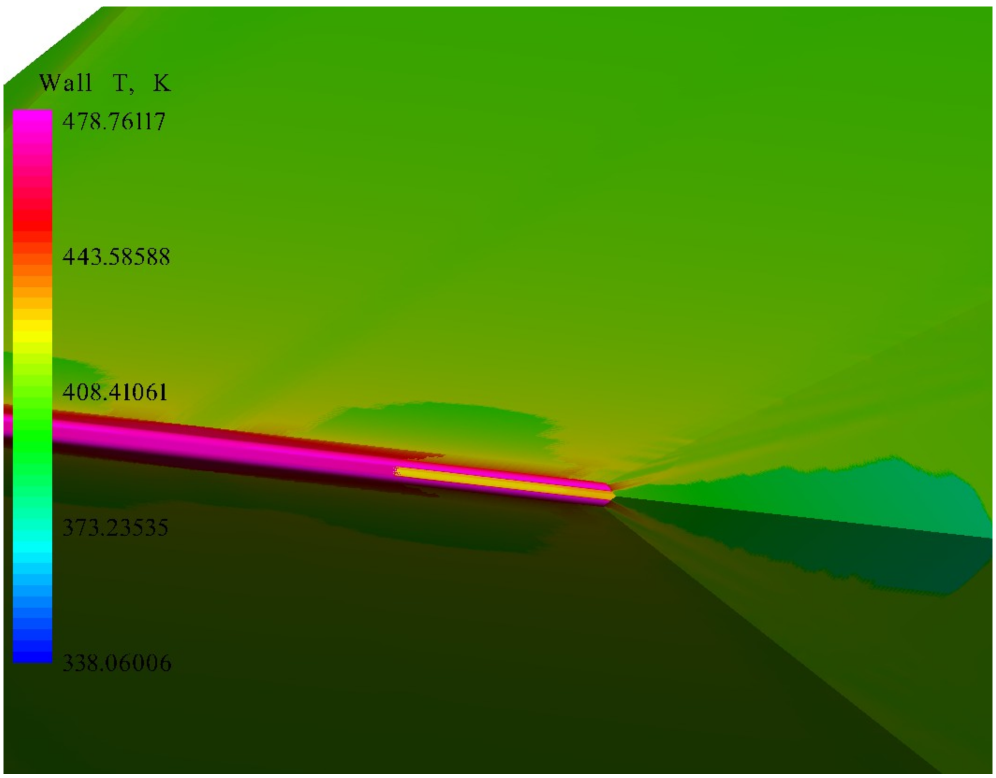

Figure 81. Proto-Waverider Nose Temp. at Mach 2.39, 28.24 km Altitude, and 0° AOA

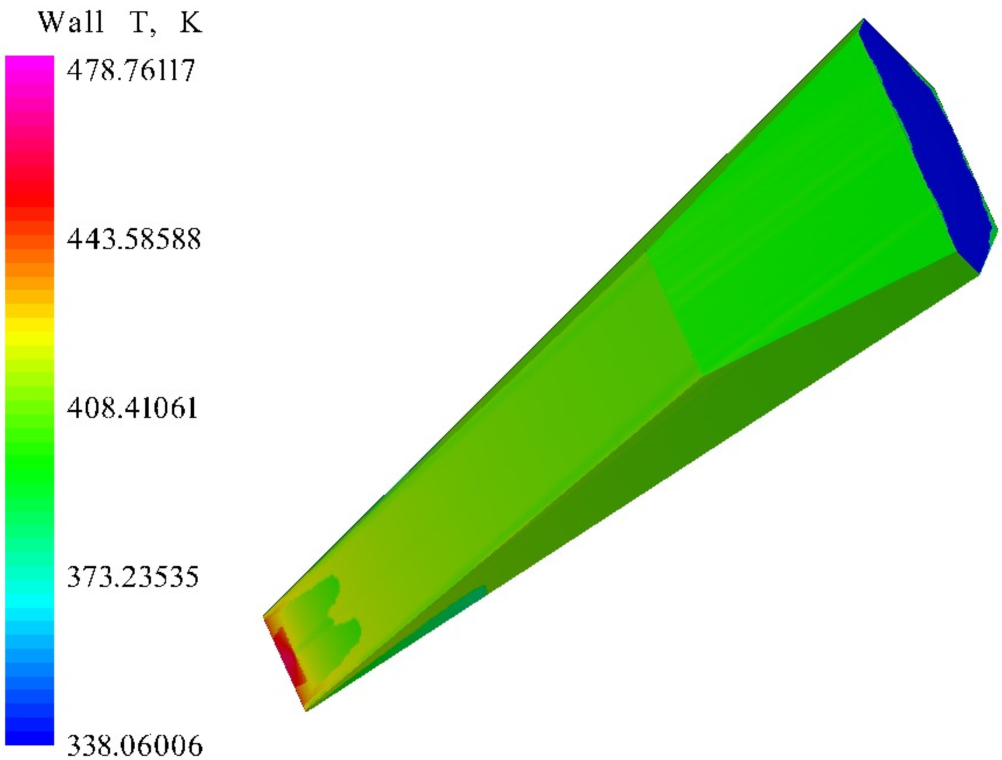

Figure 82. Proto-Waverider Bottom Temp. at Mach 2.39, 28.24 km Altitude, and 0° AOA

The C_L for this secondary maximum heating condition is -0.0221 while the C_D is 0.0273, a L/D of 0.81 in the downward direction. The angle of attack is increased to 4° for this secondary dynamic pressure spike in Figures 83 and 84.

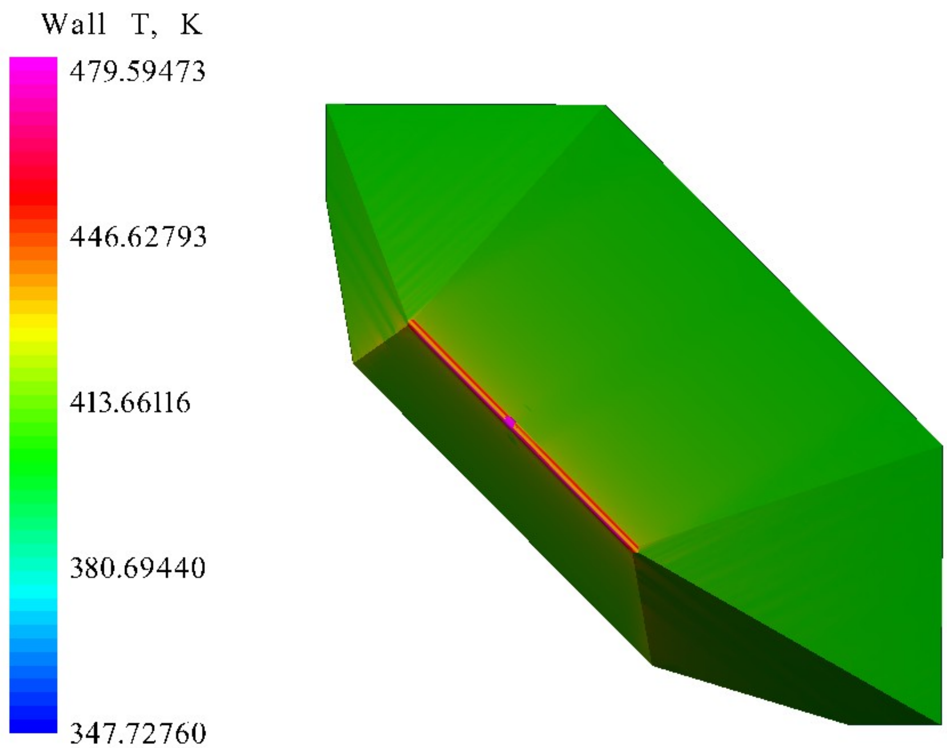

Figure 83. Proto-Waverider Temperature at Mach 2.39, 28.24 km Altitude, and 4° AOA

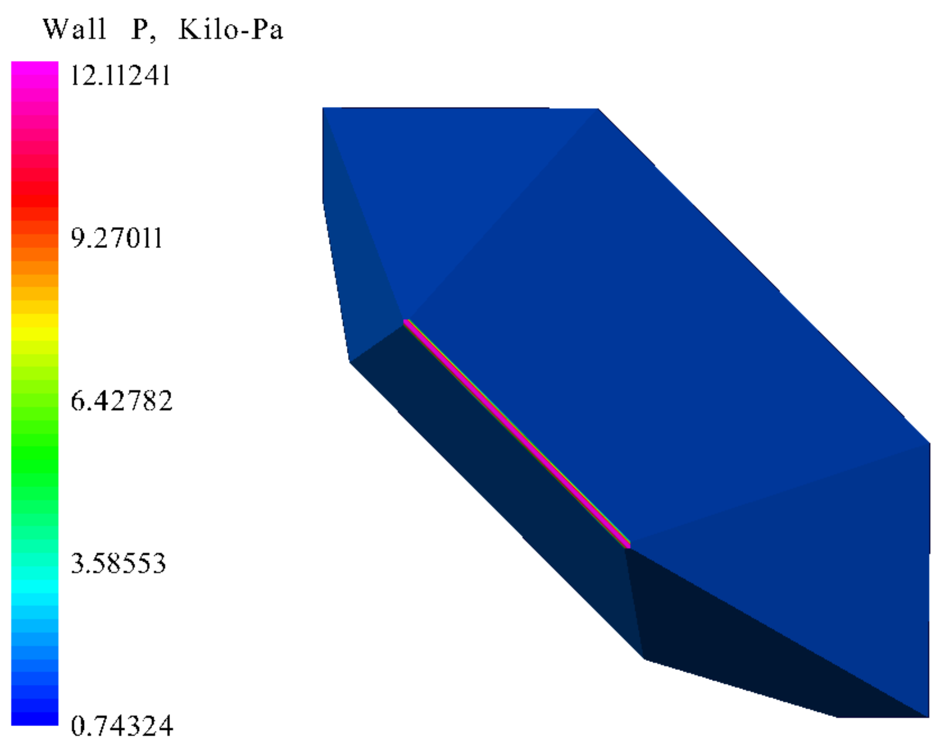

Figure 84. Proto-Waverider Pressure at Mach 2.39, 28.24 km Altitude, and 4° AOA

The proto-waverider reaches a maximum temperature around 479 K, with a maximum pressure of in the region of 12 kPa. Figure 83 once again shows the temperature anomaly. For this 4° AOA condition the C_L is 0.0184 and the C_D is 0.0279 with a L/D of 0.66. In Figures 85 and 86 the temperature and pressure values at 8° angle of attack are displayed.

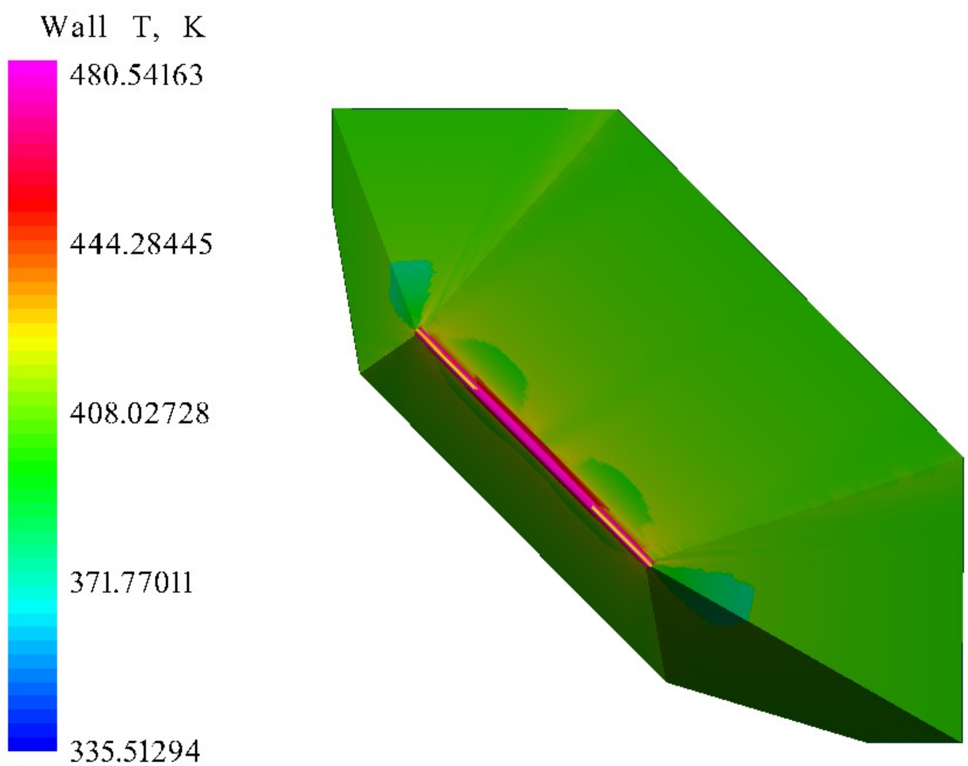

Figure 85. Proto-Waverider Temperature at Mach 2.39, 28.24 km Altitude, and 8° AOA

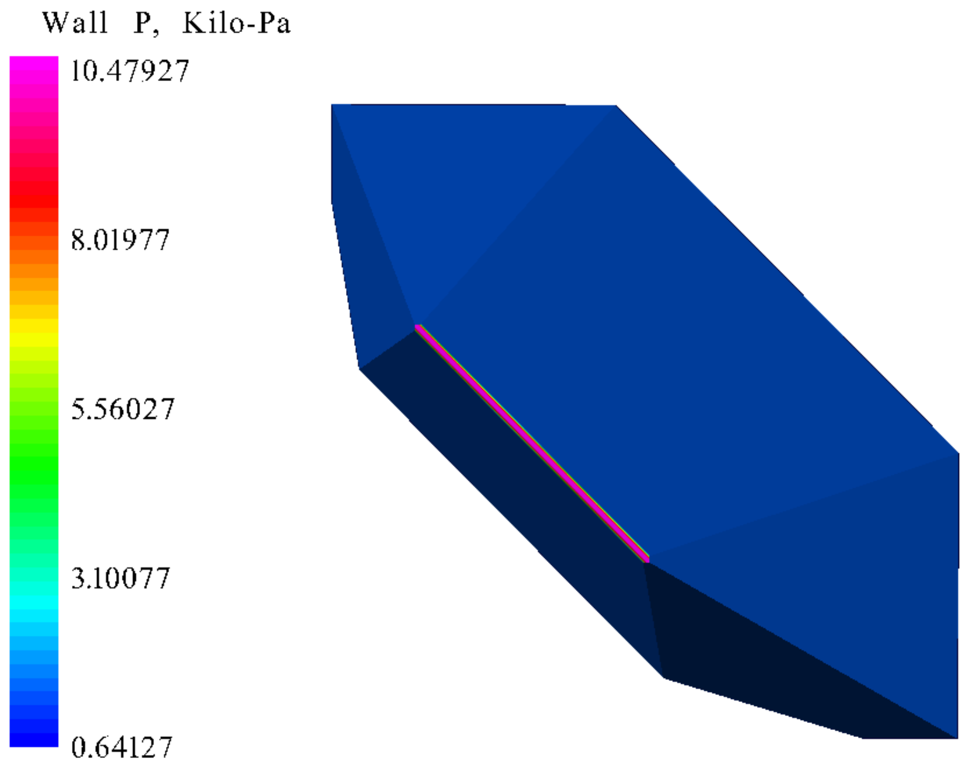

Figure 86. Proto-Waverider Pressure at Mach 2.39, 28.24 km Altitude, and 8° AOA

The wall temperatures only reach around 480 K and the maximum wall pressure is only around 10 kPa as seen in Figure 86 with a maximum total pressure of 12.11 kPa. The C_L at 8° AOA is 0.0796 while the C_D is 0.0367 resulting in a L/D of 2.17. The temperature and pressure values for a 12° angle of attack at 28.24 km altitude traveling at Mach 2.39 can be seen in Figures 87 and 88 respectively.

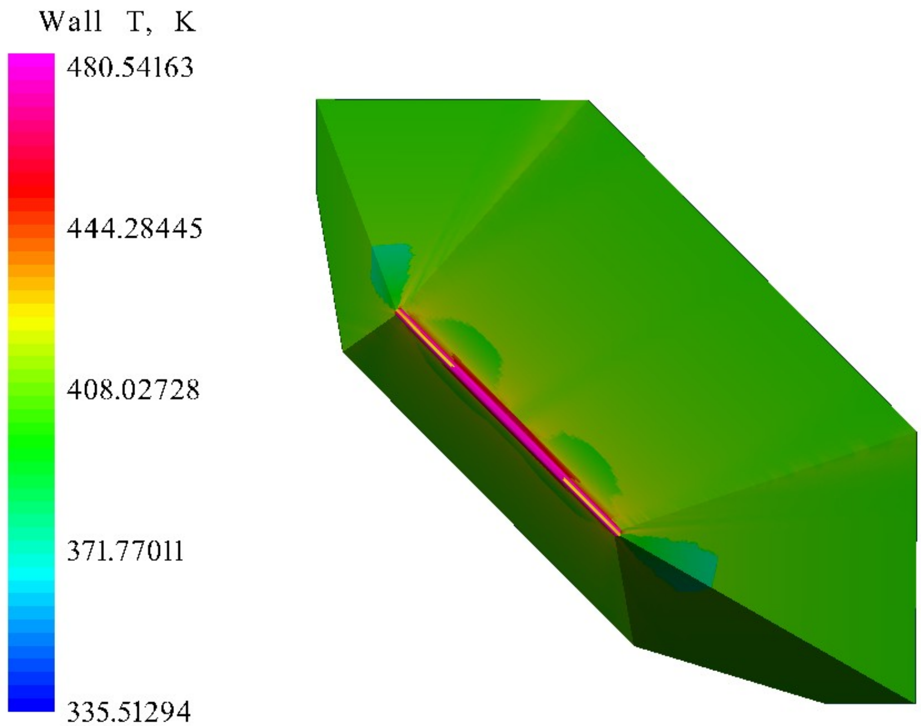

Figure 87. Proto-Waverider Temperature at Mach 2.39, 28.24 km Altitude, and 12° AOA

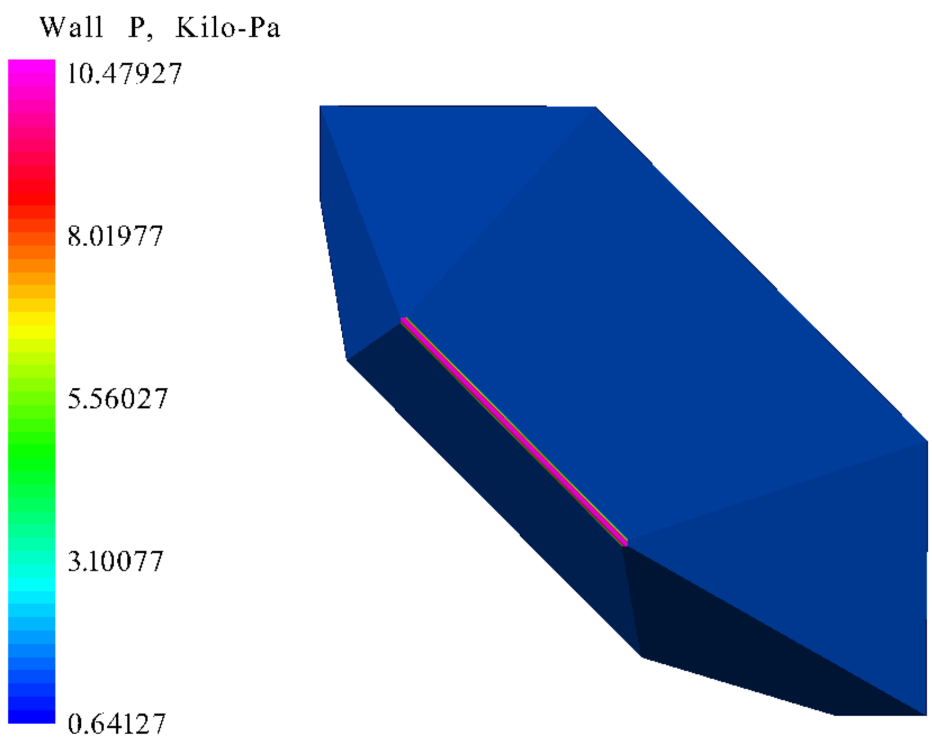

Figure 88. Proto-Waverider Pressure at Mach 2.39, 28.24 km Altitude, and 12° AOA

At an AOA of 12°, the nose of the proto-waverider reaches approximately 480 K the wall pressure is only around 10.5 kPa. Like the 8° AOA, the maximum pressure is only around 12.11 kPa. In this run the C_L is 0.1559 while the C_D is 0.0574 resulting in a L/D of 2.72.

8.3 Discussion

The CFD analysis of the proto-waverider reveals a couple important issues that must be addressed when building an actual one. The first is that the nose will experience a considerable amount of heat and will need to be able to handle temperatures in excess of 1500 K. One possible method to mitigate the higher temperatures is to use an ablative material that will burn off upon re-entry like the BOR-4. Another option is to use heat pipes within the nose of the waverider. By pulling the heat back away from the nose to the rest of the body (where temperatures are not as extreme) would help keep the waverider from disintegrating upon re-entry. While the temperature is highest at the nose of the proto-waverider, the pressure is as well. The material used will need to be able to take the forces of descent without deforming.

The CFD analysis also reveals an area of issue with the tip of the nose, perhaps indicating that the mesh along that particular region was not very uniform or that a cell had collapsed upon transferring between programs. It should be also noted that CBAERO could not compute the coefficient of lift and coefficient of drag for the 10° angle of attack. While multiple calculations were performed, the issue could not be resolved. It is advised that perhaps further direction from the code's author would be needed to address and correct this issue.

9. Conclusion

In order to support a higher down-mass, new technologies must be investigated. With hypersonic waveriders, their use provides a high-speed re-entry without the dramatic forces of a capsule re-entering the atmosphere. This application could also be suited for other missions where instrumentation or experimental materials cannot take the high re-entry forces associated with a blunt body descending. The proto-waverider could be one answer, supplying a basic vehicle with a lifting body shape. In order to determine if it is feasible we looked at previous versions of high L/D re-entry bodies and sought to determine if this proto-waverider would work using CFD. The results were positive, but there is still more that needs to be done.

Now that we are able to use a CFD solver on the proto-waverider, the results taken from these simulations can be imported into NASA's trajectory software where the aerodynamic database will be exclusively of the proto-waverider. The new trajectory results will used to conduct more CFD simulations, which in turn can be used again to refine trajectory possibilities so that more CFD runs would be conducted. This in turn will allow a thermal protection system for the waverider to be designed, and a more accurate body with a center of gravity and a well-defined thermal protection system can be simulated. Once all these results are calculated, the proto-waverider will have the wings attached and undergoes further simulations to help either change the design or to enhance its capabilities.

While there have been recent setbacks to the field of hypersonic waveriders, the idea is still strong and with CFD it can be refined without the need for constantly building and testing what may or may not work. Their use in future space missions would greatly benefit the scientific opportunities and provide additional resources that are not available with the small capsule missions.

Works Cited

1. Murbach, M. S., Boronowsky, K. M., Benton J. E., White, B., and Fritzlers, E. “Options for Returning Payloads from the ISS after the Termination of STS Flights.” American Institute of Aeronautics and Astronautics. *Proceedings of the 40th International Conference on Environmental Systems, Barcelona, Spain, July 11-15, 2010.* AIAA-2010-6223.

2. Lewis, M. J. “The Use of Hypersonic Waveriders for Aero-Assisted Orbital Maneuvering.” British Interplanetary Society, Journal vol. 46, no. 1 p. 11-20 January 1993.

3. Takashima, N., and Lewis, M. J. “Engine-Airframe Integration on Osculating Cone Waverider-Based Vehicle Designs.” American Institute of Aeronautics and Astronautics. *Joint Propulsion Conference and Exhibit, 32nd, Lake Buena Vista, FL, July 1-3, 1996.* AIAA-1996-2551.

4. Bowcutt, K. G., Anderson, J. D. Jr., Capriotti, D. “Numerical Optimization of Conical Flow Waveriders Including Detailed Viscous Effects.” AGARD, Aerodynamics of Hypersonic Lifting Vehicles, 23 p, November 1, 1987.

5. Bowcutt, K. G., Anderson, J. D. Jr., Capriotti, D. “Viscous Optimized Hypersonic Waveriders.” *Aerospace Sciences Meeting, 25th, Reno, NV, Jan 12-15, 1987*. 19 p. AIAA-1987-272.

6. Sobieczky, H., Dougherty, F. C., and Jones, K. “Hypersonic Waverider Design from Given Shock Waves.” 1st International Hypersonic Waverider Symposium, College Park, MD, Oct. 17-19, 1990. Proceedings (A91-25728 09-02), 1990, 18 p.

7. Takashima, N., and Lewis, M. J. “Wedge-Cone Waverider Configuration for Engine-Airframe Interaction.” Journal of Aircraft, 1995, 0021-8669 vol.32 no.5 (1142-1144).

8. Wade, M. “Saenger.” Encyclopedia Astronautica. Accessed Nov. 11, 2010 from <http://www.astronautix.com/lvs/saenger.htm>.

9. Wade, M. “Dynasoar.” Encyclopedia Astronautica. Accessed Nov. 11, 2010 from <http://www.astronautix.com/craft/dynasoar.htm>.

10. Wade, M. “HL-20.” Encyclopedia Astronautica. Accessed Nov. 11, 2010 from <http://www.astronautix.com/craft/hl20.htm>.

11. Wade, M. “X-38.” Encyclopedia Astronautica. Accessed Nov. 11, 2010 from <http://www.astronautix.com/craft/x38.htm>.

12. Wade, M. “X-37.” Encyclopedia Astronautica. Accessed Nov. 11, 2010 from <http://www.astronautix.com/craft/x37.htm>.

13. Wade, M. “Hermes.” Encyclopedia Astronautica. Accessed Nov. 11, 2010 from <http://www.astronautix.com/craft/hermes.htm>.

14. Wade, M. “BOR-4.” Encyclopedia Astronautica. Accessed Nov. 11, 2010 from <http://www.astronautix.com/craft/bor4.htm>.

15. Petrovitch, V. “BOR Description.” Buran Energia Project. Accessed Nov. 11, 2010 from <http://www.buran-energia.com/bor/bor-desc.php>.

16. Wade, M. “Asset.” Encyclopedia Astronautica. Accessed Nov. 11, 2010 from <http://www.astronautix.com/craft/asset.htm>.

17. Wade, M. “Prime.” Encyclopedia Astronautica. Accessed Nov. 11, 2010 from <http://www.astronautix.com/craft/prime.htm>.

18. Peebles, C. “NASA – The M2-F1: ‘Look Ma! No Wings!’.”. National Aeronautics and Space Administration. NASA Dryden Flight Research Center. Accessed Nov. 11, 2010 from <http://www.nasa.gov/topics/history/M2_F1.html>.

19. Reed, D. R. and Lister, D. <u>Wingless Flight: The Lifting Body Story</u>. NASA History Services. National Aeronautics and Space Administration. 1997.

20. Wade, M. “Kehlet Lenticular Vehicle.” Encyclopedia Astronautica. Accessed Nov. 11, 2010 from <http://www.astronautix.com/craft/kehhicle.htm>.

21. Murray, K., Armbrust, W., Pirozzoli, K., Bucad, A., Bushnell, N., and Nicholson, M. <u>SHARP Reentry Vehicle Prototype</u>. Santa Clara University. School of Engineering. 2003. Accessed Sep. 16, 2010 from < http://www.cse.scu.edu/srprojects/2003/COEN-2003-PROJECT-28.pdf >.

22. Anderson, J., Lewis, M., & Kothari, A. “Hypersonic Waveriders for Planetary Atmospheres.” American Institute of Aeronautics and Astronautics. *28th Aerospace Sciences Meeting, Reno, NV, Jan. 8-11, 1990*. 15 p. AIAA 90-0538.

23. Anderson, J. <u>Hypersonic and High-Temperature Gas Dynamics</u>. 2nd Edition. AIAA Education Series. American Institute of Aeronautics and Astronautics, United States, 2006.

Appendix A

The tables used in the following sections are all from Modern Compressible Flow by John D. Anderson, McGraw-Hill, 2003.

Solve for Region 2

1. $M_1 = 10 \xrightarrow{Table A.5} \nu(M_1) = 102.3$

2. $\nu_2 = \nu_1 + \alpha = 102.3 + 10 = 112.3$

3. $\nu_2 = 112.3 \xrightarrow{Table A.5} M_2 = 15.7$

4. $M_1 = 10 \xrightarrow{Table A.1} \dfrac{p_{01}}{p_1} = 42440$

5. $M_2 = 15.7 \xrightarrow{Table A.1} \dfrac{p_{02}}{p_2} = 917660$

Solve for Region 4

Using a θ-β-M chart for M_1=10 & θ=20°: β=26°

1. $M_{1n} = M_1 \sin\beta = 10\sin(26°) = 4.384$

2. $M_{1n} = 4.384 \xrightarrow{Table A.2} \dfrac{p_4}{p_1} = 22.26$

3. $M_{1n} = 4.384 \xrightarrow{Table A.2} \dfrac{p_{04}}{p_{01}} = 0.1008$

4. $M_{1n} = 4.384 \xrightarrow{Table A.2} M_{4n} = 0.4259$

5. $M_4 = \dfrac{M_{4n}}{\sin(\beta - 2\varepsilon)} = \dfrac{0.4259}{\sin(26° - 2(10°))} = 4.07$

6. $M_4 = 4.07 \xrightarrow{Table A.5} \nu_4 = 66.70$

7. $M_4 = 4.07 \xrightarrow{Table A.1} \dfrac{p_{04}}{p_4} = 166.7$

Solve for Region 5

1. $\nu_5 = \nu_4 + 2\varepsilon = 66.70 + 2(10) = 86.70$

2. $\nu_5 = 86.70 \xrightarrow{Table A.5} M_5 = 6.26$

3. $M_5 = 6.26 \xrightarrow{Table A.1} \frac{p_{05}}{p_5} = 2054$

Solve for C_l and C_d

1. $\frac{p_2}{p_1} = \frac{p_2}{p_{02}}\frac{p_{02}}{p_{01}}\frac{p_{01}}{p_1} = \frac{1}{917660}(1)(42440) = 0.04625$

2. $\frac{p_5}{p_1} = \frac{p_5}{p_{05}}\frac{p_{05}}{p_{04}}\frac{p_{04}}{p_{01}}\frac{p_{01}}{p_1} = \frac{1}{2054}(1)(0.1008)(42440) = 2.083$

3. $L' = p_4\cos(20°) + (p_5 - p_2)\cos(10°)$

4.
$$C_l = \frac{2}{\gamma M_1^2}\frac{l}{c}\left[\frac{p_4}{p_1}\cos(20°) + \left(\frac{p_5}{p_1} - \frac{p_2}{p_1}\right)\cos(10°)\right] =$$
$$\frac{2}{(1.4)10^2}\frac{l}{c}\left[22.26\cos(20°) + (2.083 - 0.04625)\cos(10°)\right] = 0.327\frac{l}{c}$$

5. $D' = p_4\sin(20°) + (p_5 - p_2)\sin(10°)$

6.
$$C_d = \frac{2}{\gamma M_1^2}\frac{l}{c}\left[\frac{p_4}{p_1}\sin(20°) + \left(\frac{p_5}{p_1} - \frac{p_2}{p_1}\right)\sin(10°)\right] =$$
$$\frac{2}{(1.4)10^2}\frac{l}{c}\left[22.26\sin(20°) + (2.083 - 0.04625)\sin(10°)\right] = 0.114\frac{l}{c}$$

Find L/D and Error

1. $\left(\frac{L}{D}\right)_{calc} = \frac{C_l}{C_d} = \frac{0.327\frac{l}{c}}{0.114\frac{l}{c}} = 2.88$

$$2.\ \%Error = \frac{\left|\left(\frac{L}{D}\right)_{real} - \left(\frac{L}{D}\right)_{calc}\right|}{\left(\frac{L}{D}\right)_{real}} x100\% = \frac{\left|3.5 - 2.88\right|}{3.5}\left(100\%\right) = 17.8\%$$

Appendix B

This is selective portion of the trajectory values for re-entry from a 300 km sounding rocket launch. Important conditions highlighted where maximum heating is in green and maximum dynamic pressure are in orange.

Time	Beta	qbar	az decel	Reinf	Minf	height	Vinf	Range	Phi	Qmax
1	331	3.25E-06	9.81E-09	8.62E-05	0.57037	299.99559	0.58219	0.55582	82.28926	2.08E-04
2	331	9.03E-06	2.73E-08	1.44E-04	1.58554	299.98237	0.58239	1.48254	120.37236	9.52E-04
3	331	3.26E-06	9.84E-09	8.63E-05	0.57124	299.96033	0.58273	2.03837	82.35348	2.09E-04
4	331	9.05E-06	2.73E-08	1.44E-04	1.58635	299.92947	0.5832	2.96511	120.43399	9.54E-04
5	331	3.27E-06	9.89E-09	8.66E-05	0.57298	299.8898	0.58381	3.52095	82.48187	2.10E-04
6	331	9.08E-06	2.74E-08	1.44E-04	1.58771	299.84131	0.58455	4.44771	120.53697	9.58E-04
7	331	3.30E-06	9.97E-09	8.71E-05	0.5756	299.784	0.58543	5.00358	82.67402	2.12E-04
8	331	9.13E-06	2.76E-08	1.45E-04	1.58961	299.71788	0.58643	5.93037	120.68101	9.62E-04
9	331	3.33E-06	1.01E-08	8.77E-05	0.57907	299.64294	0.58757	6.48628	82.92939	2.15E-04
10	331	9.19E-06	2.78E-08	1.46E-04	1.59204	299.55918	0.58885	7.41311	120.86596	9.68E-04
11	331	3.38E-06	1.02E-08	8.84E-05	0.58341	299.46661	0.59025	7.96906	83.2473	2.18E-04
12	331	9.26E-06	2.80E-08	1.47E-04	1.59502	299.36522	0.59178	8.89595	121.09164	9.75E-04
13	331	3.43E-06	1.04E-08	8.93E-05	0.5886	299.25501	0.59345	9.45196	83.6269	2.22E-04
14	331	9.34E-06	2.82E-08	1.48E-04	1.59853	299.13598	0.59524	10.3789	121.35782	9.84E-04
15	331	3.49E-06	1.05E-08	9.03E-05	0.59463	299.00813	0.59715	10.93498	84.0672	2.27E-04
16	331	9.44E-06	2.85E-08	1.49E-04	1.60257	298.87147	0.59919	11.862	121.66521	9.94E-04
17	331	3.56E-06	1.08E-08	9.15E-05	0.60149	298.72598	0.60136	12.41815	84.56853	2.32E-04
18	331	9.56E-06	2.89E-08	1.50E-04	1.60714	298.57168	0.60365	13.34525	122.01385	1.01E-03
19	331	3.64E-06	1.10E-08	9.28E-05	0.60918	298.40855	0.60606	13.90148	85.12845	2.38E-04
200	331	3.15E-02	9.52E-05	4.96E-01	4.83532	122.10743	1.89872	119.72475	449.67706	1.86E-01
201	331	3.91E-02	1.18E-04	6.37E-01	4.99474	120.30784	1.90765	120.33239	462.10513	2.07E-01
202	331	4.92E-02	1.49E-04	8.36E-01	5.1728	118.49895	1.91658	120.94058	475.69493	2.32E-01
203	331	6.30E-02	1.90E-04	1.12E+00	5.36938	116.68074	1.92552	121.54931	490.57375	2.63E-01
204	331	8.21E-02	2.48E-04	1.53E+00	5.58825	114.85321	1.93447	122.1586	506.88822	3.00E-01
205	331	1.10E-01	3.31E-04	2.16E+00	5.83385	113.01636	1.94342	122.76844	525.05258	3.45E-01
206	331	1.51E-01	4.55E-04	3.16E+00	6.11098	111.17019	1.95239	123.37884	545.69501	4.02E-01
207	331	2.12E-01	6.40E-04	4.75E+00	6.4105	109.31469	1.96137	123.98981	568.94522	4.75E-01
208	331	2.96E-01	8.94E-04	6.93E+00	6.62659	107.44984	1.97035	124.60134	592.42894	5.59E-01
209	331	4.14E-01	1.25E-03	9.98E+00	6.79637	105.57566	1.97935	125.21344	616.81836	6.57E-01
210	331	5.80E-01	1.75E-03	1.43E+01	6.93962	103.69213	1.98835	125.82612	642.3835	7.73E-01
211	331	8.15E-01	2.46E-03	2.05E+01	7.06316	101.79925	1.99736	126.43937	669.16658	9.10E-01
212	331	1.15E+00	3.48E-03	2.93E+01	7.17007	99.89701	2.00638	127.05321	697.18809	1.07E+00
213	331	1.64E+00	4.97E-03	4.23E+01	7.26184	97.98542	2.01541	127.66764	727.27971	1.27E+00
214	331	2.35E+00	7.11E-03	6.09E+01	7.33919	96.06446	2.02444	128.28266	758.7029	1.50E+00
215	331	3.37E+00	1.02E-02	8.75E+01	7.4024	94.13415	2.03349	128.89829	791.29502	1.78E+00
216	331	4.83E+00	1.46E-02	1.25E+02	7.45144	92.19447	2.04253	129.51454	824.96101	2.10E+00
217	331	6.89E+00	2.08E-02	1.78E+02	7.48654	90.24543	2.05158	130.13142	859.65342	2.48E+00
218	331	9.84E+00	2.97E-02	2.53E+02	7.51957	88.28703	2.06063	130.74894	895.58439	2.92E+00
219	331	1.41E+01	4.26E-02	3.61E+02	7.55259	86.31929	2.06968	131.36714	932.89469	3.44E+00
220	331	1.98E+01	5.98E-02	4.97E+02	7.52009	84.34223	2.07873	131.98605	969.67848	4.01E+00
221	331	2.76E+01	8.34E-02	6.78E+02	7.47705	82.35587	2.08776	132.60572	1006.90309	4.66E+00
222	331	3.83E+01	1.16E-01	9.22E+02	7.43515	80.36024	2.09677	133.2262	1044.71684	5.40E+00
223	331	5.29E+01	1.60E-01	1.25E+03	7.3943	78.35541	2.10576	133.84757	1083.08538	6.24E+00
224	331	7.28E+01	2.20E-01	1.68E+03	7.35441	76.34144	2.1147	134.46996	1121.94049	7.19E+00
225	331	9.97E+01	3.01E-01	2.25E+03	7.31537	74.31844	2.12357	135.09351	1162.08085	8.27E+00
226	331	1.36E+02	4.11E-01	3.01E+03	7.27707	72.28656	2.13236	135.71842	1202.9568	9.50E+00
227	331	1.83E+02	5.54E-01	3.97E+03	7.21924	70.24597	2.14104	136.34496	1243.90341	1.09E+01
228	331	2.46E+02	7.42E-01	5.18E+03	7.15675	68.19695	2.14955	136.97349	1285.17803	1.24E+01
229	331	3.27E+02	9.87E-01	6.72E+03	7.09583	66.13982	2.15786	137.60447	1326.97766	1.41E+01
230	331	4.32E+02	1.31E+00	8.69E+03	7.03617	64.07503	2.16589	138.23851	1369.31627	1.60E+01
231	331	5.68E+02	1.72E+00	1.12E+04	6.97745	62.00315	2.17356	138.87639	1412.29329	1.81E+01
232	331	7.43E+02	2.25E+00	1.43E+04	6.91927	59.92493	2.18077	139.51911	1455.901	2.04E+01
233	331	9.66E+02	2.92E+00	1.82E+04	6.86122	57.84133	2.18737	140.16797	1500.29281	2.30E+01
234	331	1.25E+03	3.77E+00	2.30E+04	6.80276	55.75359	2.19322	140.8246	1545.48309	2.59E+01
235	331	1.61E+03	4.85E+00	2.90E+04	6.74332	53.66331	2.1981	141.49107	1591.65719	2.91E+01
236	331	2.05E+03	6.20E+00	3.63E+04	6.68219	51.57252	2.20176	142.16996	1638.95973	3.27E+01
237	331	2.66E+03	8.03E+00	4.70E+04	6.683	49.48382	2.20383	142.86452	1691.66635	3.72E+01
238	331	3.44E+03	1.04E+01	6.09E+04	6.68286	47.40078	2.20379	143.57904	1748.50379	4.24E+01
239	331	4.55E+03	1.38E+01	8.19E+04	6.74389	45.32823	2.20088	144.3191	1782.36989	4.58E+01
240	331	6.02E+03	1.82E+01	1.11E+05	6.79611	43.273	2.19405	145.09225	1807.36177	4.84E+01
241	331	7.94E+03	2.40E+01	1.49E+05	6.83317	41.24458	2.18205	145.90821	1822.52372	5.00E+01
242	331	1.04E+04	3.15E+01	2.01E+05	6.84908	39.25604	2.16331	146.77916	1823.0331	5.01E+01
243	331	1.35E+04	4.09E+01	2.69E+05	6.83644	37.32527	2.13596	147.71969	1801.8836	4.78E+01
244	331	1.73E+04	5.23E+01	3.57E+05	6.78671	35.47644	2.09797	148.74613	1748.55261	4.24E+01
245	331	2.16E+04	6.52E+01	4.63E+05	6.69119	33.74132	2.04743	149.87458	1775.51728	4.51E+01
246	331	2.60E+04	7.86E+01	5.86E+05	6.54278	32.15965	1.98312	151.11728	1788.75325	4.64E+01
247	331	2.97E+04	8.96E+01	6.99E+05	6.30622	30.77674	1.90569	152.47682	1782.61375	4.58E+01
248	331	3.22E+04	9.72E+01	7.98E+05	6.03056	29.63615	1.81785	153.94	1758.74813	4.34E+01
249	331	3.31E+04	9.99E+01	8.67E+05	5.72884	28.77171	1.72362	155.47633	1718.33829	3.95E+01
250	331	3.22E+04	9.73E+01	8.97E+05	5.41763	28.19917	1.62794	157.04181	1664.62261	3.48E+01
251	331	3.00E+04	9.05E+01	8.85E+05	5.11314	27.91175	1.53547	158.58775	1602.08638	2.99E+01
252	331	2.68E+04	8.11E+01	8.40E+05	4.82783	27.88255	1.4497	160.07099	1535.34409	2.52E+01
253	331	2.34E+04	7.06E+01	7.71E+05	4.56897	28.07201	1.37254	161.46085	1468.22068	2.11E+01
254	331	1.99E+04	6.02E+01	6.92E+05	4.33911	28.43667	1.30454	162.74098	1403.35509	1.76E+01
255	331	1.68E+04	5.08E+01	6.10E+05	4.13751	28.9357	1.24529	163.9071	1342.2536	1.47E+01
256	331	1.41E+04	4.26E+01	5.32E+05	3.96163	29.5344	1.19393	164.96325	1285.56861	1.24E+01
257	331	1.18E+04	3.56E+01	4.61E+05	3.80821	30.20504	1.14937	165.91817	1233.39958	1.05E+01
258	331	9.85E+03	2.98E+01	3.98E+05	3.67391	30.9264	1.11059	166.78268	1185.53545	8.96E+00
259	331	8.25E+03	2.49E+01	3.43E+05	3.5557	31.68257	1.07662	167.56792	1141.61712	7.70E+00
260	331	6.91E+03	2.09E+01	2.94E+05	3.4469	32.46185	1.04666	168.28447	1100.93067	6.66E+00

261	331	5.78E+03	1.75E+01	2.50E+05	3.34344	33.25564	1.0201	168.94203	1063.03937	5.79E+00
262	331	4.86E+03	1.47E+01	2.14E+05	3.25005	34.05762	0.99635	169.54925	1028.09825	5.07E+00
263	331	4.11E+03	1.24E+01	1.83E+05	3.16505	34.86324	0.97491	170.11353	995.73499	4.46E+00
264	331	3.48E+03	1.05E+01	1.57E+05	3.08709	35.66918	0.95538	170.64117	965.62691	3.94E+00
265	331	2.97E+03	8.96E+00	1.36E+05	3.01504	36.47303	0.93743	171.13749	937.49787	3.50E+00
266	331	2.54E+03	7.66E+00	1.17E+05	2.948	37.27301	0.92079	171.60697	911.11326	3.13E+00
267	331	2.18E+03	6.58E+00	1.02E+05	2.88523	38.06781	0.90526	172.05338	886.27309	2.80E+00
268	331	1.87E+03	5.66E+00	8.82E+04	2.82611	38.85645	0.89065	172.47992	862.80768	2.51E+00
269	331	1.62E+03	4.89E+00	7.68E+04	2.77014	39.6382	0.87682	172.88929	840.5724	2.27E+00
270	331	1.40E+03	4.24E+00	6.71E+04	2.7169	40.41251	0.86365	173.28379	819.44325	2.05E+00
271	331	1.22E+03	3.69E+00	5.88E+04	2.66604	41.17896	0.85105	173.66535	799.3142	1.85E+00
272	331	1.06E+03	3.21E+00	5.17E+04	2.61727	41.93722	0.83892	174.03565	780.09347	1.68E+00
273	331	9.29E+02	2.81E+00	4.55E+04	2.57035	42.68704	0.82722	174.3961	761.70185	1.53E+00
274	331	8.14E+02	2.46E+00	4.02E+04	2.52507	43.42823	0.81586	174.74793	744.07037	1.39E+00
275	331	7.15E+02	2.16E+00	3.56E+04	2.48125	44.16064	0.80482	175.09217	727.13851	1.27E+00
426	331	4.42E+02	1.34E+00	2.33E+04	2.26982	46.54007	0.74542	217.87673	659.00038	8.56E-01
427	331	4.95E+02	1.50E+00	2.59E+04	2.30029	45.85959	0.75277	218.18764	671.61016	9.23E-01
428	331	5.54E+02	1.68E+00	2.89E+04	2.33056	45.17267	0.75996	218.50196	684.43159	9.95E-01
429	331	6.21E+02	1.88E+00	3.23E+04	2.36056	44.47969	0.76696	218.82009	697.45306	1.07E+00
430	331	6.97E+02	2.11E+00	3.62E+04	2.39021	43.78108	0.77374	219.14246	710.65957	1.16E+00
431	331	7.83E+02	2.36E+00	4.05E+04	2.41939	43.07734	0.78026	219.46956	724.03178	1.25E+00
432	331	8.79E+02	2.66E+00	4.54E+04	2.44799	42.36903	0.78649	219.80195	737.54546	1.34E+00
433	331	9.87E+02	2.98E+00	5.09E+04	2.47589	41.6568	0.7924	220.14022	751.17061	1.44E+00
434	331	1.11E+03	3.35E+00	5.72E+04	2.50292	40.94138	0.79794	220.48507	764.87079	1.55E+00
435	331	1.25E+03	3.77E+00	6.43E+04	2.52891	40.22361	0.80306	220.83723	778.60175	1.67E+00
436	331	1.40E+03	4.23E+00	7.23E+04	2.55368	39.50445	0.8077	221.19754	792.31058	1.79E+00
437	331	1.57E+03	4.75E+00	8.13E+04	2.57699	38.785	0.81181	221.56691	805.93445	1.91E+00
438	331	1.77E+03	5.34E+00	9.14E+04	2.59861	38.06651	0.81532	221.94631	819.39987	2.05E+00
439	331	1.98E+03	5.98E+00	1.03E+05	2.61827	37.35042	0.81816	222.33681	832.62095	2.18E+00
440	331	2.22E+03	6.69E+00	1.16E+05	2.63566	36.63836	0.82025	222.73954	845.49889	2.32E+00
441	331	2.47E+03	7.48E+00	1.30E+05	2.65046	35.93216	0.8215	223.15568	857.92114	2.46E+00
442	331	2.76E+03	8.33E+00	1.45E+05	2.66233	35.23393	0.82184	223.58645	869.76092	2.60E+00
443	331	3.06E+03	9.25E+00	1.63E+05	2.67092	34.54601	0.82117	224.03308	880.87811	2.73E+00
444	331	3.39E+03	1.02E+01	1.82E+05	2.67585	33.87103	0.81942	224.49674	891.11951	2.86E+00
445	331	3.73E+03	1.13E+01	2.02E+05	2.67677	33.21189	0.81648	224.97855	900.32159	2.98E+00
446	331	4.09E+03	1.24E+01	2.24E+05	2.67331	32.57178	0.8123	225.47944	908.31382	3.09E+00
447	331	4.44E+03	1.34E+01	2.46E+05	2.66303	31.95413	0.80681	226.00012	914.73941	3.18E+00
448	331	4.78E+03	1.44E+01	2.68E+05	2.64401	31.36251	0.80002	226.54095	919.27441	3.24E+00
449	331	5.11E+03	1.54E+01	2.89E+05	2.62048	30.80052	0.79193	227.10183	922.15455	3.28E+00
450	331	5.41E+03	1.63E+01	3.11E+05	2.59247	30.27175	0.78256	227.68218	923.27535	3.30E+00
451	331	5.67E+03	1.71E+01	3.31E+05	2.5601	29.77967	0.77196	228.28089	922.56153	3.29E+00
452	331	5.90E+03	1.78E+01	3.50E+05	2.52357	29.32751	0.76019	228.89629	919.97308	3.25E+00
453	331	6.08E+03	1.84E+01	3.67E+05	2.48322	28.91811	0.74736	229.52616	915.50983	3.19E+00
454	331	6.19E+03	1.87E+01	3.82E+05	2.43942	28.55381	0.73359	230.16774	909.21367	3.10E+00
455	331	6.25E+03	1.89E+01	3.94E+05	2.39267	28.23628	0.71903	230.81785	901.16742	2.99E+00
456	331	6.24E+03	1.89E+01	4.02E+05	2.34347	27.96644	0.70383	231.47301	891.49212	2.87E+00
457	331	6.18E+03	1.87E+01	4.07E+05	2.29239	27.74447	0.68815	232.12954	880.34029	2.72E+00
458	331	6.06E+03	1.83E+01	4.09E+05	2.23996	27.5697	0.67215	232.78377	867.888	2.57E+00
459	331	5.89E+03	1.78E+01	4.08E+05	2.18671	27.44078	0.65598	233.43215	854.32582	2.42E+00
460	331	5.67E+03	1.71E+01	4.03E+05	2.13314	27.35565	0.63979	234.07141	839.84917	2.26E+00
461	331	5.43E+03	1.64E+01	3.96E+05	2.07965	27.31173	0.62369	234.69868	824.6507	2.10E+00
462	331	5.16E+03	1.56E+01	3.86E+05	2.02663	27.30604	0.60778	235.31152	808.91281	1.94E+00
463	331	4.88E+03	1.47E+01	3.74E+05	1.97437	27.33532	0.59215	235.90797	792.80283	1.79E+00
464	331	4.58E+03	1.38E+01	3.61E+05	1.9231	27.39615	0.57685	236.48658	776.46932	1.65E+00
465	331	4.29E+03	1.30E+01	3.47E+05	1.87299	27.48511	0.56193	237.04634	760.04116	1.51E+00
466	331	4.00E+03	1.21E+01	3.32E+05	1.82417	27.59883	0.54742	237.58669	743.62703	1.39E+00
467	331	3.72E+03	1.12E+01	3.16E+05	1.7767	27.73407	0.53333	238.1074	727.31611	1.27E+00
468	331	3.45E+03	1.04E+01	3.01E+05	1.73063	27.88778	0.51968	238.60859	711.18016	1.16E+00
469	331	3.19E+03	9.63E+00	2.85E+05	1.68597	28.05713	0.50646	239.09061	695.27518	1.06E+00
470	331	2.94E+03	8.89E+00	2.70E+05	1.64269	28.23953	0.49365	239.554	679.64365	9.68E-01
471	331	2.72E+03	8.20E+00	2.55E+05	1.60077	28.43261	0.48126	239.99945	664.31651	8.84E-01
472	331	2.50E+03	7.56E+00	2.41E+05	1.56016	28.63426	0.46926	240.42774	649.3154	8.06E-01
473	331	2.30E+03	6.96E+00	2.28E+05	1.52082	28.84255	0.45764	240.83975	634.65438	7.36E-01
474	331	2.12E+03	6.41E+00	2.15E+05	1.4827	29.0558	0.44638	241.23635	620.3413	6.72E-01
475	331	1.95E+03	5.90E+00	2.02E+05	1.44573	29.27251	0.43545	241.61846	606.37948	6.13E-01
476	331	1.80E+03	5.43E+00	1.91E+05	1.40986	29.49134	0.42485	241.98697	592.76865	5.60E-01
477	331	1.65E+03	5.00E+00	1.80E+05	1.37504	29.71112	0.41456	242.34277	579.50597	5.12E-01
478	331	1.52E+03	4.60E+00	1.69E+05	1.34121	29.9308	0.40456	242.6867	566.58668	4.68E-01
479	331	1.40E+03	4.24E+00	1.60E+05	1.30834	30.14948	0.39483	243.01959	554.00491	4.27E-01
480	331	1.29E+03	3.90E+00	1.51E+05	1.27637	30.36636	0.38536	243.34222	541.75257	3.91E-01
481	331	1.19E+03	3.60E+00	1.42E+05	1.24527	30.58072	0.37615	243.65531	529.8259	3.58E-01
482	331	1.10E+03	3.32E+00	1.34E+05	1.21501	30.79193	0.36718	243.95956	518.21639	3.27E-01
483	331	1.01E+03	3.07E+00	1.27E+05	1.18555	30.99946	0.35844	244.25563	506.91747	3.00E-01
484	331	9.37E+02	2.83E+00	1.20E+05	1.15686	31.2028	0.34992	244.54412	495.92303	2.74E-01
485	331	8.67E+02	2.62E+00	1.14E+05	1.12893	31.40154	0.34162	244.8256	485.22762	2.52E-01
486	331	8.02E+02	2.42E+00	1.08E+05	1.10174	31.59529	0.33353	245.1006	474.82656	2.31E-01
487	331	7.43E+02	2.24E+00	1.02E+05	1.07527	31.78371	0.32565	245.3696	464.71602	2.12E-01
488	331	6.89E+02	2.08E+00	9.68E+04	1.04953	31.96651	0.31798	245.63306	454.89314	1.94E-01
489	331	6.39E+02	1.93E+00	9.20E+04	1.02449	32.14341	0.31051	245.89141	445.35608	1.79E-01

Appendix C

Max Temperature (in K)

Mach Range:

2.3929998875
2.5920000076
5.7290000916
6.8489999771

Dyn. Pres. (bars) Range:

0.0540600009
0.0624900013
0.1042999998
0.3305000067

AOA (°) Range:

0.0000000000
2.0000000000
4.0000000000
6.0000000000
8.0000000000
10.0000000000
12.0000000000
14.0000000000
16.0000000000
18.0000000000
20.0000000000

Function Data:

Mach	Dyn. Pres. (bars)	AOA (°)	Temp. (K)
2.3929998875	0.0540600009	0.0000000000	480.5416259766
2.3929998875	0.0540600009	2.0000000000	481.0200805664
2.3929998875	0.0540600009	4.0000000000	481.3631286621
2.3929998875	0.0540600009	6.0000000000	481.3978881836
2.3929998875	0.0540600009	8.0000000000	481.4887084961
2.3929998875	0.0540600009	10.0000000000	481.3638000488
2.3929998875	0.0540600009	12.0000000000	481.5314636230
2.3929998875	0.0540600009	14.0000000000	481.2639160156
2.3929998875	0.0540600009	16.0000000000	481.3987426758
2.3929998875	0.0540600009	18.0000000000	481.3817443848
2.3929998875	0.0540600009	20.0000000000	481.3702392578
2.3929998875	0.0624900013	0.0000000000	478.7611694336
2.3929998875	0.0624900013	2.0000000000	479.2792053223
2.3929998875	0.0624900013	4.0000000000	479.5929565430
2.3929998875	0.0624900013	6.0000000000	479.6266479492
2.3929998875	0.0624900013	8.0000000000	479.7099914551
2.3929998875	0.0624900013	10.0000000000	479.5935363770
2.3929998875	0.0624900013	12.0000000000	479.7493286133
2.3929998875	0.0624900013	14.0000000000	479.5065612793

2.3929998875	0.0624900013	16.0000000000	479.6274108887
2.3929998875	0.0624900013	18.0000000000	479.6111450195
2.3929998875	0.0624900013	20.0000000000	479.6019287109
2.3929998875	0.1042999998	0.0000000000	472.4509887695
2.3929998875	0.1042999998	2.0000000000	473.0345458984
2.3929998875	0.1042999998	4.0000000000	473.2681884766
2.3929998875	0.1042999998	6.0000000000	473.2911987305
2.3929998875	0.1042999998	8.0000000000	473.3520507812
2.3929998875	0.1042999998	10.0000000000	473.2687377930
2.3929998875	0.1042999998	12.0000000000	473.3823852539
2.3929998875	0.1042999998	14.0000000000	473.1870422363
2.3929998875	0.1042999998	16.0000000000	473.2914428711
2.3929998875	0.1042999998	18.0000000000	473.2803649902
2.3929998875	0.1042999998	20.0000000000	473.2730102539
2.3929998875	0.3305000067	0.0000000000	463.3136901855
2.3929998875	0.3305000067	2.0000000000	464.0658264160
2.3929998875	0.3305000067	4.0000000000	464.1875610352
2.3929998875	0.3305000067	6.0000000000	464.1996154785
2.3929998875	0.3305000067	8.0000000000	464.2323608398
2.3929998875	0.3305000067	10.0000000000	464.1877441406
2.3929998875	0.3305000067	12.0000000000	464.2474060059
2.3929998875	0.3305000067	14.0000000000	464.1232604980
2.3929998875	0.3305000067	16.0000000000	464.2006225586
2.3929998875	0.3305000067	18.0000000000	464.1946105957
2.3929998875	0.3305000067	20.0000000000	464.1907348633
2.5920000076	0.0540600009	0.0000000000	527.8122558594
2.5920000076	0.0540600009	2.0000000000	522.1615600586
2.5920000076	0.0540600009	4.0000000000	522.1613769531
2.5920000076	0.0540600009	6.0000000000	527.6336669922
2.5920000076	0.0540600009	8.0000000000	527.6203613281
2.5920000076	0.0540600009	10.0000000000	527.6846923828
2.5920000076	0.0540600009	12.0000000000	527.7910766602
2.5920000076	0.0540600009	14.0000000000	527.8052978516
2.5920000076	0.0540600009	16.0000000000	527.6667480469
2.5920000076	0.0540600009	18.0000000000	527.6454467773
2.5920000076	0.0540600009	20.0000000000	527.6286010742
2.5920000076	0.0624900013	0.0000000000	525.8277587891
2.5920000076	0.0624900013	2.0000000000	520.3819580078
2.5920000076	0.0624900013	4.0000000000	520.3814697266
2.5920000076	0.0624900013	6.0000000000	525.6531372070
2.5920000076	0.0624900013	8.0000000000	525.6495361328
2.5920000076	0.0624900013	10.0000000000	525.7057495117
2.5920000076	0.0624900013	12.0000000000	525.8082885742
2.5920000076	0.0624900013	14.0000000000	525.8190307617
2.5920000076	0.0624900013	16.0000000000	525.6955566406
2.5920000076	0.0624900013	18.0000000000	525.7366943359

2.5920000076	0.0624900013	20.0000000000	520.3806152344
2.5920000076	0.1042999998	0.0000000000	518.8143920898
2.5920000076	0.1042999998	2.0000000000	513.9750366211
2.5920000076	0.1042999998	4.0000000000	518.1197509766
2.5920000076	0.1042999998	6.0000000000	518.7614135742
2.5920000076	0.1042999998	8.0000000000	518.7161254883
2.5920000076	0.1042999998	10.0000000000	518.6716918945
2.5920000076	0.1042999998	12.0000000000	518.8258056641
2.5920000076	0.1042999998	14.0000000000	518.7825927734
2.5920000076	0.1042999998	16.0000000000	518.7985229492
2.5920000076	0.1042999998	18.0000000000	518.5090332031
2.5920000076	0.1042999998	20.0000000000	513.9741210938
2.5920000076	0.3305000067	0.0000000000	504.9158935547
2.5920000076	0.3305000067	2.0000000000	505.7312927246
2.5920000076	0.3305000067	4.0000000000	505.8923034668
2.5920000076	0.3305000067	6.0000000000	505.9085388184
2.5920000076	0.3305000067	8.0000000000	505.9511108398
2.5920000076	0.3305000067	10.0000000000	505.8926391602
2.5920000076	0.3305000067	12.0000000000	505.9710693359
2.5920000076	0.3305000067	14.0000000000	505.8148193359
2.5920000076	0.3305000067	16.0000000000	505.9089965820
2.5920000076	0.3305000067	18.0000000000	505.9006958008
2.5920000076	0.3305000067	20.0000000000	505.8956604004
5.7290000916	0.0540600009	0.0000000000	1607.3497314453
5.7290000916	0.0540600009	2.0000000000	1604.2390136719
5.7290000916	0.0540600009	4.0000000000	1587.6475830078
5.7290000916	0.0540600009	6.0000000000	1606.6645507812
5.7290000916	0.0540600009	8.0000000000	1606.4200439453
5.7290000916	0.0540600009	10.0000000000	1605.9062500000
5.7290000916	0.0540600009	12.0000000000	1606.3249511719
5.7290000916	0.0540600009	14.0000000000	1604.4355468750
5.7290000916	0.0540600009	16.0000000000	1603.6186523438
5.7290000916	0.0540600009	18.0000000000	1604.8723144531
5.7290000916	0.0540600009	20.0000000000	1603.9891357422
5.7290000916	0.0624900013	0.0000000000	1616.8762207031
5.7290000916	0.0624900013	2.0000000000	1612.8984375000
5.7290000916	0.0624900013	4.0000000000	1600.1646728516
5.7290000916	0.0624900013	6.0000000000	1613.9510498047
5.7290000916	0.0624900013	8.0000000000	1612.5557861328
5.7290000916	0.0624900013	10.0000000000	1613.8430175781
5.7290000916	0.0624900013	12.0000000000	1611.1660156250
5.7290000916	0.0624900013	14.0000000000	1611.9364013672
5.7290000916	0.0624900013	16.0000000000	1609.2606201172
5.7290000916	0.0624900013	18.0000000000	1611.1292724609
5.7290000916	0.0624900013	20.0000000000	1609.8715820312
5.7290000916	0.1042999998	0.0000000000	1621.3077392578

5.7290000916	0.1042999998	2.0000000000	1607.7739257812
5.7290000916	0.1042999998	4.0000000000	1568.8293457031
5.7290000916	0.1042999998	6.0000000000	1568.8289794922
5.7290000916	0.1042999998	8.0000000000	1617.5368652344
5.7290000916	0.1042999998	10.0000000000	1568.8293457031
5.7290000916	0.1042999998	12.0000000000	1568.8293457031
5.7290000916	0.1042999998	14.0000000000	1614.1906738281
5.7290000916	0.1042999998	16.0000000000	1612.6398925781
5.7290000916	0.1042999998	18.0000000000	1616.0744628906
5.7290000916	0.1042999998	20.0000000000	1568.8293457031
5.7290000916	0.3305000067	0.0000000000	1541.2177734375
5.7290000916	0.3305000067	2.0000000000	1535.7932128906
5.7290000916	0.3305000067	4.0000000000	1519.6728515625
5.7290000916	0.3305000067	6.0000000000	1538.0732421875
5.7290000916	0.3305000067	8.0000000000	1539.6464843750
5.7290000916	0.3305000067	10.0000000000	1538.8194580078
5.7290000916	0.3305000067	12.0000000000	1535.5675048828
5.7290000916	0.3305000067	14.0000000000	1537.9731445312
5.7290000916	0.3305000067	16.0000000000	1540.8625488281
5.7290000916	0.3305000067	18.0000000000	1539.1201171875
5.7290000916	0.3305000067	20.0000000000	1537.8530273438
6.8489999771	0.0540600009	0.0000000000	1999.0098876953
6.8489999771	0.0540600009	2.0000000000	1996.8747558594
6.8489999771	0.0540600009	4.0000000000	1996.8750000000
6.8489999771	0.0540600009	6.0000000000	1996.8464355469
6.8489999771	0.0540600009	8.0000000000	1996.8757324219
6.8489999771	0.0540600009	10.0000000000	1996.8753662109
6.8489999771	0.0540600009	12.0000000000	1996.8464355469
6.8489999771	0.0540600009	14.0000000000	1997.0507812500
6.8489999771	0.0540600009	16.0000000000	1994.8719482422
6.8489999771	0.0540600009	18.0000000000	1996.6922607422
6.8489999771	0.0540600009	20.0000000000	1996.8754882812
6.8489999771	0.0624900013	0.0000000000	2008.9912109375
6.8489999771	0.0624900013	2.0000000000	2005.7431640625
6.8489999771	0.0624900013	4.0000000000	2005.7454833984
6.8489999771	0.0624900013	6.0000000000	2005.0682373047
6.8489999771	0.0624900013	8.0000000000	2005.7612304688
6.8489999771	0.0624900013	10.0000000000	2005.7609863281
6.8489999771	0.0624900013	12.0000000000	2005.7604980469
6.8489999771	0.0624900013	14.0000000000	2005.7607421875
6.8489999771	0.0624900013	16.0000000000	2004.5412597656
6.8489999771	0.0624900013	18.0000000000	2005.7583007812
6.8489999771	0.0624900013	20.0000000000	2005.7612304688
6.8489999771	0.1042999998	0.0000000000	2110.6752929688
6.8489999771	0.1042999998	2.0000000000	2022.0988769531
6.8489999771	0.1042999998	4.0000000000	2022.0987548828

6.8489999771	0.1042999998	6.0000000000	2022.0981445312
6.8489999771	0.1042999998	8.0000000000	2069.4401855469
6.8489999771	0.1042999998	10.0000000000	2089.4331054688
6.8489999771	0.1042999998	12.0000000000	2022.0968017578
6.8489999771	0.1042999998	14.0000000000	2091.1853027344
6.8489999771	0.1042999998	16.0000000000	2088.9399414062
6.8489999771	0.1042999998	18.0000000000	2068.8229980469
6.8489999771	0.1042999998	20.0000000000	2058.3857421875
6.8489999771	0.3305000067	0.0000000000	2028.2999267578
6.8489999771	0.3305000067	2.0000000000	2015.6783447266
6.8489999771	0.3305000067	4.0000000000	1988.5168457031
6.8489999771	0.3305000067	6.0000000000	2016.0169677734
6.8489999771	0.3305000067	8.0000000000	2016.9382324219
6.8489999771	0.3305000067	10.0000000000	1988.5238037109
6.8489999771	0.3305000067	12.0000000000	1988.5238037109
6.8489999771	0.3305000067	14.0000000000	2025.1604003906
6.8489999771	0.3305000067	16.0000000000	2022.1230468750
6.8489999771	0.3305000067	18.0000000000	2021.9052734375
6.8489999771	0.3305000067	20.0000000000	2017.8781738281

Appendix D

Total Pressure (in Pascal)
Mach Range:
2.3929998875
2.5920000076
5.7290000916
6.8489999771
Dyn. Pres. (bars) Range:
0.0540600009
0.0624900013
0.1042999998
0.3305000067
AOA (°) Range:
0.0000000000
2.0000000000
4.0000000000
6.0000000000
8.0000000000
10.0000000000
12.0000000000
14.0000000000
16.0000000000
18.0000000000
20.0000000000

Function Data:

Mach	Dyn. Pres. (bars)	AOA (°)	Total Pres. (Pa)
2.3929998875	0.0540600009	0.0000000000	10010.6484375000
2.3929998875	0.0540600009	2.0000000000	10476.9511718750
2.3929998875	0.0540600009	4.0000000000	10478.8496093750
2.3929998875	0.0540600009	6.0000000000	10478.3613281250
2.3929998875	0.0540600009	8.0000000000	10478.9130859375
2.3929998875	0.0540600009	10.0000000000	10479.1660156250
2.3929998875	0.0540600009	12.0000000000	10478.9921875000
2.3929998875	0.0540600009	14.0000000000	10441.8105468750
2.3929998875	0.0540600009	16.0000000000	10479.0000000000
2.3929998875	0.0540600009	18.0000000000	10478.9580078125
2.3929998875	0.0540600009	20.0000000000	10477.5830078125
2.3929998875	0.0624900013	0.0000000000	11571.1396484375
2.3929998875	0.0624900013	2.0000000000	12110.8535156250
2.3929998875	0.0624900013	4.0000000000	12097.9599609375
2.3929998875	0.0624900013	6.0000000000	12111.7597656250
2.3929998875	0.0624900013	8.0000000000	12112.3984375000
2.3929998875	0.0624900013	10.0000000000	12100.9667968750

2.3929998875	0.0624900013	12.0000000000	12112.4892578125
2.3929998875	0.0624900013	14.0000000000	12069.5107421875
2.3929998875	0.0624900013	16.0000000000	12112.4970703125
2.3929998875	0.0624900013	18.0000000000	12111.5595703125
2.3929998875	0.0624900013	20.0000000000	12112.3935546875
2.3929998875	0.1042999998	0.0000000000	19309.7617187500
2.3929998875	0.1042999998	2.0000000000	20203.5195312500
2.3929998875	0.1042999998	4.0000000000	20212.8710937500
2.3929998875	0.1042999998	6.0000000000	20193.5390625000
2.3929998875	0.1042999998	8.0000000000	20199.5820312500
2.3929998875	0.1042999998	10.0000000000	20213.4824218750
2.3929998875	0.1042999998	12.0000000000	20213.1464843750
2.3929998875	0.1042999998	14.0000000000	20213.5000000000
2.3929998875	0.1042999998	16.0000000000	20202.4375000000
2.3929998875	0.1042999998	18.0000000000	20211.5957031250
2.3929998875	0.1042999998	20.0000000000	20210.4277343750
2.3929998875	0.3305000067	0.0000000000	61187.1250000000
2.3929998875	0.3305000067	2.0000000000	64037.1640625000
2.3929998875	0.3305000067	4.0000000000	63992.1914062500
2.3929998875	0.3305000067	6.0000000000	64007.2304687500
2.3929998875	0.3305000067	8.0000000000	64011.4882812500
2.3929998875	0.3305000067	10.0000000000	63988.7109375000
2.3929998875	0.3305000067	12.0000000000	63988.4101562500
2.3929998875	0.3305000067	14.0000000000	64050.7617187500
2.3929998875	0.3305000067	16.0000000000	64042.6953125000
2.3929998875	0.3305000067	18.0000000000	64044.7265625000
2.3929998875	0.3305000067	20.0000000000	64041.0234375000
2.5920000076	0.0540600009	0.0000000000	9902.1708984375
2.5920000076	0.0540600009	2.0000000000	9587.6914062500
2.5920000076	0.0540600009	4.0000000000	9619.8085937500
2.5920000076	0.0540600009	6.0000000000	9951.7119140625
2.5920000076	0.0540600009	8.0000000000	9895.7998046875
2.5920000076	0.0540600009	10.0000000000	9944.7470703125
2.5920000076	0.0540600009	12.0000000000	9897.1240234375
2.5920000076	0.0540600009	14.0000000000	9878.5292968750
2.5920000076	0.0540600009	16.0000000000	9925.4541015625
2.5920000076	0.0540600009	18.0000000000	9938.0517578125
2.5920000076	0.0540600009	20.0000000000	9908.1835937500
2.5920000076	0.0624900013	0.0000000000	11445.1562500000
2.5920000076	0.0624900013	2.0000000000	11134.5185546875
2.5920000076	0.0624900013	4.0000000000	11150.5244140625
2.5920000076	0.0624900013	6.0000000000	11502.4169921875
2.5920000076	0.0624900013	8.0000000000	11437.7929687500
2.5920000076	0.0624900013	10.0000000000	11494.3671875000
2.5920000076	0.0624900013	12.0000000000	11439.3232421875
2.5920000076	0.0624900013	14.0000000000	11417.8310546875

2.5920000076	0.0624900013	16.0000000000	11472.0673828125
2.5920000076	0.0624900013	18.0000000000	11486.6289062500
2.5920000076	0.0624900013	20.0000000000	11158.5742187500
2.5920000076	0.1042999998	0.0000000000	19383.5937500000
2.5920000076	0.1042999998	2.0000000000	19092.0175781250
2.5920000076	0.1042999998	4.0000000000	19063.4921875000
2.5920000076	0.1042999998	6.0000000000	19459.1308593750
2.5920000076	0.1042999998	8.0000000000	19313.5546875000
2.5920000076	0.1042999998	10.0000000000	19459.6191406250
2.5920000076	0.1042999998	12.0000000000	19429.9199218750
2.5920000076	0.1042999998	14.0000000000	19438.4003906250
2.5920000076	0.1042999998	16.0000000000	19320.3378906250
2.5920000076	0.1042999998	18.0000000000	19167.2734375000
2.5920000076	0.1042999998	20.0000000000	19106.0019531250
2.5920000076	0.3305000067	0.0000000000	60660.8554687500
2.5920000076	0.3305000067	2.0000000000	63552.0039062500
2.5920000076	0.3305000067	4.0000000000	63559.8867187500
2.5920000076	0.3305000067	6.0000000000	63556.8632812500
2.5920000076	0.3305000067	8.0000000000	63560.2812500000
2.5920000076	0.3305000067	10.0000000000	63561.8476562500
2.5920000076	0.3305000067	12.0000000000	63560.7773437500
2.5920000076	0.3305000067	14.0000000000	63561.9140625000
2.5920000076	0.3305000067	16.0000000000	63560.8164062500
2.5920000076	0.3305000067	18.0000000000	63555.7929687500
2.5920000076	0.3305000067	20.0000000000	63552.0429687500
5.7290000916	0.0540600009	0.0000000000	8406.5615234375
5.7290000916	0.0540600009	2.0000000000	8360.9550781250
5.7290000916	0.0540600009	4.0000000000	6925.7270507812
5.7290000916	0.0540600009	6.0000000000	8379.0175781250
5.7290000916	0.0540600009	8.0000000000	8635.1611328125
5.7290000916	0.0540600009	10.0000000000	8212.7158203125
5.7290000916	0.0540600009	12.0000000000	8478.6328125000
5.7290000916	0.0540600009	14.0000000000	8406.0693359375
5.7290000916	0.0540600009	16.0000000000	8660.5429687500
5.7290000916	0.0540600009	18.0000000000	8587.6572265625
5.7290000916	0.0540600009	20.0000000000	8466.7900390625
5.7290000916	0.0624900013	0.0000000000	9717.1523437500
5.7290000916	0.0624900013	2.0000000000	9664.4355468750
5.7290000916	0.0624900013	4.0000000000	9862.0166015625
5.7290000916	0.0624900013	6.0000000000	9685.3144531250
5.7290000916	0.0624900013	8.0000000000	9981.3896484375
5.7290000916	0.0624900013	10.0000000000	9493.0869140625
5.7290000916	0.0624900013	12.0000000000	9800.4599609375
5.7290000916	0.0624900013	14.0000000000	10089.2900390625
5.7290000916	0.0624900013	16.0000000000	10010.7275390625
5.7290000916	0.0624900013	18.0000000000	9926.4804687500

5.7290000916	0.0624900013	20.0000000000	9786.7705078125
5.7290000916	0.1042999998	0.0000000000	17140.1269531250
5.7290000916	0.1042999998	2.0000000000	17130.1835937500
5.7290000916	0.1042999998	4.0000000000	14208.5312500000
5.7290000916	0.1042999998	6.0000000000	14236.8964843750
5.7290000916	0.1042999998	8.0000000000	17364.7636718750
5.7290000916	0.1042999998	10.0000000000	14223.9101562500
5.7290000916	0.1042999998	12.0000000000	14214.5537109375
5.7290000916	0.1042999998	14.0000000000	17449.5058593750
5.7290000916	0.1042999998	16.0000000000	17276.0078125000
5.7290000916	0.1042999998	18.0000000000	17689.0019531250
5.7290000916	0.1042999998	20.0000000000	14204.0419921875
5.7290000916	0.3305000067	0.0000000000	57013.9843750000
5.7290000916	0.3305000067	2.0000000000	56215.1953125000
5.7290000916	0.3305000067	4.0000000000	52405.6757812500
5.7290000916	0.3305000067	6.0000000000	59864.3164062500
5.7290000916	0.3305000067	8.0000000000	56401.7539062500
5.7290000916	0.3305000067	10.0000000000	57549.5117187500
5.7290000916	0.3305000067	12.0000000000	51740.3671875000
5.7290000916	0.3305000067	14.0000000000	59275.9023437500
5.7290000916	0.3305000067	16.0000000000	57853.7617187500
5.7290000916	0.3305000067	18.0000000000	57631.5585937500
5.7290000916	0.3305000067	20.0000000000	57180.4609375000
6.8489999771	0.0540600009	0.0000000000	8256.9785156250
6.8489999771	0.0540600009	2.0000000000	6743.9707031250
6.8489999771	0.0540600009	4.0000000000	6743.8798828125
6.8489999771	0.0540600009	6.0000000000	6810.6533203125
6.8489999771	0.0540600009	8.0000000000	6731.5727539062
6.8489999771	0.0540600009	10.0000000000	6722.3383789062
6.8489999771	0.0540600009	12.0000000000	6810.8461914062
6.8489999771	0.0540600009	14.0000000000	8065.7553710938
6.8489999771	0.0540600009	16.0000000000	7929.2524414062
6.8489999771	0.0540600009	18.0000000000	8213.5263671875
6.8489999771	0.0540600009	20.0000000000	6732.7153320312
6.8489999771	0.0624900013	0.0000000000	9539.2226562500
6.8489999771	0.0624900013	2.0000000000	7811.2949218750
6.8489999771	0.0624900013	4.0000000000	7951.1977539062
6.8489999771	0.0624900013	6.0000000000	8319.1113281250
6.8489999771	0.0624900013	8.0000000000	7880.6547851562
6.8489999771	0.0624900013	10.0000000000	7879.0336914062
6.8489999771	0.0624900013	12.0000000000	7871.3027343750
6.8489999771	0.0624900013	14.0000000000	7878.1313476562
6.8489999771	0.0624900013	16.0000000000	9160.6064453125
6.8489999771	0.0624900013	18.0000000000	7855.7583007812
6.8489999771	0.0624900013	20.0000000000	7883.1245117188
6.8489999771	0.1042999998	0.0000000000	16909.8378906250

6.8489999771	0.1042999998	2.0000000000	13399.8798828125
6.8489999771	0.1042999998	4.0000000000	13397.6503906250
6.8489999771	0.1042999998	6.0000000000	13367.1347656250
6.8489999771	0.1042999998	8.0000000000	12851.6337890625
6.8489999771	0.1042999998	10.0000000000	12710.9404296875
6.8489999771	0.1042999998	12.0000000000	13348.2597656250
6.8489999771	0.1042999998	14.0000000000	12308.3222656250
6.8489999771	0.1042999998	16.0000000000	12005.4384765625
6.8489999771	0.1042999998	18.0000000000	14334.4531250000
6.8489999771	0.1042999998	20.0000000000	14922.4384765625
6.8489999771	0.3305000067	0.0000000000	53455.7148437500
6.8489999771	0.3305000067	2.0000000000	52247.4570312500
6.8489999771	0.3305000067	4.0000000000	47329.5156250000
6.8489999771	0.3305000067	6.0000000000	58279.7382812500
6.8489999771	0.3305000067	8.0000000000	52686.3984375000
6.8489999771	0.3305000067	10.0000000000	47724.9453125000
6.8489999771	0.3305000067	12.0000000000	47742.5781250000
6.8489999771	0.3305000067	14.0000000000	53260.7226562500
6.8489999771	0.3305000067	16.0000000000	52842.5585937500
6.8489999771	0.3305000067	18.0000000000	54304.0546875000
6.8489999771	0.3305000067	20.0000000000	53886.9218750000

Appendix E

Coefficient of Lift
Mach Range:
2.3929998875
2.5920000076
5.7290000916
6.8489999771
Dyn. Pres. (bars) Range:
0.0540600009
0.0624900013
0.1042999998
0.3305000067
AOA (°) Range:
0.0000000000
2.0000000000
4.0000000000
6.0000000000
8.0000000000
10.0000000000
12.0000000000
14.0000000000
16.0000000000
18.0000000000
20.0000000000

Function Data:

Mach	Dyn. Pres. (bars)	AOA (°)	C_L
2.3929998875	0.0540600009	0.0000000000	-0.0221080538
2.3929998875	0.0540600009	2.0000000000	-0.0013090177
2.3929998875	0.0540600009	4.0000000000	0.0184249133
2.3929998875	0.0540600009	6.0000000000	0.0441883057
2.3929998875	0.0540600009	8.0000000000	0.0795788988
2.3929998875	0.0540600009	10.0000000000	nan
2.3929998875	0.0540600009	12.0000000000	0.1558928043
2.3929998875	0.0540600009	14.0000000000	0.1959918886
2.3929998875	0.0540600009	16.0000000000	0.2360392064
2.3929998875	0.0540600009	18.0000000000	0.2760632038
2.3929998875	0.0540600009	20.0000000000	0.3167361617
2.3929998875	0.0624900013	0.0000000000	-0.0221031643
2.3929998875	0.0624900013	2.0000000000	-0.0013071796
2.3929998875	0.0624900013	4.0000000000	0.0184293985
2.3929998875	0.0624900013	6.0000000000	0.0441888794
2.3929998875	0.0624900013	8.0000000000	0.0795825943
2.3929998875	0.0624900013	10.0000000000	nan

2.3929998875	0.0624900013	12.0000000000	0.1558805704
2.3929998875	0.0624900013	14.0000000000	0.1959684491
2.3929998875	0.0624900013	16.0000000000	0.2360067219
2.3929998875	0.0624900013	18.0000000000	0.2760395706
2.3929998875	0.0624900013	20.0000000000	0.3167419136
2.3929998875	0.1042999998	0.0000000000	-0.0220899694
2.3929998875	0.1042999998	2.0000000000	-0.0012954620
2.3929998875	0.1042999998	4.0000000000	0.0184388030
2.3929998875	0.1042999998	6.0000000000	0.0441955365
2.3929998875	0.1042999998	8.0000000000	0.0795866400
2.3929998875	0.1042999998	10.0000000000	nan
2.3929998875	0.1042999998	12.0000000000	0.1558990479
2.3929998875	0.1042999998	14.0000000000	0.1959472895
2.3929998875	0.1042999998	16.0000000000	0.2359924614
2.3929998875	0.1042999998	18.0000000000	0.2760564685
2.3929998875	0.1042999998	20.0000000000	0.3167564571
2.3929998875	0.3305000067	0.0000000000	-0.0220676959
2.3929998875	0.3305000067	2.0000000000	-0.0012915519
2.3929998875	0.3305000067	4.0000000000	0.0184468143
2.3929998875	0.3305000067	6.0000000000	0.0442117974
2.3929998875	0.3305000067	8.0000000000	0.0795782954
2.3929998875	0.3305000067	10.0000000000	nan
2.3929998875	0.3305000067	12.0000000000	0.1559269577
2.3929998875	0.3305000067	14.0000000000	0.1959788799
2.3929998875	0.3305000067	16.0000000000	0.2360207587
2.3929998875	0.3305000067	18.0000000000	0.2761034667
2.3929998875	0.3305000067	20.0000000000	0.3168314993
2.5920000076	0.0540600009	0.0000000000	-0.0199607573
2.5920000076	0.0540600009	2.0000000000	0.0000383703
2.5920000076	0.0540600009	4.0000000000	0.0189998988
2.5920000076	0.0540600009	6.0000000000	0.0433740839
2.5920000076	0.0540600009	8.0000000000	0.0764207095
2.5920000076	0.0540600009	10.0000000000	nan
2.5920000076	0.0540600009	12.0000000000	0.1483912915
2.5920000076	0.0540600009	14.0000000000	0.1859513521
2.5920000076	0.0540600009	16.0000000000	0.2244597375
2.5920000076	0.0540600009	18.0000000000	0.2631147206
2.5920000076	0.0540600009	20.0000000000	0.3022570014
2.5920000076	0.0624900013	0.0000000000	-0.0199347213
2.5920000076	0.0624900013	2.0000000000	0.0000514799
2.5920000076	0.0624900013	4.0000000000	0.0190032423
2.5920000076	0.0624900013	6.0000000000	0.0433535911
2.5920000076	0.0624900013	8.0000000000	0.0763881281
2.5920000076	0.0624900013	10.0000000000	nan
2.5920000076	0.0624900013	12.0000000000	0.1483278424
2.5920000076	0.0624900013	14.0000000000	0.1858587712

2.5920000076	0.0624900013	16.0000000000	0.2243178338
2.5920000076	0.0624900013	18.0000000000	0.2629338503
2.5920000076	0.0624900013	20.0000000000	0.3021674454
2.5920000076	0.1042999998	0.0000000000	-0.0198873114
2.5920000076	0.1042999998	2.0000000000	0.0000759069
2.5920000076	0.1042999998	4.0000000000	0.0190208890
2.5920000076	0.1042999998	6.0000000000	0.0433459766
2.5920000076	0.1042999998	8.0000000000	0.0763395205
2.5920000076	0.1042999998	10.0000000000	nan
2.5920000076	0.1042999998	12.0000000000	0.1481888890
2.5920000076	0.1042999998	14.0000000000	0.1857465059
2.5920000076	0.1042999998	16.0000000000	0.2241827548
2.5920000076	0.1042999998	18.0000000000	0.2628405094
2.5920000076	0.1042999998	20.0000000000	0.3019692302
2.5920000076	0.3305000067	0.0000000000	-0.0198538974
2.5920000076	0.3305000067	2.0000000000	0.0001006001
2.5920000076	0.3305000067	4.0000000000	0.0190576147
2.5920000076	0.3305000067	6.0000000000	0.0433845446
2.5920000076	0.3305000067	8.0000000000	0.0763443485
2.5920000076	0.3305000067	10.0000000000	nan
2.5920000076	0.3305000067	12.0000000000	0.1482361257
2.5920000076	0.3305000067	14.0000000000	0.1857948899
2.5920000076	0.3305000067	16.0000000000	0.2242890298
2.5920000076	0.3305000067	18.0000000000	0.2629965842
2.5920000076	0.3305000067	20.0000000000	0.3020799458
5.7290000916	0.0540600009	0.0000000000	-0.0079848440
5.7290000916	0.0540600009	2.0000000000	0.0078666164
5.7290000916	0.0540600009	4.0000000000	0.0224561244
5.7290000916	0.0540600009	6.0000000000	0.0382745080
5.7290000916	0.0540600009	8.0000000000	0.0582611337
5.7290000916	0.0540600009	10.0000000000	nan
5.7290000916	0.0540600009	12.0000000000	0.1068498716
5.7290000916	0.0540600009	14.0000000000	0.1345291883
5.7290000916	0.0540600009	16.0000000000	0.1644150168
5.7290000916	0.0540600009	18.0000000000	0.1957853287
5.7290000916	0.0540600009	20.0000000000	0.2278333902
5.7290000916	0.0624900013	0.0000000000	-0.0079981685
5.7290000916	0.0624900013	2.0000000000	0.0078567127
5.7290000916	0.0624900013	4.0000000000	0.0224554818
5.7290000916	0.0624900013	6.0000000000	0.0382829905
5.7290000916	0.0624900013	8.0000000000	0.0582817681
5.7290000916	0.0624900013	10.0000000000	nan
5.7290000916	0.0624900013	12.0000000000	0.1068764329
5.7290000916	0.0624900013	14.0000000000	0.1345590949
5.7290000916	0.0624900013	16.0000000000	0.1644225121
5.7290000916	0.0624900013	18.0000000000	0.1958234608

5.7290000916	0.0624900013	20.0000000000	0.2278639823
5.7290000916	0.1042999998	0.0000000000	-0.0080295997
5.7290000916	0.1042999998	2.0000000000	0.0078516193
5.7290000916	0.1042999998	4.0000000000	0.0224585664
5.7290000916	0.1042999998	6.0000000000	0.0383101888
5.7290000916	0.1042999998	8.0000000000	0.0583199374
5.7290000916	0.1042999998	10.0000000000	nan
5.7290000916	0.1042999998	12.0000000000	0.1069570854
5.7290000916	0.1042999998	14.0000000000	0.1346415430
5.7290000916	0.1042999998	16.0000000000	0.1644900590
5.7290000916	0.1042999998	18.0000000000	0.1959895194
5.7290000916	0.1042999998	20.0000000000	0.2279354185
5.7290000916	0.3305000067	0.0000000000	-0.0080231400
5.7290000916	0.3305000067	2.0000000000	0.0078521809
5.7290000916	0.3305000067	4.0000000000	0.0224779360
5.7290000916	0.3305000067	6.0000000000	0.0383637957
5.7290000916	0.3305000067	8.0000000000	0.0584028438
5.7290000916	0.3305000067	10.0000000000	nan
5.7290000916	0.3305000067	12.0000000000	0.1070948765
5.7290000916	0.3305000067	14.0000000000	0.1348424554
5.7290000916	0.3305000067	16.0000000000	0.1646978259
5.7290000916	0.3305000067	18.0000000000	0.1961404830
5.7290000916	0.3305000067	20.0000000000	0.2281195074
6.8489999771	0.0540600009	0.0000000000	-0.0068839784
6.8489999771	0.0540600009	2.0000000000	0.0086401161
6.8489999771	0.0540600009	4.0000000000	0.0228331201
6.8489999771	0.0540600009	6.0000000000	0.0379201099
6.8489999771	0.0540600009	8.0000000000	0.0567917712
6.8489999771	0.0540600009	10.0000000000	nan
6.8489999771	0.0540600009	12.0000000000	0.1034136638
6.8489999771	0.0540600009	14.0000000000	0.1304578632
6.8489999771	0.0540600009	16.0000000000	0.1596833020
6.8489999771	0.0540600009	18.0000000000	0.1905838400
6.8489999771	0.0540600009	20.0000000000	0.2222114503
6.8489999771	0.0624900013	0.0000000000	-0.0068825395
6.8489999771	0.0624900013	2.0000000000	0.0086370800
6.8489999771	0.0624900013	4.0000000000	0.0228417628
6.8489999771	0.0624900013	6.0000000000	0.0379267111
6.8489999771	0.0624900013	8.0000000000	0.0567990951
6.8489999771	0.0624900013	10.0000000000	nan
6.8489999771	0.0624900013	12.0000000000	0.1033977643
6.8489999771	0.0624900013	14.0000000000	0.1304588467
6.8489999771	0.0624900013	16.0000000000	0.1596796662
6.8489999771	0.0624900013	18.0000000000	0.1906098425
6.8489999771	0.0624900013	20.0000000000	0.2222062051
6.8489999771	0.1042999998	0.0000000000	-0.0069141318

6.8489999771	0.1042999998	2.0000000000	0.0086352471
6.8489999771	0.1042999998	4.0000000000	0.0228324421
6.8489999771	0.1042999998	6.0000000000	0.0379396304
6.8489999771	0.1042999998	8.0000000000	0.0567908101
6.8489999771	0.1042999998	10.0000000000	nan
6.8489999771	0.1042999998	12.0000000000	0.1033449247
6.8489999771	0.1042999998	14.0000000000	0.1304541975
6.8489999771	0.1042999998	16.0000000000	0.1596277356
6.8489999771	0.1042999998	18.0000000000	0.1906085610
6.8489999771	0.1042999998	20.0000000000	0.2221726030
6.8489999771	0.3305000067	0.0000000000	-0.0068968823
6.8489999771	0.3305000067	2.0000000000	0.0086375745
6.8489999771	0.3305000067	4.0000000000	0.0228334777
6.8489999771	0.3305000067	6.0000000000	0.0379151441
6.8489999771	0.3305000067	8.0000000000	0.0567699708
6.8489999771	0.3305000067	10.0000000000	nan
6.8489999771	0.3305000067	12.0000000000	0.1033018008
6.8489999771	0.3305000067	14.0000000000	0.1303753853
6.8489999771	0.3305000067	16.0000000000	0.1595838964
6.8489999771	0.3305000067	18.0000000000	0.1905301362
6.8489999771	0.3305000067	20.0000000000	0.2222134471

Appendix F

Coefficient of Drag
Mach Range:
2.3929998875
2.5920000076
5.7290000916
6.8489999771
Dyn. Pres. (bars) Range:
0.0540600009
0.0624900013
0.1042999998
0.3305000067
AOA (°) Range:
0.0000000000
2.0000000000
4.0000000000
6.0000000000
8.0000000000
10.0000000000
12.0000000000
14.0000000000
16.0000000000
18.0000000000
20.0000000000

Function Data:

Mach	Dyn. Pres. (bars)	AOA (°)	C_D
2.3929998875	0.0540600009	0.0000000000	0.0274121743
2.3929998875	0.0540600009	2.0000000000	0.0266966969
2.3929998875	0.0540600009	4.0000000000	0.0280459691
2.3929998875	0.0540600009	6.0000000000	0.0310986228
2.3929998875	0.0540600009	8.0000000000	0.0368331484
2.3929998875	0.0540600009	10.0000000000	nan
2.3929998875	0.0540600009	12.0000000000	0.0575695746
2.3929998875	0.0540600009	14.0000000000	0.0730167255
2.3929998875	0.0540600009	16.0000000000	0.0916935056
2.3929998875	0.0540600009	18.0000000000	0.1137066260
2.3929998875	0.0540600009	20.0000000000	0.1392088681
2.3929998875	0.0624900013	0.0000000000	0.0272516776
2.3929998875	0.0624900013	2.0000000000	0.0265473984
2.3929998875	0.0624900013	4.0000000000	0.0278701279
2.3929998875	0.0624900013	6.0000000000	0.0309269987
2.3929998875	0.0624900013	8.0000000000	0.0366567150
2.3929998875	0.0624900013	10.0000000000	nan

2.3929998875	0.0624900013	12.0000000000	0.0573890060
2.3929998875	0.0624900013	14.0000000000	0.0728270710
2.3929998875	0.0624900013	16.0000000000	0.0914955288
2.3929998875	0.0624900013	18.0000000000	0.1135104969
2.3929998875	0.0624900013	20.0000000000	0.1390295476
2.3929998875	0.1042999998	0.0000000000	0.0267255288
2.3929998875	0.1042999998	2.0000000000	0.0260365698
2.3929998875	0.1042999998	4.0000000000	0.0272907261
2.3929998875	0.1042999998	6.0000000000	0.0303850863
2.3929998875	0.1042999998	8.0000000000	0.0360922255
2.3929998875	0.1042999998	10.0000000000	nan
2.3929998875	0.1042999998	12.0000000000	0.0568063371
2.3929998875	0.1042999998	14.0000000000	0.0722273216
2.3929998875	0.1042999998	16.0000000000	0.0908871293
2.3929998875	0.1042999998	18.0000000000	0.1128002629
2.3929998875	0.1042999998	20.0000000000	0.1384056062
2.3929998875	0.3305000067	0.0000000000	0.0258416403
2.3929998875	0.3305000067	2.0000000000	0.0251424480
2.3929998875	0.3305000067	4.0000000000	0.0263978690
2.3929998875	0.3305000067	6.0000000000	0.0294400696
2.3929998875	0.3305000067	8.0000000000	0.0351404063
2.3929998875	0.3305000067	10.0000000000	nan
2.3929998875	0.3305000067	12.0000000000	0.0557925105
2.3929998875	0.3305000067	14.0000000000	0.0711883903
2.3929998875	0.3305000067	16.0000000000	0.0897092447
2.3929998875	0.3305000067	18.0000000000	0.1116903946
2.3929998875	0.3305000067	20.0000000000	0.1374123245
2.5920000076	0.0540600009	0.0000000000	0.0254967771
2.5920000076	0.0540600009	2.0000000000	0.0249791127
2.5920000076	0.0540600009	4.0000000000	0.0263335798
2.5920000076	0.0540600009	6.0000000000	0.0293981805
2.5920000076	0.0540600009	8.0000000000	0.0349538624
2.5920000076	0.0540600009	10.0000000000	nan
2.5920000076	0.0540600009	12.0000000000	0.0549546517
2.5920000076	0.0540600009	14.0000000000	0.0696969032
2.5920000076	0.0540600009	16.0000000000	0.0877132714
2.5920000076	0.0540600009	18.0000000000	0.1090721712
2.5920000076	0.0540600009	20.0000000000	0.1338073611
2.5920000076	0.0624900013	0.0000000000	0.0253122449
2.5920000076	0.0624900013	2.0000000000	0.0248006918
2.5920000076	0.0624900013	4.0000000000	0.0261451248
2.5920000076	0.0624900013	6.0000000000	0.0291664731
2.5920000076	0.0624900013	8.0000000000	0.0347657241
2.5920000076	0.0624900013	10.0000000000	nan
2.5920000076	0.0624900013	12.0000000000	0.0547585934
2.5920000076	0.0624900013	14.0000000000	0.0694825575

2.5920000076	0.0624900013	16.0000000000	0.0874850601
2.5920000076	0.0624900013	18.0000000000	0.1088194847
2.5920000076	0.0624900013	20.0000000000	0.1335775405
2.5920000076	0.1042999998	0.0000000000	0.0247374158
2.5920000076	0.1042999998	2.0000000000	0.0242193993
2.5920000076	0.1042999998	4.0000000000	0.0255167987
2.5920000076	0.1042999998	6.0000000000	0.0286077745
2.5920000076	0.1042999998	8.0000000000	0.0341976583
2.5920000076	0.1042999998	10.0000000000	nan
2.5920000076	0.1042999998	12.0000000000	0.0541247688
2.5920000076	0.1042999998	14.0000000000	0.0688968673
2.5920000076	0.1042999998	16.0000000000	0.0868990570
2.5920000076	0.1042999998	18.0000000000	0.1082039326
2.5920000076	0.1042999998	20.0000000000	0.1328496337
2.5920000076	0.3305000067	0.0000000000	0.0237803347
2.5920000076	0.3305000067	2.0000000000	0.0232089292
2.5920000076	0.3305000067	4.0000000000	0.0245407298
2.5920000076	0.3305000067	6.0000000000	0.0276466645
2.5920000076	0.3305000067	8.0000000000	0.0331995450
2.5920000076	0.3305000067	10.0000000000	nan
2.5920000076	0.3305000067	12.0000000000	0.0531683899
2.5920000076	0.3305000067	14.0000000000	0.0678994581
2.5920000076	0.3305000067	16.0000000000	0.0858997256
2.5920000076	0.3305000067	18.0000000000	0.1070609093
2.5920000076	0.3305000067	20.0000000000	0.1318918616
5.7290000916	0.0540600009	0.0000000000	0.0127732847
5.7290000916	0.0540600009	2.0000000000	0.0129184071
5.7290000916	0.0540600009	4.0000000000	0.0148392711
5.7290000916	0.0540600009	6.0000000000	0.0180896576
5.7290000916	0.0540600009	8.0000000000	0.0232264549
5.7290000916	0.0540600009	10.0000000000	nan
5.7290000916	0.0540600009	12.0000000000	0.0399270765
5.7290000916	0.0540600009	14.0000000000	0.0521805696
5.7290000916	0.0540600009	16.0000000000	0.0672585741
5.7290000916	0.0540600009	18.0000000000	0.0853566751
5.7290000916	0.0540600009	20.0000000000	0.1063879058
5.7290000916	0.0624900013	0.0000000000	0.0125401840
5.7290000916	0.0624900013	2.0000000000	0.0127091957
5.7290000916	0.0624900013	4.0000000000	0.0146368975
5.7290000916	0.0624900013	6.0000000000	0.0178599097
5.7290000916	0.0624900013	8.0000000000	0.0229918100
5.7290000916	0.0624900013	10.0000000000	nan
5.7290000916	0.0624900013	12.0000000000	0.0396638513
5.7290000916	0.0624900013	14.0000000000	0.0518999994
5.7290000916	0.0624900013	16.0000000000	0.0669862255
5.7290000916	0.0624900013	18.0000000000	0.0850827694

5.7290000916	0.0624900013	20.0000000000	0.1060950980
5.7290000916	0.1042999998	0.0000000000	0.0120770596
5.7290000916	0.1042999998	2.0000000000	0.0122653777
5.7290000916	0.1042999998	4.0000000000	0.0140479468
5.7290000916	0.1042999998	6.0000000000	0.0172869023
5.7290000916	0.1042999998	8.0000000000	0.0223045535
5.7290000916	0.1042999998	10.0000000000	nan
5.7290000916	0.1042999998	12.0000000000	0.0389819816
5.7290000916	0.1042999998	14.0000000000	0.0511444397
5.7290000916	0.1042999998	16.0000000000	0.0662160069
5.7290000916	0.1042999998	18.0000000000	0.0842475072
5.7290000916	0.1042999998	20.0000000000	0.1051930934
5.7290000916	0.3305000067	0.0000000000	0.0111168791
5.7290000916	0.3305000067	2.0000000000	0.0112911249
5.7290000916	0.3305000067	4.0000000000	0.0130771995
5.7290000916	0.3305000067	6.0000000000	0.0161916129
5.7290000916	0.3305000067	8.0000000000	0.0212367531
5.7290000916	0.3305000067	10.0000000000	nan
5.7290000916	0.3305000067	12.0000000000	0.0377595648
5.7290000916	0.3305000067	14.0000000000	0.0498600788
5.7290000916	0.3305000067	16.0000000000	0.0648219138
5.7290000916	0.3305000067	18.0000000000	0.0828011408
5.7290000916	0.3305000067	20.0000000000	0.1036799625
6.8489999771	0.0540600009	0.0000000000	0.0119011868
6.8489999771	0.0540600009	2.0000000000	0.0119994953
6.8489999771	0.0540600009	4.0000000000	0.0139812157
6.8489999771	0.0540600009	6.0000000000	0.0172763206
6.8489999771	0.0540600009	8.0000000000	0.0223914236
6.8489999771	0.0540600009	10.0000000000	nan
6.8489999771	0.0540600009	12.0000000000	0.0389220901
6.8489999771	0.0540600009	14.0000000000	0.0510729924
6.8489999771	0.0540600009	16.0000000000	0.0659794137
6.8489999771	0.0540600009	18.0000000000	0.0838925615
6.8489999771	0.0540600009	20.0000000000	0.1047607511
6.8489999771	0.0624900013	0.0000000000	0.0116134761
6.8489999771	0.0624900013	2.0000000000	0.0117539894
6.8489999771	0.0624900013	4.0000000000	0.0136961034
6.8489999771	0.0624900013	6.0000000000	0.0170088187
6.8489999771	0.0624900013	8.0000000000	0.0220949315
6.8489999771	0.0624900013	10.0000000000	nan
6.8489999771	0.0624900013	12.0000000000	0.0386068113
6.8489999771	0.0624900013	14.0000000000	0.0507284105
6.8489999771	0.0624900013	16.0000000000	0.0656193867
6.8489999771	0.0624900013	18.0000000000	0.0835189298
6.8489999771	0.0624900013	20.0000000000	0.1043971479
6.8489999771	0.1042999998	0.0000000000	0.0109942472

6.8489999771	0.1042999998	2.0000000000	0.0111538423
6.8489999771	0.1042999998	4.0000000000	0.0130238570
6.8489999771	0.1042999998	6.0000000000	0.0163062345
6.8489999771	0.1042999998	8.0000000000	0.0213580579
6.8489999771	0.1042999998	10.0000000000	nan
6.8489999771	0.1042999998	12.0000000000	0.0377740823
6.8489999771	0.1042999998	14.0000000000	0.0498042256
6.8489999771	0.1042999998	16.0000000000	0.0646354854
6.8489999771	0.1042999998	18.0000000000	0.0825587139
6.8489999771	0.1042999998	20.0000000000	0.1033819690
6.8489999771	0.3305000067	0.0000000000	0.0098306993
6.8489999771	0.3305000067	2.0000000000	0.0100981705
6.8489999771	0.3305000067	4.0000000000	0.0119687598
6.8489999771	0.3305000067	6.0000000000	0.0151460730
6.8489999771	0.3305000067	8.0000000000	0.0201701093
6.8489999771	0.3305000067	10.0000000000	nan
6.8489999771	0.3305000067	12.0000000000	0.0364194624
6.8489999771	0.3305000067	14.0000000000	0.0483519919
6.8489999771	0.3305000067	16.0000000000	0.0631026700
6.8489999771	0.3305000067	18.0000000000	0.0808500051
6.8489999771	0.3305000067	20.0000000000	0.1015557051